

Development of Manufacturing Processes for Solid State Self-Healing Composites

Richard V. Grainger

June 2013



A thesis submitted for the degree of Doctor of Philosophy in

The Department of Materials Science and Engineering

The University Of Sheffield

Acknowledgements

I am deeply indebted to my supervisors Dr. Simon Hayes, Prof. Alma Hodzic, Prof. Russell Hand and Prof. Frank Jones for their invaluable help, guidance and support during the course of this project. Your tireless efforts, patient proof-reading and constant encouragement and reassurance pushed me to accomplish something which I never could have on my own.

Thank you to all those in Composite Systems Innovation Centre for their interminable patience and for teaching me more about composites than I could ever hope to take in, and for their help and assistance whenever I needed it, particularly Dr. Austin Lafferty, Dr. Pete Bailey, Dr. Tim Swait, Mr. Elliot Fleet and Dr. Mohd Suzeren Md Jamil.

Thank you to David Light from Airbus UK for his effort as project manager and my industrial mentor, who took a special interest in my work and my badminton and for me was an inspiration both professionally and personally.

I would also like to thank all the technical and administrative staff who helped me carry out my research and in the preparation of this manuscript and to the University of Sheffield, the EPSRC and to Airbus for funding this work.

Finally, I would like to thank Helen Pasquier from EADS UK who went out of her way to give me the opportunity and encouragement to continue my studies, and along with Jeremy Greaves from EADS UK and Ian Risk from EADS Innovation Works made this PhD possible with a generous studentship.

Abstract

This project was aimed at providing the next step in manufacturing capability for modified matrix self-healing composite panels. Modified matrix self-healing composites use a sense-and-heal approach for which both the resin and the heating actuation must be tailored for industrial processes.

The high viscosity imposed by the healing agent has made composite layup difficult in previous trials. This however has never been quantified, and projects which have looked at this resin system before have focused on recovery of mechanical properties only. This study has investigated and quantified the viscosity of the self-healing blend with a view to reducing it for industrial manufacture. Several routes were investigated for their viscosity reduction and the effect on their healing properties was quantified as much as possible in terms of fracture toughness recovery, as measured by a modified compact tension geometry.

A steered self-heating method has also been trialled. Different methods of track manufacture were used including photoresist, inkjet mask printing and direct silver printing. Track widths were compared for their effect on the resistance of the channels and their ability to heat up the composite and focus their heating.

Contents

1	Introduction	13
1.1	Materials History	13
1.2	Aims and Objectives	16
2	Literature Review	18
2.1	Composites	18
2.2	Composite Design Limitations	18
2.3	Damage Tolerant Design	19
2.4	Self-healing Technologies	20
2.4.1	Hollow-fibre method	21
2.4.2	Microcapsule Method	23
2.4.3	Vascular Method	24
2.4.4	Epoxy Particulate System	27
2.4.5	Limitations of Resin Delivery Systems	27
2.4.6	Remendable Polymers	30
2.4.7	Thermoplastic Healing Agents	32
2.5	Rheological Studies	35
2.6	Self-sensing	36
2.7	Summary	38
3	Experimental	40
3.1	Introduction to Epoxy Resins	40
3.2	Epoxy Resin Systems	41
3.2.1	Bisphenol-A Resins	41
3.2.2	Bisphenol-F Resins	41
3.2.3	Curing Agents	42
3.3	Epoxy-Acid Anhydride Cure Chemistry	43
3.3.1	Uncatalysed Reaction	43
3.3.2	Catalysed Reaction	44
3.3.3	Calculating the Epoxy-Anhydride Equivalent Weight	45
3.4	Preparation of chemicals	47
3.4.1	Healing Agents	47
3.4.2	End-cap Deactivation	47
3.5	Formulations	48
3.5.1	Previous Formulation	48
3.6	Resin Preparation	49
3.6.1	Resins and Nomenclature	50
3.7	Healing Procedure	51

3.8	Rheology	52
3.8.1	Theory	52
3.8.2	Equipment	53
3.9	Compact Tension Testing	53
3.9.1	K_{Ic} Calculation	55
3.9.2	G_{Ic} Calculation	56
3.9.3	Specimen Creation	57
3.9.4	Setup	58
3.9.5	Calibration	58
3.9.6	Assessment of Healing Efficiency	59
3.10	Tensile Testing	59
3.10.1	Assessment of Mechanical Properties	59
3.10.2	Specimen Creation	60
3.11	Composites Manufacture	61
3.11.1	Manufacture of Self-sensing Plies	61
3.12	Composite Specimen Preparation	65
4	Characterisation of Resin System	67
4.1	Introduction	67
4.2	Developmental Research	67
4.2.1	Uniaxial Compression Testing	68
4.2.2	Tensile Testing	70
4.3	Compact Tension Self-Healing	71
4.4	Rheology of System	72
4.5	Discussion	76
4.6	Conclusion	79
5	Development of Resin System	80
5.1	Introduction	80
5.2	Characterisation of Systems	80
5.2.1	Concentration Effects	80
5.2.2	Molecular Weight Variance	81
5.2.3	Reactive Diluents	83
5.2.4	Bisphenol-F Blend	87
5.3	Discussion	88
5.3.1	Compact Tension Testing Fracture	92
5.3.2	Irwin and the development of Standards	93
5.3.3	Difficulties in implementation of Standard Testing	93
5.3.4	Standard assessment of self-healing materials	97
5.4	Conclusion	100

6	Manufacture of Sensing Panel	102
6.1	Introduction	102
6.2	Self-Sensing Plies	102
6.2.1	Inkjet Masking	103
6.2.2	Direct Silver Printing	107
6.3	Small Panel Resistive Heating	109
6.3.1	Thermography	109
6.4	Large Panel Targeted Heating	120
6.4.1	Thermography	120
6.5	Discussion	122
6.6	Conclusion	125
7	Concluding Summary	126
8	Future Work	129
	References	131
	Appendix	147

List of Figures

1	Frank Whittle’s original gas turbine jet design, which could provide air speeds which demanded more advanced materials [4].	14
2	Schematic representation of the composite self-sensing system. Electrical contact was made with flexible circuit boards.	16
3	Classification of self-healing materials into Autonomic and Non-autonomic systems [47].	21
4	SEM of fractured glass fibres containing uncured repair resin [49]. . .	22
5	The microcapsule self-healing concept [32].	23
6	Mechanism of DCPD ring-opening metathesis polymerisation (ROMP) reaction with Grubbs’ catalyst [64].	24
7	Microvascular-based healing of polymers: (a) microchannels in the substrate contain a supply of healing agent (red) fill surface cracks with self-healing resin(purple), (b) excess healing agent (dicyclopentadiene, DCPD) released on the surface of the sample after transverse cracks were healed [76].	26
8	Micrograph of matrix tensile fatigue damage before(left) and after(right) a repair cycle [75].	27
9	Different types of hollow-fibre resin delivery systems [49].	28
10	Damaged samples showing bleeding of UV-fluorescent dye at 45x magnification [79].	29
11	Maleimide and furan react to form a DA-step growth polymer.	31
12	A dynamic equilibrium between a monomer species (left) and a organometallic polymer (right) that is controlled via an external stimulus such as heat [89].	31
13	Photo-dimerisation of anthracene using UV light	32

14	Structure of epoxypropane, a basic epoxy, with epoxy ring.	40
15	Reaction of epichlorohydrin and bisphenol A to form bisphenol-A diglycidyl ether.	41
16	Structure of bisphenol A diglycidyl ether epoxy resin.	41
17	Reaction of phenol and formaldehyde into the isomers of bisphenol-F [13].	42
18	NMA reacts with a hydroxyl group to form a half acid ester.	44
19	The new carboxyl reacts with epoxy to form hydroxy di-ester.	44
20	Epoxy groups react with free hydroxyl.	44
21	Initiation of reaction, NMA activated by the tertiary amine catalyst.	45
22	Epoxy group reacting with activated acid anhydride.	45
23	Continuation of reaction, opening second anhydride ring.	45
24	Reaction of PDGBA and benzoic acid to provide end-capping.	48
25	Structural formulae of the three main constituents of the self-healing resin system: resin, curing agent and healing agent.	49
26	Compact Tension Schematic according to the British Standard ISO 13586:2000.	54
27	Load-displacement graph for a compact tension test.	55
28	Tensile Testing Specimen Dimensions [132].	60
29	Schematic representation of the composite self-sensing system. Electrical contact was made with flexible circuit boards.	65
30	Composite manufacture bagging arrangement recommended by Cytac	66
31	200 mm x 200 mm carbon fibre panel with self-sensing polyimide circuit board inserts. Two connectors on left are for 0° and 90° directions.	66
32	Stress/Strain curves of resin in uniaxial compression test.	68
33	Yield Strength of base resin with varying concentration of healing agent from uniaxial compression testing.	69

34	Yield Strain of base resin with varying concentration of healing agent from uniaxial compression testing.	70
35	Recovery of K_{IC} for varying concentration of healing agent.	71
36	Recovery of K_{IC} across 3 healing cycles, with very concentration of healing agent.	72
37	Temperature dependance of viscosity of resin with varying concentration of healing agent (0 wt%, 3 wt%, 5 wt%, 7.5 wt% and 10 wt%).	73
38	Log plot of viscosity vs temperature detail. Shaded area represents viscosity usable (light) and ideal (dark) for use in resin transfer moulding.	74
39	Normal stress recorded during the flow mode viscosity testing shown in Figure 37.	75
40	Loss and Storage moduli of the isothermal curing reaction at 90°C of the pure 828 resin with no modifying healing agent. The crossing point of the loss and storage moduli represents the gel point of the reaction.	75
41	Log complex viscosity of epoxy resin modified with increasing concentration of healing agent. Healing agent Mw: approx. 44,000 g/mol	81
42	Viscosity of epoxy resin modified with 7.5 wt% of healing agents with different molecular weights as a function of temperature. Also shown is viscosity of the control resin, unmodified Epon 828. Shaded areas represent the usable (light) and ideal (dark) viscosity ranges for resin transfer moulding.	82
43	Recovery of fracture toughness with 7.5% of healing agents with a range of different molecular weights. Healing cycle '0' refers to virgin properties. The 'Unmodified Resin' is the control with no healing agent.	83

44	Change in viscosity with temperature of unmodified 828 resin, with increasing concentrations of propylene carbonate (PC) diluent	84
45	Log viscosity of resin without healing agent, modified by propylene carbonate	85
46	Change in viscosity of modified self-healing resin, with 5% healing agent and a range of concentrations of propylene carbonate (PC). Also shown is unmodified control.	85
47	Log viscosity of self-healing resin modified with propylene carbonate (PC).	86
48	Recovery of fracture toughness of resin modified by healing agent and propylene carbonate (PC) diluent. ‘Unmodified’ resin contains no healing agent or diluent and represents the control	87
49	Change in viscosity with changing concentration of Bisphenol F resin (PY306).	88
50	The effect on calculated K_{IC} of measuring the width of the specimen	94
51	The effect on calculated K_{IC} of measuring the initial crack length . .	94
52	Comparison of ASTM and BSI polynomials for calculating the geometry factor from the initial crack length (a) and specimen width (w)	95
53	The three stages of crack propagation by razor tapping from [147] . .	99
54	Images of Inkjet mask printed with various colours, with a 20 minute oven air dry post-print cycle. Right hand side of each image shows the mask partially removed with acetone. a) standard quality. b) photo quality	104
55	Detail of track quality: a) standard quality, and b) photo quality . . .	104

56	Track quality comparison of flexible circuit boards created by using a mask printed with the 4 colours of the inkjet printer head: a) cyan, b) magenta, c) yellow, and d) black.	105
57	Mask created with a copper pre-treatment of 15 minutes in an air convection oven at 90°C.	106
58	Final print mask quality.	106
59	Artwork produced with direct silver printing.	107
60	Silver printed artwork detail. a) Inclusion causing track damage. b) Line spacing causing track break.	108
61	Infra-red thermography of a panel with 1.25mm contact widths targeting damage using 2W of heating power: a) Front face, and b) Back face	110
62	Infra-red thermography of a panel with 2.5mm contact widths targeting damage using 2W of heating power: a) Front face, and b) Back face	110
63	Infra-red thermography of a panel with 5mm contact widths targeting damage using 2W of heating power: a) Front face, and b) Back face	110
64	Infra-red thermography of a panel with 7mm contact widths targeting damage using 2W of heating power: a) Front face, and b) Back face	111
65	3-dimensional graphical representation of temperature increase across the panel area during single-channel heating of a damaged specimen (damage can be seen as a temperature spike in the centre). Both tests were done on a panel with 5mm contact widths like those in Figure 63. a) 6W of heating power, and b) 2W of heating power.	113

66	Intensity of the infra-red camera pixels down the centre of the heated channel. Comparison of contact widths (colour) and heating power (upper and lower traces).	116
67	Temperature-calibrated profile through the cross-section of the panel with the damage in the centre.	117
68	Calculation areas for the targeting characteristics of the resistive heating. Green: Panel area. Purple: Ambient panel temperature. Red: Channel area. Blue: Damage zone, the ‘Hotspot’ is in the centre of this zone. Orange: Contact area.	118
69	Damage-targeting ability of self-heating panels with changing contact width. Calculation zones can be seen in Figure 68.	119
70	Thermography of 200 mm x 200 mm self-heating panel targeting 2 arbitrary sites on an undamaged panel to demonstrate steerable heating effects. 6W of power applied. Large contact heating noticeable.	121
71	A 3-dimensional plot showing the pixel intensity of the infrared camera viewing an undamaged large carbon-fibre panel which is being resistively heated down an arbitrary X and Y channel.	122
72	Primary amine-epoxy addition reaction.	147
73	Secondary amine-epoxy addition reaction.	147
74	Hydroxyl-epoxy etherification reaction.	148
75	Epoxy-epoxy homopolymerisation reaction.	148
76	Mechanism of hydroxyl-catalysed epoxy-amine addition.	149

1 Introduction

The aerospace industry is highly dependent on emerging materials technologies to provide more sophisticated transport systems for military as well as civil use. From the use of wing-warping by the Wright Brothers' Flyer [1] (enabled by its spruce frame) through the self-annealing titanium alloy skin of the SR-71 Blackbird [2], to the multi-functional composite coatings of the F-22 Raptor (which allow radar absorption and damage detection [3]), materials technology has always been at the heart of advances in aerospace performance. However, the use of advanced materials for structural applications has, of necessity, been a gradual process due to the workability of the materials, their availability and the performance required.

1.1 Materials History

Early aircraft before the First World War consisted of predominantly plywood frames with fabric covering. Once the purpose of aircraft became largely for offensive use rather than purely for reconnaissance this design did not provide adequate strength. Anthony Fokker, a Dutch entrepreneur working in Germany during the war, developed a welded-tube steel fuselage, braced with steel wire to provide stability and strength at higher speeds and to enable the mounting of armaments. Such was the design of many Sopwith bi- and tri-planes and their rival Fokker aircraft such as the DR-1 flown by the infamous Red Baron. In World War II the need for air superiority became more important. Advancements in aerospace technology progressed rapidly and included the invention of a gas-turbine jet engine [4] for the Gloster E.28/39, the advancement of aerodynamics [5] for the Spitfire, and improvements in arms deployment [6]. The new engine enabled heavier aircraft to take off and fly faster. Hugo Junkers, a German engineer, had developed all-metal aircraft design in 1915 during the first world war for the J-1 whose wings were composed of 0.08-inch corrugated aluminum alloy skin riveted to an internal framework of aluminum alloy

tubing. However, these new advancements allowed these once slow and heavy aircraft to become a lethal threat. Aircraft developed subsequently by the Axis Powers were built upon Junkers' development of all-metal designs, first using sheet-iron and then duralumin which is a high-strength aluminium alloy.

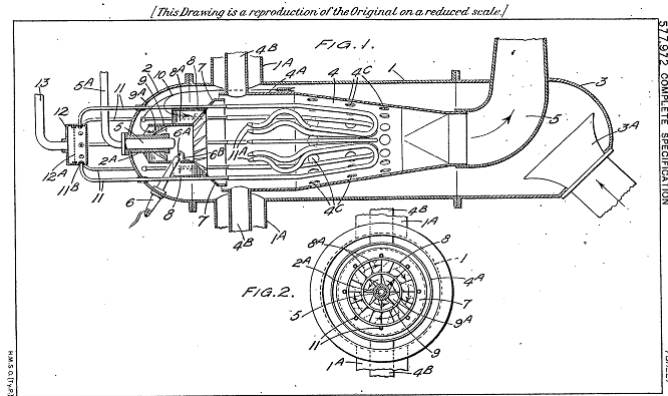


Figure 1: Frank Whittle's original gas turbine jet design, which could provide air speeds which demanded more advanced materials [4].

Following the war, all-metal construction started around the world, the US aeronautics advisory NACA declaring that “metal does not splinter, is more homogeneous, and the properties of the material are much better known and can be relied upon”[7]. Further development of metallic processes and manufacturing techniques led to more exotic designs enabling supersonic travel in the Bell X-1, Fairey Delta-2 and North American X-15 [2].

Until the late 1960s, almost all tactical aircraft were composed primarily of aluminium and its alloys. Titanium alloys became increasingly used mainly owing to their high specific strength, but as bulk titanium needed to be purchased from Russia during the Cold War, costs were prohibitive and concealing its use was almost impossible. After extensive use in the SR-71 high-speed reconnaissance aircraft, titanium was considered unfeasible due to weight and cost issues for anything but the highest-performance components. An alternative was therefore sought: composite materials.

Synthetic composite materials have played a significant role in the advancement of

many areas of industry, including most prominently aerospace, automotive and construction. However they have one major weakness in that their failure can seem unpredictable due to microcracks within the structure which compromise mechanical performance and often evade detection. Non-destructive evaluation techniques, such as radiography and ultrasonic testing, are time-consuming and require expert technicians and tools. Even then this is not always possible with certain geometries, and most often not economically feasible. This has somewhat inhibited the introduction of these materials into more diverse markets where technological advancement is a less crucial factor in product profitability. Nevertheless this desire to overcome the limitations of composites in order to reap their benefits has led to the conceptualisation of an entirely new class of materials; ‘self-healing’ materials. Several methods for the regeneration of mechanical properties have been proposed, each with their own advantages which make them suitable for particular applications or environments. Active or ‘non-autonomic’ methods have been developed, where the reformation of bonds within the matrix is instigated by an external stimulus, such as ‘modified-matrix’ which regains structural integrity with the application of heat to a damage site. This is the technology under investigation in the current project. One of the main disadvantages of this method is that the healing agent imparts a high viscosity to the blend, making it unsuitable for many industrial manufacturing processes, including injection moulding, resin transfer and filament winding.

The modified matrix method relies a distinct sense and heal mechanisms. The self-sensing concept is based on the principle that the resistance of the carbon fibres is low, and that when the ply is damaged or strained the resistance will change as the electrical signal pathways in the laminate are altered. This enables a sensing system attached to the panel to detect where damage has occurred, and if this is done simultaneously in 2 directions then the damage may be triangulated. This method is shown in Figure 2.

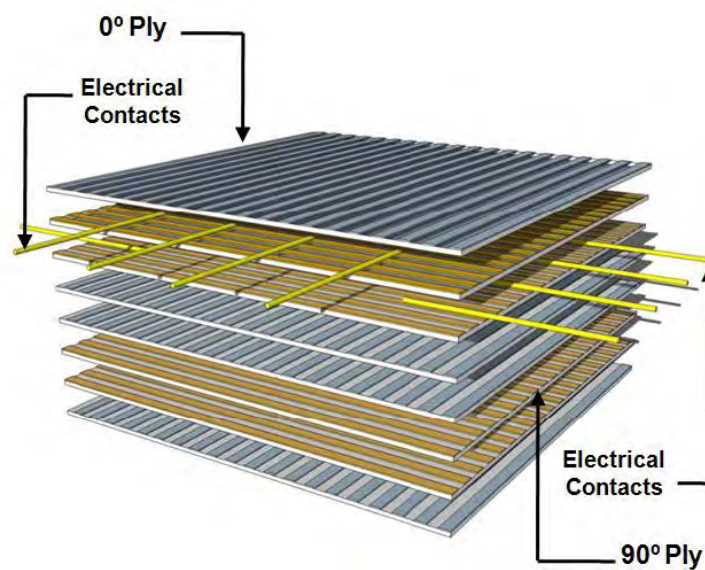


Figure 2: Schematic representation of the composite self-sensing system. Electrical contact was made with flexible circuit boards.

1.2 Aims and Objectives

The overall aim of the current research is to improve the manufacturing performance of the solid state sense and heal system to increase the potential for its use in a commercial setting. It is important to investigate which development routes would provide possible areas of exploitation for the advancement of the solid state epoxy healing system for use in fibre composites. There are two main aims of this project addressing issues with this technology which are:

- 1) The viscosity of the blend is too high and must be reduced.
- 2) The self-sensing plies are inconsistent and the tracks require optimisation.

These aims will be achieved by covering the following objectives:

- 1) The analysis of current system performance, including an assessment of the effectiveness of the resin to recover mechanical properties, predominantly fracture toughness. The mechanical performance which has already been published must be correlated with characteristics for ease of manufacture, most importantly rheological

profile.

2) The formulation of new resin blends with reduced viscosity. It will be important to document the knock-down in healing performance associated with each route.

3) The manufacture of the flexible circuit boards must be assessed. The width of the tracks is thought to be key to providing heating actuation to the damage zone. Different manufacturing techniques should be explored to improve this process.

For the resin system, it is hoped to reduce the viscosity of the overall resin while maintaining or improving self-healing performance. It is likely to be the case that ideal healing ability may be achieved through the correct calculation of the optimum combination of resin, curing agent, diluents and healing polymer molecular weights. Previous results have supported this hypothesis so far and it shall be an important part of this investigation to provide evidence for this. Other elements of the manufacturing route include development of the sensors, connectors, flexible circuit boards, layup and ply inclusions which will be investigated.

2 Literature Review

2.1 Composites

Composite materials are materials made from two or more distinct constituent phases, generally with significantly different physical or chemical properties. This enables the net or macroscopic properties of the material to be enhanced, often gaining beneficial properties and losing detrimental ones. This enables engineers to combine materials with a specific weakness with a second phase to counteract the effect. An example of this is one of the most common types of composite, carbon-fibre polymer-matrix composites. Both combine the extremely high tensile strength inherent to brittle fibres with a polymer ‘matrix’ to provide cohesion and some geometric and compression strength.

To improve the performance of advanced aerospace composites, much research has been done on the individual phases which can be tested and compared for their intrinsic properties, and the interactions between the different combinations. There are many different types of fibre, even in the specialised area of carbon fibres, and thousands of different resin systems, which can be used in combination with a huge range of curing agents. Once additives, diluents and fillers have been considered, it becomes clear that the selection of these parameters for the best material for a specific application must be the subject of a long-term research initiative.

2.2 Composite Design Limitations

Although composite materials have displayed improved ballistic protection against projectile damage over metal equivalents with respect to weight, the failure characteristics of composites are far more complex and to some extent misunderstood. It was argued by Hogg [24] that even in the field of composite armour the development of new systems depends largely on experience, empiricism, and intuition,

and it has been reported by the Federal Aviation Authority (FAA) that the most trusted sources of information for design of new sandwich structures by Boeing and Sikorsky are empirically based [25]. Due to the lack of in-depth knowledge of the structural effects of impact damage, the allowable strain is limited to 0.3-0.4% [29], despite the fact that allowing a strain of 0.6% would provide significant weight savings and material exploitation. It has been reported that most commercially available carbon-fibres have a failure strain of 0.5-2.4% [30] and that an improvement in damage tolerance could allow for a 50% increase in the current 0.4% strain limit while maintaining a conservative safety factor [31]. Strain allowables in composite structures are a useful way of determining safe operating regions for different load bearing areas within a composite structure. They are usually calculated from tensile and compression tests as these are dominated by the carbon fibre and the resin properties respectively.

2.3 Damage Tolerant Design

To provide materials with greater allowable strains a composite system must be designed to be resistant to damage. This can be achieved through several different mechanisms. Unlike metallic materials which exhibit only two major failure modes, brittle and ductile, composites have many more which can be used to their advantage. Impact damage can be distributed to matrix cracking and other modes which often do not affect the integrity of the structure. However this makes damage detection even more difficult. Damage in metallic materials starts at the impacted surface, in contrast to composites in which it often begins on non-impacted surfaces [30], or in the form of internal delamination, matrix cracking, fibre pull-out or a number of other mechanisms. It is important to note that in addition to the compromise of many mechanical and structural properties of the material, cracking provides initiation sites for moisture absorption and swelling which can further degrade properties [32]. There is much concern that composites can rapidly deteri-

orate in strength due to so-called Barely-Visible Impact Damage (BVID) which is very difficult to detect [30, 33, 34, 35], as suggested by its name. It is stated by the FAA in the US that “defects that are not detectable during manufacturing inspections and service inspections must withstand [the] ultimate load and not impair operation of the aircraft for its lifetime, in this region it is assumed that the damage may never be discovered during the aircraft’s lifetime and must support ultimate design load” [25]. By this definition it can be seen that without improvement brittle-matrix composites would be difficult to use and improvements are required if polymer-matrix composites are to supercede metallics for primary structures, as defects in brittle matrix composites can generally not withstand small defects in the same way as metallics, and are much more difficult to detect.

In order to solve the problem of damage detection and to improve the damage tolerance of composite systems several solutions have been developed. One solution to this lack of damage tolerance of composites is a concept where the materials are able to heal in a biomimetic approach taken from the natural world. There are many other concepts which can be designed into structures or extra technologies added to them which can make composites more able to tolerate a certain amount of damage. These methods include approaches such as thermoplastic toughening[26], z-pinning[27] and damage deflection[28], which all mitigate the effects of damage.

2.4 Self-healing Technologies

A novel material design concept was conceived whereby the material heals itself through active or passive means to restore strength from areas affected by impact damage, originally proposed by Dry for the repair of cracks in concrete with a methyl methacrylate resin [37, 38]. This gave rise to a group of innovative materials known collectively as ‘self-healing’ materials, due to their biomimetic functionality [36]. However the methods employed to achieve this functionality have been widely varied. Many excellent reviews are available on the topic of self-healing materials

[39, 45, 46, 40, 41, 42, 43, 44, 83, 47, 36, 52], and only work which provides specific detail related to the direction of the current research will be presented here.

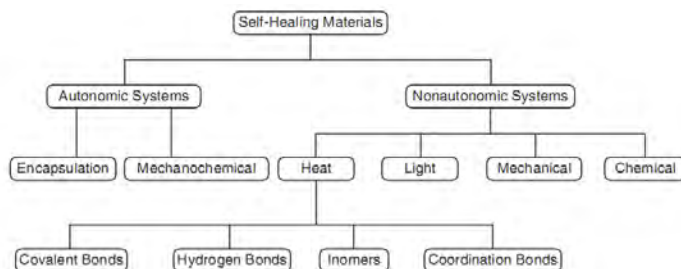


Figure 3: Classification of self-healing materials into Autonomic and Non-autonomic systems [47].

As shown in Figure 3, methods fall into two main categories: Autonomous and Nonautonomous systems, of which the dominating solutions are ‘Liquid-resin delivery systems’ and ‘Modified matrix systems’ respectively. The most common systems will therefore be investigated, with a primary focus on the relative benefits and obstacles for each solution. Resin delivery methods are reviewed first, followed by a critical analysis and a brief treatment of the solid-state system.

2.4.1 Hollow-fibre method

Bond et al. [48] have developed a system to use hollow glass fibres to deliver uncured resin into cracks that occur through the material as a result of impact. The resin then either mixes with a liquid catalyst or curing agent from another ruptured vessel, or comes into contact with a solid catalyst dispersed within the matrix in a similar manner to the microcapsule method described below. This original method of self-healing was developed from Dry’s initial work with concrete composites[38]. A Scanning Electron Microscope (SEM) image of fractured ‘hollow’ glass fibres containing unreacted resin can be seen in Figure 4.

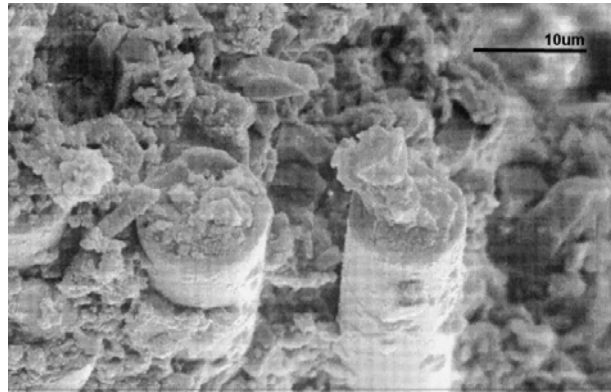


Figure 4: SEM of fractured glass fibres containing uncured repair resin [49].

Similar work by Motuku et al. [50] used two different two-part epoxy resin systems as shown in Figure 4. Epon 862 is a Bis-F based system and was cured with Epicure 9550, an aliphatic amine. VE C50 is a Bis-A based resin and was cured with cobalt naphthenate (CoNap) promoter and 2,4 pentanedione (acetyl acetone) gel time retarder. The two-part system was used as these systems retain a lower viscosity until cured, which allows for a longer shelf life and for faster filling of the narrow hollow glass fibres.

This approach can provide large benefits when fracture surfaces are not aligned, as the material may still regain significant strength. However, the inclusion of non-structural fibres may cause a reduction in mechanical properties, particularly where the glass fibre healing system is incorporated by the inclusion of a discrete glass-fibre reinforced plastic (GFRP) ply within a carbon-fibre (CFRP) laminate. If the fibres are included in the ply with structural fibres, there tends to be a large diameter difference between them, which can cause deleterious effects. In order to reduce the problem of fibre-diameter mismatch, Bleay et al. report the use of extremely thin hollow fibres for self-healing [51]. With extremely thin fibres it is necessary to dilute the resin with up to 40% acetone in order to improve processability, even with a specially developed vacuum-assisted capillary filling technique [52].

2.4.2 Microcapsule Method

Another approach similar to this is to embed microcapsules containing either epoxy monomer [53] or solvent [60, 59] or a mixture of both into an epoxy matrix to provide healing resin in the event of damage. White [53] has shown this to be an effective healing system, reportedly now capable of complete recovery of fracture toughness after crack propagation with non-toxic solvents. Capsules have been shown to rupture as a crack in the host matrix breaks them apart and releases the DCPD monomer, which is drawn into the crack plane by capillary action. When this monomer contacts the Grubbs' catalyst a ring-opening metathesis polymerisation (ROMP) reaction is initiated [54] which cures the monomer and rebonds the crack. Papers have reported a recovery of over 90% of fracture toughness [57] as well as delamination damage recovery using fibre composite specimens [55, 56].

In addition to providing an efficient mechanism for self-healing, the presence of DCPD-filled polymeric microcapsules also increased the inherent fracture toughness of the epoxy. Under monotonic loading the maximum toughness with microcapsules was 127% greater than neat epoxy [57]. The increased toughening associated with fluid-filled microcapsules was attributed to crack pinning along with increased hackle marking and subsurface microcracking. Brown et al. [58] also investigated the influence of microcapsules on fatigue crack propagation behavior of epoxy. The addition of microcapsules significantly decreased the fatigue crack-growth rate and increased the fatigue life [61].

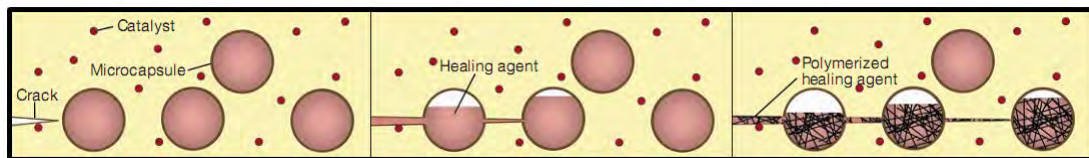


Figure 5: The microcapsule self-healing concept [32].

The resin system currently in use is a monomer healing agent of dicyclopentadiene (DCPD) and a chemical catalyst of Bis(tricyclohexylphosphine)benzylidene ruthe-

niium (IV) dichloride (Grubbs' catalyst [62]) as the healing trigger as shown in Figure 6. DCPD is a low viscosity monomer commercially produced from petrochemicals and is relatively inexpensive. However, it is important to notice that the Grubbs catalyst is both expensive and contains potentially toxic heavy metals which would require careful manufacturing processes and efficient use to reduce costs and fulfil the recent guidelines for green chemistry [63].

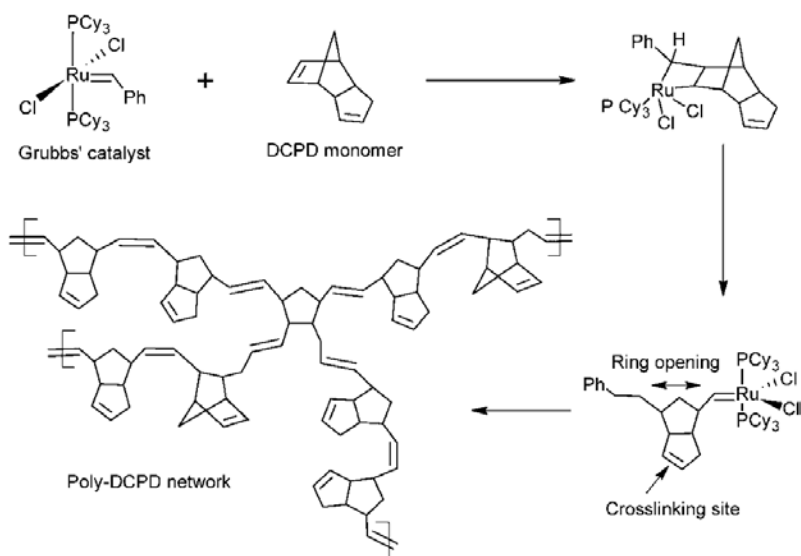


Figure 6: Mechanism of DCPD ring-opening metathesis polymerisation (ROMP) reaction with Grubbs' catalyst [64].

Another obstacle for liquid resin delivery systems is that the vessels must not rupture during the manufacturing process in order to keep their functionality, and survival of these microcapsules during large-scale manufacturing has yet to be demonstrated. As with the previous solution, these methods rely on the crack developing through the container of uncured resin, be it capsule or hollow fibre, in order to impart healing (Figure 5).

2.4.3 Vascular Method

Self-healing polymers composed of microencapsulated healing agents exhibit remarkable mechanical performance and regenerative ability, but are limited to autonomous

repair of a single damage event in a given location. Self-healing is triggered by crack-induced rupture of the embedded capsules; thus, once a localized region is depleted of healing agent, further repair is precluded. A biomimetic approach is to adopt a system used commonly in nature to recreate a circulatory system which can supply large quantities of repair material to an affected site which allows for, in theory, infinite healing cycles [65, 66, 67, 68]. Using a vascular method, a self-healing system capable of autonomously repairing repeated damage events has been reported [69]. The coating-substrate design delivers healing agent to cracks in a polymer coating via a three-dimensional microvascular network embedded in the substrate as shown in Figure 7.

Toohey et al. [71] reported a self-healing architecture in which three-dimensional microvascular network capable of repeated healing performance was proposed. In this system, a microvascular network within the epoxy resin is embedded by direct-write assembly of a fugitive organic ink. When a crack is formed in the coating the microvascular network in the substrate supplies the healing agent (DCPD) to the crack [72]. Using the same chemistry described in Figure 6, the DCPD in the network has sufficiently low viscosity to allow a significant amount of resin to be drawn into the crack, and the Grubbs' catalyst which is dispersed in the coating enables damage in the epoxy coating to be healed repeatedly with a well-crosslinked resin [70]. After resting for 48 h at room temperature, 70% of peak recovery was recorded with a repeated healing of up to seven four-point bend fracture-heal cycles. However, beyond this point, healing ceases due to depletion of catalyst in the crack plane.

To overcome this limitation, the vascular system was improved [73] by using two independent vascular networks within the matrix polymer to supply two monomers of a two-part epoxy to the damaged site. By infilling the networks with a photocurable resin and selectively photopolymerizing thin parallel sections of these resin-filled microchannels, isolated networks are produced. These microvascular networks can

independently house different healing agents until a crack forms in the coating. In this work, healing efficiencies of over 60% was achieved for up to 16 intermittent healing cycles of a single crack.

These systems however do not lend themselves to mass production, and it has not yet been demonstrated that large scale production of microvascular networked substrate material can be economical.

The successful implementation of this technology could substantially enhance the integrity, reliability and robustness of composite structures, whilst offering benefits through reduced operational costs and extended lifetimes. However, establishing the benefits of such novel systems to existing design criteria is challenging, suggesting that bespoke design tools will be required to fully attain the potential benefits of self-healing technologies.

As it stands, the above findings do not justify the incorporation of self-healing in real-life structural, safety critical components as they are currently designed. However, the results strongly suggest that fast, reliable, repeated self-healing can offer a step-change in material performance, thereby justifying the investment required to evaluate such systems beyond the coupon level, and to develop tailored healing chemistries [74].

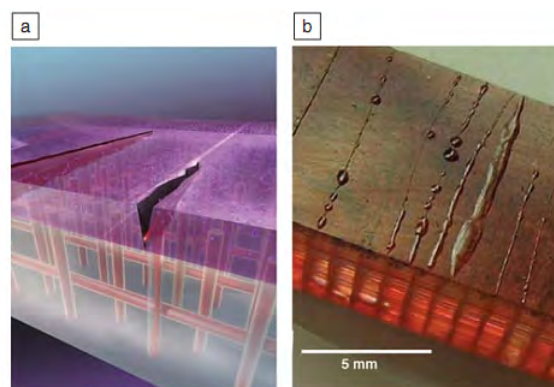


Figure 7: Microvascular-based healing of polymers: (a) microchannels in the substrate contain a supply of healing agent (red) fill surface cracks with self-healing resin(purple), (b) excess healing agent (dicyclopentadiene, DCPD) released on the surface of the sample after transverse cracks were healed [76].

2.4.4 Epoxy Particulate System

Zako et al. [75] investigated an epoxy ‘particulate’ system which is akin to the microcapsule method. Epoxy-based adhesive particles, Toa-Gosei AP-700, are mixed into a coldsetting epoxy matrix. When damage occurs, these particles cause a healing action on the application of heat, by melting and then adhering surfaces of the crack together. Information available about this method is limited possibly due to commercial involvement. This system sees many benefits; including an inexpensive and simple manufacturing route, and effective healing at least from a visual inspection standpoint. This method does require external heating, as with most other self-healing methods, and will likely suffer from an inability to repeatedly heal damage which reoccurs in the same area. Although it is quoted that “the embedded epoxy particles do not deteriorate the stiffness by comparison with a specimen without particles,” it is not clear what the virgin mechanical properties of this resin system are.

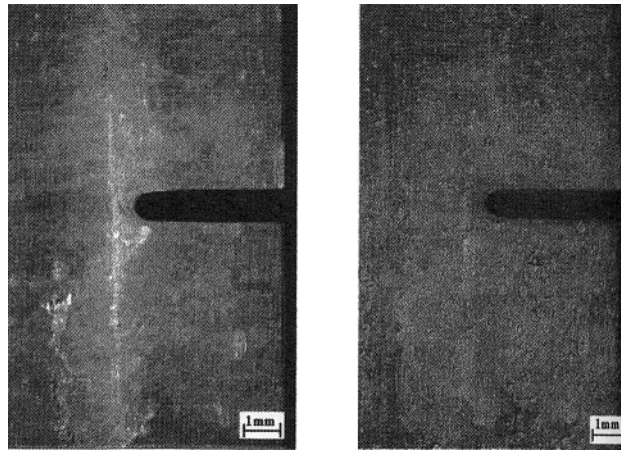


Figure 8: Micrograph of matrix tensile fatigue damage before(left) and after(right) a repair cycle [75].

2.4.5 Limitations of Resin Delivery Systems

Most of the methods discussed so far fit into a category which can broadly be defined as ‘liquid resin delivery’ systems as all the varieties of this method require

the addition of new unreacted resin material to fill cracks which have developed. Although these approaches need no manual intervention in order to repair, a feature which excludes them from being defined as truly 'smart' materials, they remain limited by their inherent design.

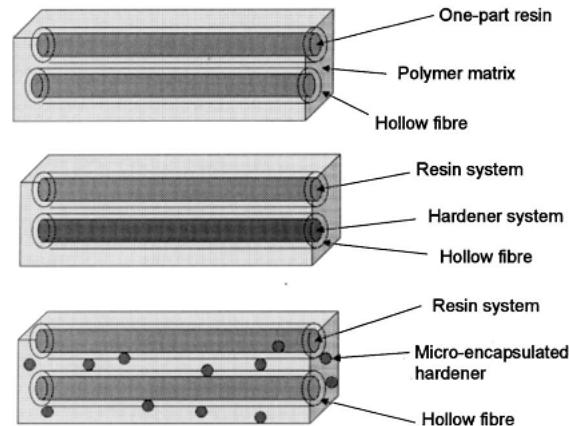


Figure 9: Different types of hollow-fibre resin delivery systems [49].

A vessel of liquid resin must be incorporated into the composite material, and must fracture at the same time as the matrix, when either hollow-fibres or microcapsules are employed, and yet these vessels must be of sufficient strength to survive the manufacturing and processing procedures without fracture, a problem which has not been adequately addressed, nor a solution proposed or demonstrated in the published literature. It is also important that the vessels do not provide a stress concentration in the material, and to notice that larger structures have generally lower strengths than small coupons, and that scaling effects in these composites may require vessels to be prohibitively dominating [77].

As there is no intelligent or control system in place as with a smart system, there is no external knowledge of damage within the material, which is an important limiting factor for these technologies as they require extensive continued use of current non-destructive testing (NDT) techniques in order to detect damaged panels which would need replacing. A further refinement is to include UV fluorescent additives within the healing polymer which can enable damage to be more easily located, particularly

in Barely-Visible Impact Damage (BVID) detection [78]. Images of this type of NDT being used can be seen in Figure 10, with damage being shown as luminous under ultra-violet light, and therefore cracks and even subsurface damage can be detected.

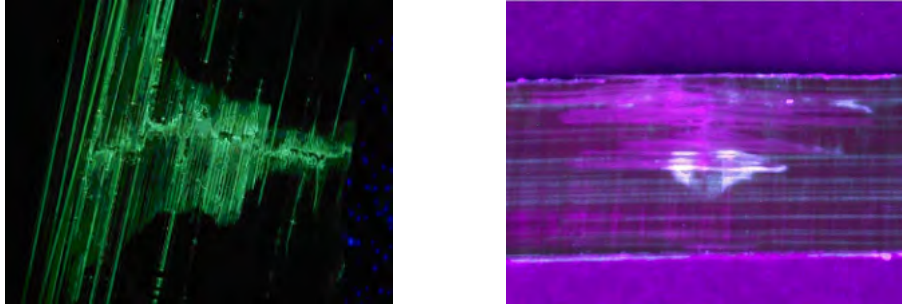


Figure 10: Damaged samples showing bleeding of UV-fluorescent dye at 45x magnification [79].

It has been reported by Kessler [80] that the unimpacted toughness of the composite decreases slightly when an unintended catalyst cluster is found in the matrix which can cause stress concentration. These clusters therefore contribute to unstable crack propagation, one of the main reasons to avoid composite materials entirely due to its unpredictability. It has also been reported that voids left after the healing of a crack by thermoplastic particles have an erratic effect on the integrity of the healed specimen [81]. Bond [82] has recently demonstrated an alleviation of the problem of unstable crack propagation by the judicious introduction of toughening agents into certain regions.

As all resin delivery methods require the deposition of resin to a damage site, there are difficulties in providing both adequate quantities to a specific site, and in delivery to a repeat fracture in the same location, a not uncommon presentation. Hollow glass fibres have been used most for their good combination of storage and mechanical performance but the liquid resin and therefore the healing capacity of the fibres is limited, and there is no possibility of knowing when resin reserves in a particular area are depleted.

Microcapsules have similar problems in that their size must be extremely limited in order to avoid distorting the host matrix. This creates problems for adequate resin

delivery by this method.

2.4.6 Remendable Polymers

Another class of self-healing polymeric materials may be known by the collective term 'remendable polymers'. These materials, although not directly related to aerospace composites yet, are in themselves worthy of academic note. In general these materials exploit reversible polymerisation reactions, whose reactions are catalysed by a variety of methods. Often this results in experimental data supporting extremely impressive healing capability, but with either unfavourable commercial economics or inadequate virgin thermomechanical properties for widespread application.

Externally mendable polymers are those upon crack formation stay in their failed state until healed by external intervention [83]. This can be in the form of thermo-, photo- or chemical-induced healing.

Thermally Induced Healing

Diels-Alder The Diels-Alder reaction is a cycloaddition reaction between a conjugated diene and a substituted alkene [84]. This is an important reaction for remendable polymers as it is often thermally decomposable, the reverse reaction being termed retro-Diels-Alder. Even though a large amount of literature has been published on the subject of Diels-Alder reactions and their mechanisms, their use in self-healing has only recently been demonstrated.

The first system used was that shown in Figure 11 where a tris-maleimide (3M) and tetra-furan (4F) react to form a DA-step growth polymer (3M4F) which was subject to repeated healing cycles and its structural changes monitored by solid-state ^{13}C NMR spectroscopy [85].

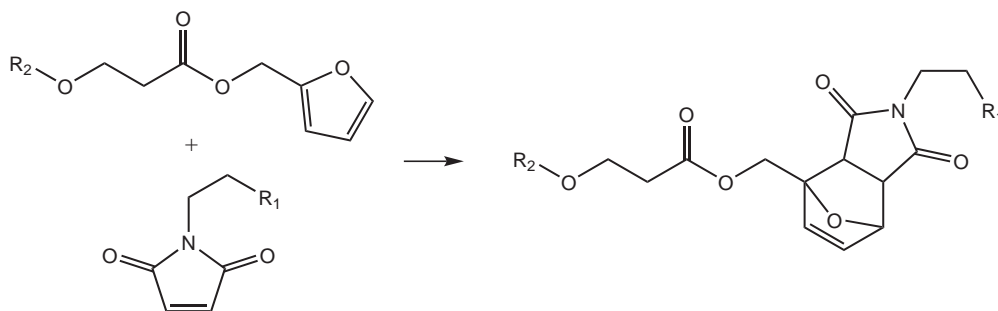


Figure 11: Maleimide and furan react to form a DA-step growth polymer.

Dipolar Bonds Dipolar or coordination bonding supplies another heat-activated solution to self-healing, which can be either autonomous or non-autonomous depending on the application. A novel class of materials were conceived which are electrically conductive self-healing polymers. These materials can be used to both self-monitor and heal simultaneously, as a constant current flow can both health-monitor and, in the event of crack developing, the resulting increase in resistance will cause targeted heating of the affected zone, causing a healing-activated repolymerisation.

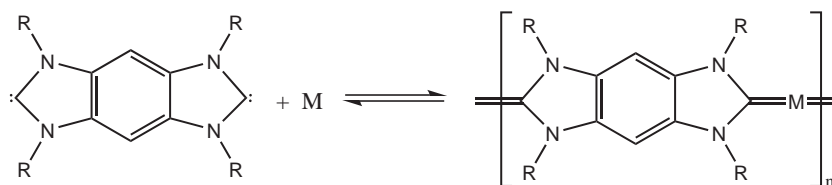


Figure 12: A dynamic equilibrium between a monomer species (left) and an organometallic polymer (right) that is controlled via an external stimulus such as heat [89].

Although an impressive range of dynamic polymerisations are known, the fundamental reversible reactions involved do not meet the conductivity requirement. One exception are complexes formed between N-heterocyclic carbenes (NHCs) and transition metals. These are not only known to form reversibly with tunable equilibrium constants, but also their electronic communications within these systems are well studied (Lewis et al. 2003; Scott & Nolan 2005)

Photo-induced Polymerisation

Photodimerisation There have been several studies of reversible photo-induced cross-linking of polymer networks based on photo-dimerisation of anthracene (Figure 13), sulfides and benzopyranones. Chung has shown that highly crosslinked structures may be produced and subsequently healed by photodimerisation using light of wavelength greater than 280nm [87]. Although doubts have been expressed [86] about the flexural strength measurements of the healed samples, insufficient data is available to draw conclusions about the long-term viability of this approach.

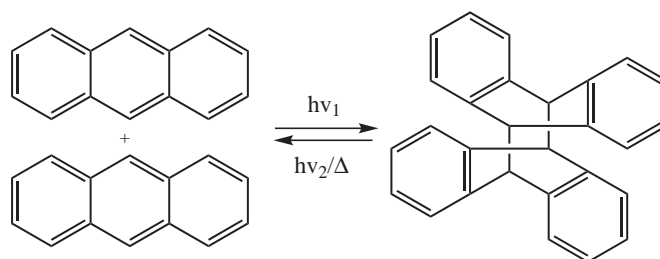


Figure 13: Photo-dimerisation of anthracene using UV light

Thiol-chain Transfer Another method in the area of photo-polymerisation is based on thiol-ene chemistry, lead by Bowman [88]. This method utilises addition-fragmentation chain transfer of mid-chain functional groups in order to induce plasticity, healing and will remove residual stresses.

2.4.7 Thermoplastic Healing Agents

Wool et al. [41] systematically studied the theory of crack healing in thermoplastic polymeric material and can be summarised through five phases of crack healing:

- (i) surface rearrangement, which affects initial diffusion function;
- (ii) surface approach, related to the time-dependent contact of the different parts of the surfaces to create the interface;
- (iii) wetting, to wet and form an interface and continue healing
- (iv) diffusion, the main factor that controls recovery of mechanical properties; and

(v) randomization, ensuring disappearance of cracking interface

which led to the development of a model [91] of strength recovery by diffusion in polymer crack interfaces known as the “Reptation Model”, originally proposed by de Gennes [92]. This model states that a polymer chain can be thought of as moving through the structure like a snake with intermolecular interactions with neighbouring polymer chains, known as entanglement couplings. Strength is gained across and interface by these chains randomly ‘walking’ across a polymer weld line and forming new entanglements with polymer chains on opposing sides of the weld [93]. This process of random ‘walking’ through the polymer structure is known as reptation [94]. This model is time and temperature dependant.

Solid-State Method A final approach which is the subject of this study is to use a solid-state method for healing whereby the composite recovers its strength by the reformation of bonds within the matrix by the application of heat to a damaged area [95]. Thus no volume is lost to unreacted resins, catalysts or other healing agents and therefore mechanical performance is maximised. This method employs a thermosetting resin, into which a linear polymer is dissolved, providing rehealable functionality similar to conventional thermoplastic resin systems.

The healing agent for solid state healing should have the following properties in order that it provide effective healing [96]:

1. The healing agent should be reversibly bonded to the cross-linked network of the cured epoxy resin through intermolecular bonds such as hydrogen.
2. The healing agent should be mobile above the minimum healing temperature to induce diffusional bridging of a crack and provide recovery of strength.
3. The addition of the linear chain molecule should not significantly reduce the thermomechanical properties of the original resin.

The solid-state healing chemistry is currently provided by a blend of a commonly used epoxy-based thermoset resin, its curing agent and a thermoforming polymer to provide the healable properties.

Work on this method first investigated the qualitative effects of the blend on the healability of impact damage in fibre reinforced composites[97]. The blend used 20 wt% of the healing agent but it was shown that much lower healing agents could be used in the future. Initial results showed the reduction of damage area visible on photographs of impact sites by approximately 30%, and it was thought that matrix cracking was entirely eliminated.

Further work determined that an optimum concentration of 7.5 wt% healing agent was effective in significant healing of impact damage across multiple healing cycles[96]. A smart system was identified in this paper for using the carbon fibre which would make up the final composite as both a damage sensor and heat source for the healing actuation. It was also demonstrated that the testing methodology for healability of resins needed to be defined more precisely in future to allow more precise and quantitative assessment of the technology.

Work on the solid state method then looked to a new method of healing assessment and began using compact tension testing to evaluate the recovery of fracture toughness after a damage event[98]. Results were extremely good, with recovery showing up to 70% and a much more reliable method for quantitative assessment. Self sensing was also introduced to demonstrate the potential for a fully 'smart' system.

Work more recently has focussed on the mechanism of healing[133]. Further investigation into the basic science of the healing method revealed that at higher concentrations of the healing agent a phase separation occurs which has a dramatic effect on the healability of the resin.

2.5 Rheological Studies

Before curing, resins generally are composed of low viscosity liquid polymers comprising elements such as the epoxy prepolymer, curing agent, additives, catalysts etc. During the cure the solution goes through several states between a blend to a fully cured resin.

Rheology is the study of flow of liquids or solids under conditions in which they flow rather than deform elastically. In polymer science the rheological properties are important as they relate closely to the morphology, just as the mechanical properties describe the morphology of solids. This dependence of the rheological properties on melt morphology has been demonstrated quite comprehensively by Han [100, 102, 101].

Rheological studies have been done on blends of epoxy with a variety of thermoplastics. Epoxy toughened with Polyether Sulphone (PES) has been studied extensively using rheometry because it has a variety of structural transitions during cure, due to phase separations and cross-linking reactions [103]. Kim and Char used rheology to measure fluctuations in epoxy/PES curing reactions, and attributed this anomaly to the movement of thermoplastic into phase-separated domains [104]. Small-angle and time-resolved light scattering techniques (SALS and TLS) have also been used to investigate this process [104, 105].

During the first stage of the cure, the liquid reacts into a gel. This is known as the gelation process and means the thermoset can no longer be processed as a liquid. Low molecular weight molecules can however continue to reach reaction sites through diffusion, which will continue until the reaction proceeds to the next stage. When the glass transition temperature (T_g) of the reactive system becomes equal to the curing temperature the resin will undergo vitrification. This is the transformation from an elastic gel into a glassy solid state. This will cause the cure to slow and finally stop because molecular mobility is extensively reduced. Although this polymer is

now described as ‘cured’, the cure is not complete, as there will still be unreacted polymers locked within the structure which are unable to reach a reaction site. This is often the reason for a ‘post-cure’ processing stage, to reheat the partially cured thermoset above its T_g to allow unreacted molecules to be involved in further cure. Thermosetting polymers are used in a wide variety of applications as discussed mostly due to their intrinsic good mechanical properties. In an effort to further improve these properties, particularly the low fracture toughness, much work has been done on trying to modify thermoset polymers with thermoplastic additives. This approach has been achieved by incorporating a liquid rubber, such as CTBN (carboxyl-terminated butadiene acrylonitrile) into epoxy [107]. However it was shown that this is not an effective toughening agent for epoxy thermosets with a high crosslink density. As an improvement to this, Ratna used CTPEHA (carboxyl-terminated poly(2-ethylhexyl acrylate)) which is another liquid rubber but one which does not introduce double bonds which can provide sites for oxidation [108]. As a further improvement, instead of liquid rubber, thermoplastic additives were used such as PES and polycarbonate which were found to be much more effective [109].

2.6 Self-sensing

Most structural health monitoring (SHM) systems make use of embedded sensors within a structure to detect changes in its state or properties. Information can be gathered about the temperature, pressure, strain condition, damage, shock etc depending on what type of sensor system is used, and what data is to be gained. There are many types of extrinsic sensors, including electronic, such as a thermistor, electromechanical, eg. piezoelectrics, optical, eg fibre-bragg gratings (FBGs) etc.

Self-sensing materials are those which can monitor the strain or damage inside themselves without the need for additional sensing elements. Information may be gathered about damage inside the composite laminate which has been distributed throughout the volume including delamination, matrix cracking or fibre pullout. This

may be monitored by the measurement of intrinsic properties. Smart materials can also monitor damage with the use of sensors such as piezoelectrics, optical fibres, strain gauges or acoustic sensors. Self-sensing materials have several advantages including scalability, lower cost, lower complexity and large sensing volumes.

One method of self-sensing in carbon-fibre reinforced polymer (CFRP) composites is by monitoring the resistance down the carbon fibres. As the carbon fibres are low resistance, but the polymer matrix is insulating, any movement in the fibres which affects the conduction pathways will result in a change of resistance across the panel. These changes may be due to strain in the panel, or to damage.

This type of structural health monitoring has been proposed and used by Todoroki [110], Abry [111], Irving [112], Chung [113] and Hou [114]. The attachment of contacts to the carbon fibres at the edges of the panel however remains a problem for manufacture. This problem has been solved by several different methods by the groups investigating. This may be done by co-curing of the contacts into the structure [110], by electroplating of the fibres to create a contact point [115], by electrolytic deposition of a conducting medium onto the fibres [111] or by the application of a conducting adhesive [116].

All of the methods for attaching contacts to a panel leave these delicate points exposed at the edges. As such these contacts are vulnerable to damage or chemical degradation. The resistance of the connection between the carbon fibres and the electronic sensing circuitry is of the highest importance for sensitive resistive measurement, as the carbon fibres are very low resistance and this contact will dominate the signal. Slight changes to this signal caused by the changing resistance of the contacts due to chemical decomposition, or galvanic corrosion from the fibres, or any other sort of damage may have a dramatic effect on the perceived damage within the laminate as recorded by the sensing hardware [117, 118]. If the contacts are attached to the laminate after manufacture they can only be placed on either surface ply, or connected across all the plies of the layup. Both of these methods have significant

problems when it comes to triangulating damage. The advantage of this approach, however, is that the contacts need not be incorporated during the manufacturing stages and may be added later which makes an overall sense and heal system much easier to implement. Alternatively the contacts may be cured into the laminate which allows them some physical protection, better electrical contact with the fibres and most importantly it allows individual plies to be selected for sensing.

2.7 Summary

There are currently many solutions to the problem of damage tolerance in polymer-matrix composites. While some resin delivery systems have weakness as outlined, they provide an extremely competitive solution which is cost-effective and nearing trial or in some cases in production implementation[121]. They can often provide self-healing ability tailored to specific damage types or impact levels, but by simply adding self-healing functionality to a conventionally designed laminate that has already been optimised for damage tolerance is unlikely to yield any appreciable enhancement in performance or weight saving [74].

The solid state technology has reached a level which suggests a potential for commercial application. In order for this technology to move forward to this stage there are a number of barriers particularly with regard to manufacturing. The self-healing resins must be developed further. In reference to the specific objectives laid out in Section 1.2 on page 16, it is required that the viscosity must be lowered for almost any manufacturing process.

Self-sensing techniques have been discussed for structural health monitoring of carbon fibre composites. The scalability and cost-effectiveness of intrinsic self-sensing as opposed to embedded extrinsic sensors are considered the drivers towards this type of technology as long as the manufacturing challenges can be overcome and the cost benefit is demonstrated. There have been many approaches taken to solve the high electrical resistance associated with the contacts in the resistive damage sens-

ing system. The studies have outlined why it is an important barrier for the system that the manufacturing problems must be solved as this has a profound influence on the resolution and sensitivity of the system.

It is important to note that each healing solution lends itself to particular applications, and that an expansive market such as that of self-healing materials has areas that have different demands on their cost, healable volume, ease of implementation, parasitic weight and functionality of any self-healing solution. It is believed that there is an area of applications for the solid-state method which is inadequately addressed by any other method, and that if it proves possible to optimised this technology it will be worthwhile research for the materials of tomorrow.

It is clear from the published research that no self-healing solution has as yet yielded its full potential. Trials with multiple specimens have shown varying degrees of success, none of which have provided the statistical backing required to advance this technology to a level ready for design implementation in the aerospace sector. It is therefore an aim of the current study to provide additional evidence of the benefits of the solid state self-healing technology over current engineering solutions.

3 Experimental

All experimental procedures used for this research are presented in this chapter, including materials selection and the types of specimens used for the mechanical tests. Compact tension testing was used to measure the healing efficiency of resin samples. Tensile testing was used to measure the ultimate tensile stress of resin specimens to compare mechanical properties. Rheology was used to measure the viscosity of previous formulations and to help develop new ones, and also to monitor the cure of some example reactions.

3.1 Introduction to Epoxy Resins

Epoxy resins are a large and very versatile group of polymeric materials, all of which make use of the functional group known as the epoxy ring, from which this class of materials get their name. Its properties and reaction mechanism with various curing agents have been reported extensively [122]. This is an extremely important functional group, as it contains a high energy carbon/oxygen ring (the epoxy ring), which is extremely susceptible to nucleophilic attack, which causes a ‘ring opening’ reaction. The structure of the functional group can be seen in Figure 14, and while the epoxypropane structure shown is the most basic type of epoxy, the terminal methyl can be any organic chain or moiety which may have its own chemical or bonding properties.

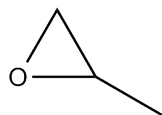


Figure 14: Structure of epoxypropane, a basic epoxy, with epoxy ring.

A common non-IUPAC nomenclature convention is to use the prefix ‘glycidyl’ when naming epoxy compounds, which will become noticeable during the discussion of common systems.

3.2 Epoxy Resin Systems

3.2.1 Bisphenol-A Resins

Bisphenol-A was first created by condensation of acetone (hence the suffix A) with two molar equivalents of phenol[12]. It is a more complex structure than bisphenol-F but its processing route is cheaper and easier and has therefore become most widely used.

The reaction of bisphenol-A diglycidyl ether from its constituents, epichlorohydrin and bisphenol A, is shown in Figure 15. The form shown is only the simplest example, in reality the reaction may be controlled to yield products of extremely varied molecular weight, which have a wide variety of physical attributes, ranging from low viscosity liquids to dense solids.

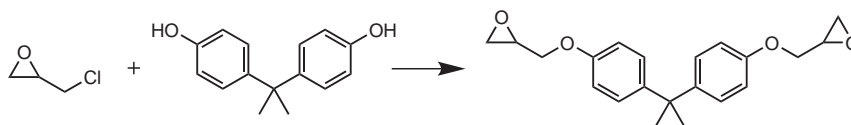


Figure 15: Reaction of epichlorohydrin and bisphenol A to form bisphenol-A diglycidyl ether.

The structure of these higher weight species can be seen in Figure 16, where n can range in value from 0 to 12. An 'n' value of 0 produces the structure seen on the right of Figure 15, which is the lightest species possible.

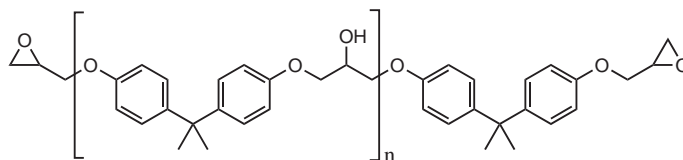


Figure 16: Structure of bisphenol A diglycidyl ether epoxy resin.

3.2.2 Bisphenol-F Resins

Bisphenol-F is the simplest novolac, which are now known as phenol formaldehyde resins, and is created by reacting formaldehyde (hence the suffix F) with a large

excess of phenol under acidic conditions. Although it is the simplest, Bisphenol-F is also the most difficult to obtain due to its propensity to undergo oligomerisation to higher MW species [13]. Epoxy resins based on Bisphenol-F, in other words diglycidyl ethers of bisphenol-F (DGEBF), tend to be more expensive due to processing costs but can provide improved mechanical and chemical properties compared to those of their bisphenol-A equivalents. In reality, many declared DGEBF resins contain detectable amounts of DGEBA resin due to the difficulty in its processing [14].

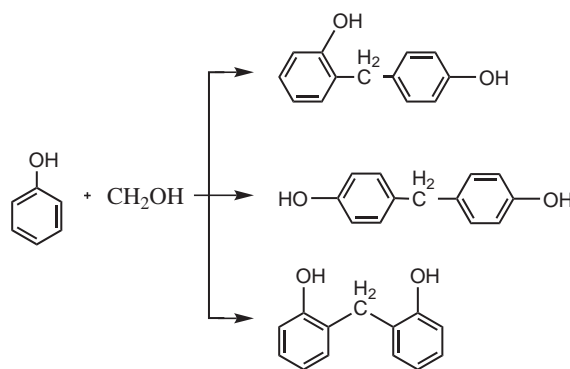


Figure 17: Reaction of phenol and formaldehyde into the isomers of bisphenol-F [13].

3.2.3 Curing Agents

For a curing reaction to take place, the epoxy species must react with a hardener, normally amine-based curing agents. For the reaction and mechanisms of the reaction of epoxy resins with amine-based curing agents, refer to Appendix A. Table 1 lists a range of commonly used amine curing agents for use with epoxy systems. Each has its own characteristics and therefore lends itself to specific applications, which are also listed.

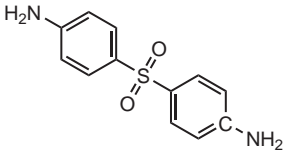
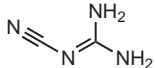
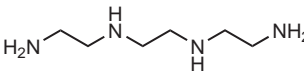
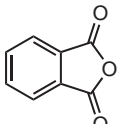
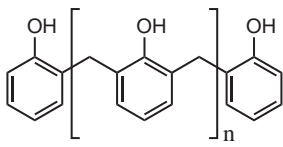
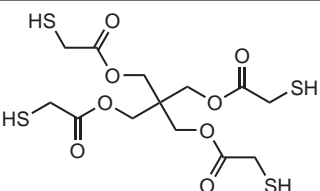
Agent Type	Example Structure	Chemical Name	Typical Uses
Aromatic amines and cycloaliphatic amines		4,4 diaminodiphenylsulphone	Coatings, adhesives and composites.
Dicyandiamide		2 cyanoguanidine	PCBs, composites and adhesives.
Aliphatic amines		triethylenetetramine	Flooring, paints, adhesives and tooling compounds.
Acid anhydrides		phthalic anhydride	Electrical castings and coatings.
Phenol formaldehyde		phenol-novolac	Drum and can linings.
Thiol curing agents		pentaerythritol tetra (thioglycolate)	Fast-curing adhesives.

Table 1: Common epoxy curing agents [15].

3.3 Epoxy-Acid Anhydride Cure Chemistry

3.3.1 Uncatalysed Reaction

In the absence of acidic or basic catalysts, epoxide reacts with acid anhydrides to yield esters. The curing of the diglycidyl ethers of bisphenol A with acid anhydrides without a catalyst can be considered to be initiated by water, hydroxy or carboxy compounds contained in either reactant. For acid anhydride-epoxy reactions without a catalyst, Fisch and Hofmann [21] proposed the following reaction:

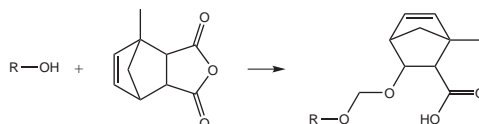


Figure 18: NMA reacts with a hydroxyl group to form a half acid ester.

The anhydride, in this case NMA, reacts with a hydroxyl group such as a secondary hydroxyl found in the higher homologs of DGEBA to generate the half acid ester.

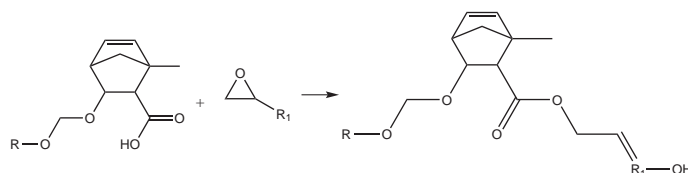


Figure 19: The new carboxyl reacts with epoxy to form hydroxy di-ester.

The newly formed carboxyl group reacts with an epoxy group to form a hydroxy di-ester. This new hydroxyl can react with the anhydride to form another carboxyl group and so on to give exclusively diester chains. However, Fisch and Hofmann found that in some anhydride cures the consumption of epoxy was greater than could be accounted for by the diester groups produced. On this basis they proposed a third reaction route between epoxy and hydroxyl groups, Figure 20.



Figure 20: Epoxy groups react with free hydroxyl.

3.3.2 Catalysed Reaction

Use of a tertiary amine in small quantities in the reaction gives more control over the route of the reaction, and initiates an alternating copolymerisation of epoxy and anhydride. The amine initiates the reaction by opening the acid anhydride ring which promotes electrophilic attack on the newly-charged oxygen.

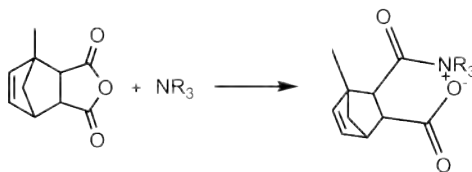


Figure 21: Initiation of reaction, NMA activated by the tertiary amine catalyst.

Once the curing agent is in this form, it reacts with an epoxy group from the resin to create a new species which can open the next curing agent molecule in the same way.

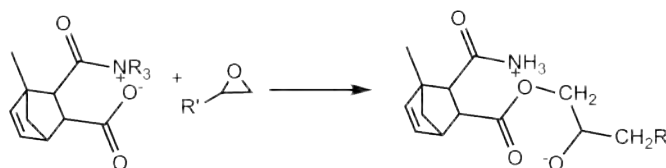


Figure 22: Epoxy group reacting with activated acid anhydride.

Thus the alternating copolymerisation structure is created, and this self-controlled reaction is said to contribute to the consistency of the cure and mechanical properties.

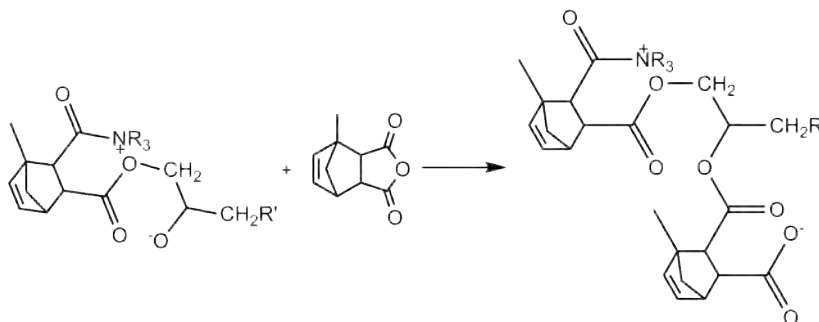


Figure 23: Continuation of reaction, opening second anhydride ring.

3.3.3 Calculating the Epoxy-Anhydride Equivalent Weight

During the uncatalysed reaction there are competing mechanisms, leading to some controversy in the literature. The possibility of epoxy reacting with either a hydroxyl groups in an etherification reaction (Figure 18), or with an anhydride in an esterification reaction (Figure 20), means that epoxy groups are consumed faster

than would be expected for just the curing-agent reaction. This leads to the ideal equivalents of anhydride to be 0.85 for ideal properties rather than the expected 1 [22] for uncatalysed reactions.

The literature mostly agrees that the catalysed reaction removes the likelihood of etherification, and therefore a stoichiometric mixture is recommended. This is confirmed by the testing done in the 1950s where it is remarked that “if the reaction goes to completion, the ratio reaches the exact value of unity within the experimental error of locating the maximum in the yield point-composition curves.” [23]

Calculations have been made in previous work [133] for solid state self-healing resins using an industrial formulation of this resin which was based on the 0.85 equivalents calculation, despite being an amine-catalysed reaction. This standard will continue to be adhered to in order to provide the most meaningful comparison with previous results and industrial formulations.

The equation used:

$$\text{WeightOfAnhydride} = \frac{\text{WeightOfEpoxy}}{\text{WeightPerEpoxy}} \times M_w^A \times \text{EquivalentsRatio} \quad (1)$$

Where: M_w^A is the molecular weight per anhydride.

The resin systems which have been used in the past are based on epon 828 which is a bisphenol-a epoxy resin. In order to achieve the main objectives of the project, further data is required about the handling properties of this resin, along with new aerospace-grade resins for particular applications or industrial procedures. The previous formulation was not ideal at high temperatures and had generally poorer mechanical performance compared to resins based on the T-GAP/TGDDM/DDS system.

As one of the main aims of this study (aim 1, objective 2, see Section 1.2 on page 16) is to reduce the viscosity of the overall resin while maintaining or improving self-healing performance, several routes must be examined for their mechanical proper-

ties to demonstrate which procedure is the most effective for achieving these aims. In the first instance, a lower molecular weight healing agent was used. Higher molecular weight variants of the same chemicals have by definition a higher viscosity. This method is likely to reduce the viscosity but possibly at the cost of ‘healability’, as shorter chains will have fewer entanglements and therefore will recover less strength. ‘Healability’ is used to refer to the effectiveness of the materials recovery of fracture toughness.

3.4 Preparation of chemicals

3.4.1 Healing Agents

The healing agent used in the past [95] was Phenoxy PKHB-100 from Inchem Corp. This was a bisphenol-A type resin with a molecular weight of approx. 25,000. The Phenoxy healing agent has been superseded by a similar bisphenol-A based chemical produced by Aldrich, poly(bisphenol-A-co-epichlorohydrin) which has been chosen for its compatibility with the host matrix. This chemical has a glass transition around 86 °C. This is shown in Figure 25. This is also a bisphenol-A but with a higher molecular weight, approximately 44000, and a lower polydispersity. Three different molecular weights of healing agents were procured for the study involving different chain lengths, but unfortunately the two lower molecular weight versions had a reactive epoxy end group.

3.4.2 End-cap Deactivation

The lower molecular weight healing agents which have been obtained from Sigma Aldrich have functional epoxide end groups. In order that they become mobile solid-state healing agents they must not covalently bond into the matrix. Therefore as chemical preparation the epoxide groups must be deactivated by reacting them with benzoic acid as detailed below, in a process which has become known as ‘end-

capping’. This, however, is a confused term in the literature, sometimes meaning a molecule has a reactive end group, and sometimes meaning the reactive group has been deactivated. For this reason, ‘end-capping’ as a term will be avoided where possible.

The chemical structures of the reactants are shown in Figure 24. The processes of deactivating the linear healing agent was based on a method by Oprea [134]:

Excess Benzoic Acid 20 g of PDGGBA (6100g/mol and 5 g of benzoic acid were stirred in 100 ml distilled water at 85 °C for 1 h. Another 50 ml of distilled water was added to the mixture before being filtered in a Buchner funnel. The sample was then crushed into powder and washed repeatedly with water at 70 °C before being dried under vacuum at 70 °C.

To create the self-healing resin, the new healing agents were then dissolved in the Epon 828 at 90 °C for approximately 24 hours as previously described. Once mixed with NMA and BDMA, the resin was cured at 90 °C for 4 h followed by a post cure at 150 °C for 2 h before cooling to 25 °C at 2 °C/min.

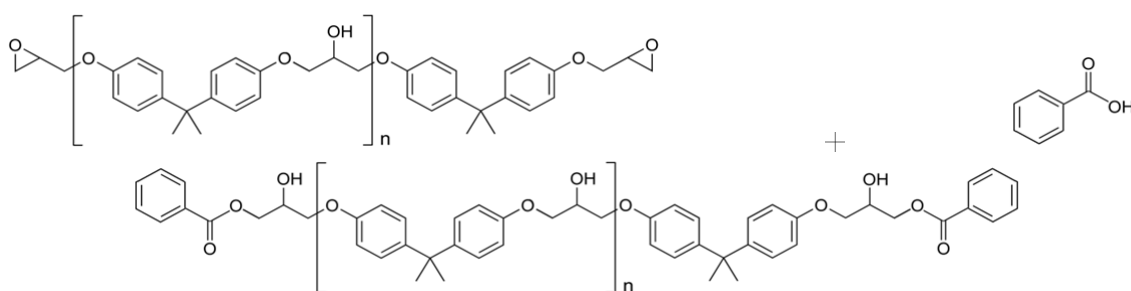


Figure 24: Reaction of PDGGBA and benzoic acid to provide end-capping.

3.5 Formulations

3.5.1 Previous Formulation

The formulation used in earlier versions of the solid-state healing method involved the chemical composition:

A base of Araldite LY1556, which is a Bisphenol A epoxy resin, Huntsman Araldite GY 298, a flexibilising aliphatic epoxy resin, and cured with nadic methyl anhydride (NMA) curing agent, shown in Figure 25b, and Capcure 3-800 (Cognis Chemicals), a thiol-terminated epoxy hardener, which also catalyses the NMA cure reaction.

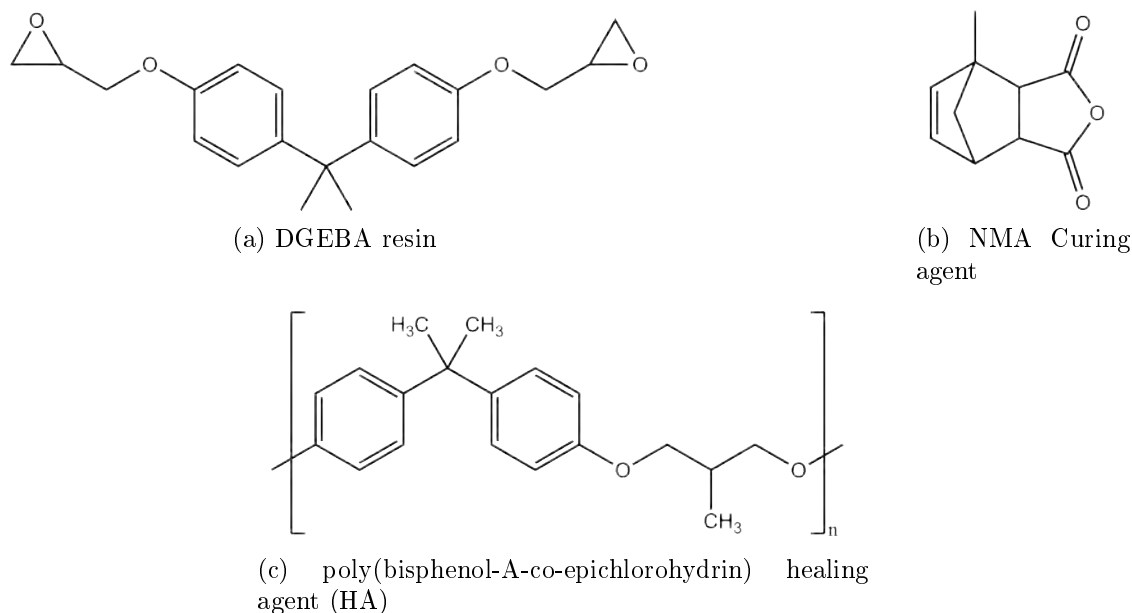


Figure 25: Structural formulae of the three main constituents of the self-healing resin system: resin, curing agent and healing agent.

Added to this base epoxy thermoset was the thermoplastic resin, which consists of poly(bisphenol-A-co-epichlorohydrin) (Sigma-Aldrich 181196), shown in Figure 25c. This was selected based on previous favorable results[95], originally chosen for its high compatibility with the host resin's main constituent, the Araldite LY 1556.

3.6 Resin Preparation

The control resin was prepared according to manufacturer's guidelines. The Epikote 828 was prepared by heating to 50 °C for 15 minutes to reduce the viscosity for stirring. The NMA hardener was added and the BDMA accelerant was added in the quantities listed in table.

Component	Chemical	Quantity by weight (phr)
Epoxy Resin	Epon 828	100
Hardener	NMA	81.2
Catalyst	BDMA	1

Table 2: Formulation of the acid-anhydride cured epoxy resin.

The components were stirred together by hand for 10 minutes and then the mixture was degassed in a vacuum oven at approximately 1 bar to eliminate any gaseous elements. The mixture was then poured carefully into the required mould and placed in the oven programmed for the appropriate cure cycle. A discussion of the weight equivalents calculation can be found in Section 3.3.3, which describes how this may not be a stoichiometric formulation but will be kept consistent with previous work [133].

The healing resin was prepared by first dissolving the healing agent into the 828 host matrix. This had to be done at elevated temperature as the extremely long chains in the healing agent were difficult to ‘dissolve’. The 828 and healing agent were weighed into a glass beaker, and stirred together using a mechanical stirrer at 90 °C for approximately 24 hours. Some concentrations required longer to fully disperse the healing agent homogeneously throughout the resin. Healing agent in these higher concentrations could be seen as translucent particles at the bottom of the beaker, and if these were still evident, further stirring was required. Once all the healing agent had been dissolved, the mixture was degassed, and then the standard mixing procedure was followed for the addition of the curing components.

3.6.1 Resins and Nomenclature

The resin systems used in this project are all bisphenol A epoxy resins. Epon 828 (“resin”) is well used as a formulation resin as it has good general properties and is

therefore used as the 'base' epoxy resin in all cases. Epon 825 is a higher 'purity' epoxy resin, in that it has a lower molecular weight and weight distribution, meaning a lower polydispersity index. This is due to a distillation process which separates the 'ideal' (i.e. highest reactivity per weight) bisphenol A epoxy from the longer chains, shown as the structure in Figure 16 with an 'n' value of 0. This resin may be used in industrial formulations to obtain higher properties and a lower viscosity but the principles are all demonstrated using the lower purity version.

A 'healing resin' is epon 828 with healing agent ("HA") dissolved into it. The healing agent used in this study is poly(bisphenol-A-co-epichlorohydrin) shown in Figure 25c. Healing agents have been obtained from 2 different manufacturers, Aldrich and Inchem Corp., but are the same chemical system.

The 'reactive diluent' refers to propylene carbonate ("PC") which was used to lower the viscosity of the resin.

The 'handling properties' of the resin is used as a qualitative term to refer to the viscosity of the resin, and its ease of use around the lab including difficulty of cleaning and its solubility in common solvents.

3.7 Healing Procedure

For the healing of the resin, the specimens were put through a heating and cooling program referred to as a 'healing cycle'. The Tg of the healing agent is 88 °C, and the healing cycle was higher than this to give the healing agent more energy to flow. The Tg of the healing resin was found by DMTA to be approximately 90 °C. The healing cycle was achieved in an air convection oven at 140 °C for 6 hours. The temperature was ramped up from room temperature at 2 °C/min and held at the healing temperature. After healing, the oven was programmed to reduce in temperature at approximately 2 °C/min, although the actual rate of temperature drop was slightly slower as the oven had no ability to cool quicker than

just turning the element off. As this is well over the glass transition of the resin it should be expected that some damage would be done to the resin over time, with a consequence with respect to the mechanical properties. This would normally be a resin embrittlement as the resin oxidises, resulting in a lower fracture toughness and a higher hardness.

3.8 Rheology

3.8.1 Theory

Rheology is one of the primary tools of the current work. The previous work on the solid state self healing technology had attempted to provide the highest amounts of healing without considering the feasibility of implementing this technology in an industrial environment. Rheology, as the study of the flow of the liquid resin, was used to evaluate the ability of the technology to be used in other manufacturing processes. The viscosity of the resin during cure can give an indication of the degree of polymerisation. The gel point of the cure process can therefore also be assessed by its rheological properties. It indicates the beginning of crosslinking for the cure reaction, where the resin system changes from a liquid to a rubbery state. The gel time can be determined according to different criteria [123, 124]. The commonly used criteria for gel time are as follows:

1. The crossing point between the base line and the tangent drawn from the turning point of G' curve [125, 126]
2. The time where $\tan \delta$ equals 1, or G' and G'' curves crossover [127, 125]
3. The point where $\tan \delta$ is independent of frequency [128, 129]
4. The time required for viscosity to reach a very large value or tends to infinity [130]

In this study, the determination of gel time was based on the second criterion.

3.8.2 Equipment

The testing was done on a TA Instruments AR2000 rheometer. Steady-shear rheological profile was measured during flow mode evaluation. Tests were also done on curing samples to determine some aspects of their cure behaviour. These were done by fixing PTFE film onto the base plate and geometry, and by using an oscillation mode instead of flow to measure changing properties, during a thermal cycle the same as the cure cycle for the normal samples. Steady-shear rheological behaviour was investigated using a parallel plate geometry of 40 mm diameter, and a gap of 1 mm. For each test, a volume (approximately 2 cm³) of well-mixed sample was placed on the base plate of the rheometer. The shear rate was set at 100 s⁻¹ while the temperature was ramped between 100 and 20 °C at the rate of 5 °C/min. All the rheological measurements were carried out in duplicate. The viscosity (η) of specimen at specific temperature or time was obtained directly from the software. Software used for these tests was the Rheology Advantage, TA version 5.2.26.

Cure monitoring was also done using the same equipment. An oscillation mode can be used on samples as they cure to apply a stress to a material and release it whether the material is liquid, gel or solid. PTFE film was applied to the geometry to prevent the cured epoxy from adhering permanently to it. It is still possible to gain information about the rheological profile while the cure is advancing to determine the gel point of the reaction. Resin was mixed according to the same method described in Section 3.6 on page 49, and the curing cycle was programmed into the rheometer which was set in oscillation mode using a multiple wave-form dynamic test.

3.9 Compact Tension Testing

Compact tension testing is the main tool for the assessment of healing efficiency. It is a standard test to quantify the resistance to crack growth in mode I tensile

fracture, as determined by the critical stress intensity factor, K_{Ic} . It is also possible to quantify healing efficiency in terms of the recovery of the critical energy release rate, G_{Ic} . The testing was completed in accordance with the British Standard ISO 13586:2000, with one notable modification. In order that the fracture surfaces remain aligned during the curing procedure, a 3mm diameter hole was machined into each specimen in the crack growth plane in order to arrest the approaching crack.

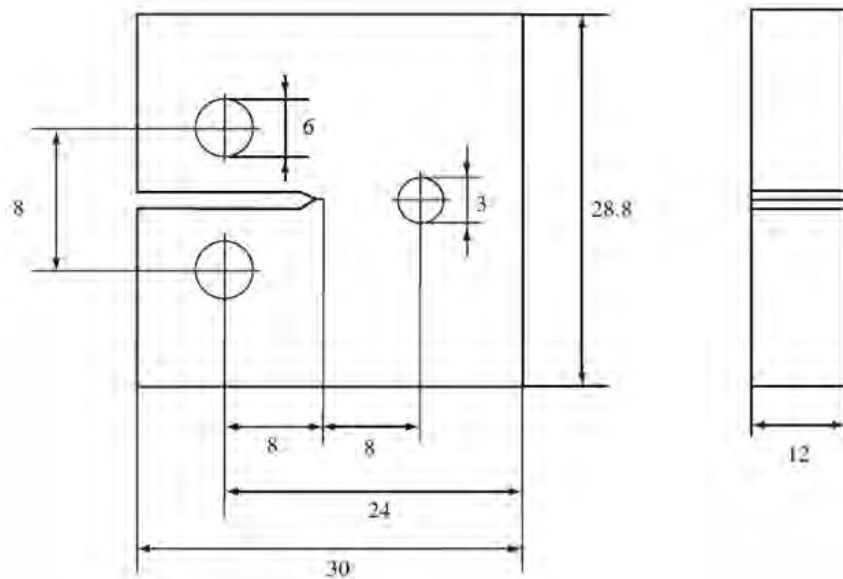


Figure 26: Compact Tension Schematic according to the British Standard ISO 13586:2000.

Where:

w	width	
W	overall width	$W = 1.25w \pm 0.01w$
l1	Length	$l_1 = 1.2w \pm 0.01w$
l2	Distance between holes	$l_2 = 0.55w \pm 0.0005w$
R	radius	$R = 0.125w \pm 0.005w$
h	thickness	$0.4w < h < 0.6w$
a	crack length	$0.45w \leq a \leq 0.55w$

With the crack plane prevented from propagating through the entire width of the specimen, it was possible to measure the fracture toughness, and then place the samples in the oven for a curing cycle whilst keeping the fracture surfaces in intimate contact as would be the case for a matrix crack in a composite system. The arrest hole was created 8mm from the tip of the pre-crack notch.

From the data received from the load cell and displacement transducer a graph can be plotted as load (F) against displacement (s) shown in Figure 27. An idealized load-displacement plot from a compact tension test can be seen in Figure 27.

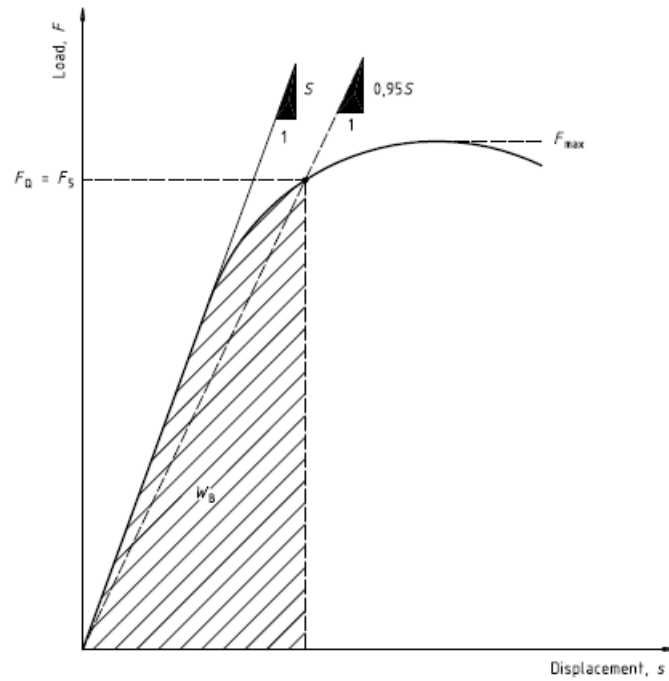


Figure 27: Load-displacement graph for a compact tension test.

3.9.1 K_{Ic} Calculation

In order to evaluate the critical stress intensity factor, K_{Ic} , calculations must be done on the data which are described in the Standard and reproduced here.

$$K_{Ic} = f\left(\frac{a}{w}\right) \frac{F_Q}{h\sqrt{w}} \quad (2)$$

Where:

- F_Q Load to break
- h Specimen thickness
- w Specimen width
- $f\left(\frac{a}{w}\right)$ Geometry calibration factor

Evaluation of the geometry calibration factor can also be found in the standard, and is shown to be:

$$\alpha = \frac{a}{w} \quad (3)$$

$$f = \frac{(2 + \alpha)}{(1 - \alpha)^{\frac{3}{2}}} (0.886 + 4.64\alpha - 13.32\alpha^2 + 14.72\alpha^3 - 5.6\alpha^4) \quad (4)$$

In order to provide detail for the method applied to real data, a worked example for the calculation of K_{IC} from the data is shown. For the geometry used in the standard setup, with dimensions detailed above, it can be taken that $\alpha = 0.008m$, $h = 0.012m$ and $w = 0.024m$. A load to break has been taken to be 200N for the purposes of the calculation, but would be gained experimentally. i.e. $F_Q = 200N$.

$$f\left(\frac{a}{w}\right) = f\left(\frac{0.008}{0.024}\right) = f(0.33) = 6.182 \quad (5)$$

$$\therefore K_{Ic} = 6.182 \times \frac{200N}{0.012m\sqrt{0.024m}} = 665077.31 \frac{N}{m\sqrt{m}} = 0.67MPa.m^{\frac{1}{2}} \quad (6)$$

3.9.2 G_{Ic} Calculation

The calculation for G_{Ic} can be done in a similar manner from equations specified in the standard.

$$G_{Ic} = \frac{W_B}{h \times w \times \phi\left(\frac{a}{w}\right)} \quad (7)$$

Where:

W_B	Energy to break
h	Specimen thickness
w	Specimen width
$\phi(\frac{a}{w})$	Energy calibration factor

Evaluation of the energy calibration factor can also be found in the standard, and is shown to be:

$$\phi(\frac{a}{w}) = \phi(\alpha) = \frac{A(1 - \alpha)}{B + 2A} \quad (8)$$

$$A = 1.9118 + 19.118\alpha - 2.5122a^2 - 23.226\alpha^3 + 20.54\alpha^4 \quad (9)$$

$$B = (19.118 - 5.0244\alpha - 69.678\alpha^2 + 82.16\alpha^3)(1 - \alpha) \quad (10)$$

In the current assessment the strain energy release rate will not be used as it was thought that the critical stress intensity factor would be a more appropriate criterion. Both are indicators of a toughness, but KIC is used far more commonly for self-healing materials assessment.

3.9.3 Specimen Creation

To create the specimens, rectangular blocks of resin were cast in a silicone rubber mould. The moulds were created using RTV134 from Alchemie, a two-component condensation cure, low viscosity silicone rubber. The two parts (RTV 134 and C134) were mixed in the ratio 100:5 as per manufacturers guidelines [131], degassed, and poured into disposable cups until the plug was covered as shown in diagram. The mixture had a cure cycle of 2-8 hours at room temperature.

Once the moulds were created, resin was cast into them using the mixing ratios and procedure described in Section 3.6 on page 49. Once the samples were removed from

the mould, they could be machined to the requirements shown above, and finally a sharp pre-crack was created in the machined notch by the tapping of a fresh razor blade; this extremely sharp crack tip is required by the standard to ensure crack propagation in the correct mode.

3.9.4 Setup

The samples were loaded into the tensile testing machine as shown. Specimens were mounted using the two machined loading holes onto pins on the support grips. Tests were carried out using a J.J.Lloyd Instrument's T5002 in displacement control mode. A load cell of 500 N was used. All tests were carried out at room temperature and pressure and at a test speed of 10 mm/min in accordance with the British Standard. At the test speed of 10 mm/min the equipment is effectively free from inertial lag. The load cell data was logged during the test as with the corresponding displacements. Healing samples were measured with a range of concentrations of modifying agents, as well as unmodified samples of pure resin as a control.

3.9.5 Calibration

Unfortunately no external extensometer was available for use with the instrument which would have recorded more precise displacement of the sample during testing. Therefore careful calibration of the load cell and displacement transducer were necessary to ensure that readings were as accurate as the instrument allowed with its internal components, in order to avoid introducing unnecessary systematic errors. Internal accuracy of the equipment is within 1% of actual values. Calibration for this instrument involves the direct conversion from mV output from the load cell to Newtons and mm recorded by the logging software. By loading the instrument gradually with a series of known 1 kg weights, the gradients of the output data produce a mV/g and mV/mm conversion factor to apply to results collected later.

3.9.6 Assessment of Healing Efficiency

This technology has been designed to regain strength after an impact event and a healing cycle. Therefore, demonstration of recovery of properties, in this case the fracture toughness, is essential. One of the objectives of this research into the self-healing materials is to demonstrate functional recovery in the healing material, see Objective 1 in Section 1.2 on page 16. The extent of healing is calculated from the recovery of any one of a range of materials properties: fracture toughness, tensile strength, elongation at break etc. Thus, the performance of a material can be obtained from the following equation:

$$R_x = \frac{X_{healed}}{X_{virgin}} \quad (11)$$

where X is a measured materials property of the healed material and X_{virgin} is the virgin property.

The unmodified epoxy resin control without healing agent does also show some recovery of properties which is often wrongly attributed to self-healing, but is in fact latent unreacted cure species which, after fracture, are given the freedom to react with new curing agent. In many studies this is not compensated for, and to allow for this in this study, an adjusted healing efficiency has been proposed and re-estimated from Equation 11.

$$H_x = R_x - R_x^{control} \quad (12)$$

3.10 Tensile Testing

3.10.1 Assessment of Mechanical Properties

The maximum tensile stress was measured using the BSI standard BS EN ISO 527-4:1997 [132]. Tensile properties were measured using a Hounsfield Universal

(H100KS/05) testing instrument with a 10 kN load cell. The specimen was marked with a gauge length of 50 mm as shown in Figure 28 and clamped securely in the grips of the machine. Only fractures which occurred in the gauge length of the specimen were accepted. The load cell and extensometer were connected to a computer system and output the force and strain information using the S-Series software. A displacement rate of 2mm/min was used as per the standard.

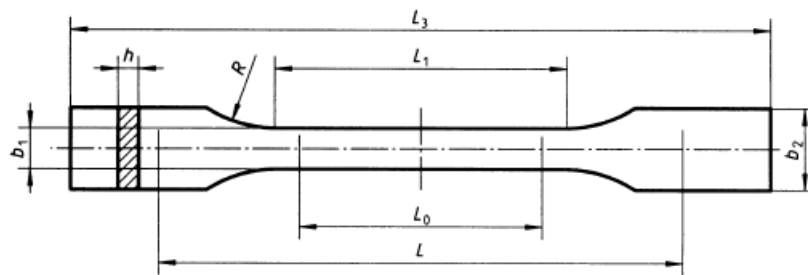


Figure 28: Tensile Testing Specimen Dimensions [132].

Where:

L_3	Overall Length	=	$\geq 150\text{mm}$
L_1	Length of narrow parallel-sided portion	=	$60 \pm 0.5\text{mm}$
R	Radius	=	$\geq 60\text{mm}$
b_2	Width at ends	=	$20 \pm 0.2\text{mm}$
b_1	Width of narrow portion	=	$10 \pm 0.2\text{mm}$
h	Thickness	=	2 to 10mm
L_0	Gauge length	=	$50 \pm 0.5\text{mm}$
L	Initial distance between grips	=	$115 \pm 1\text{mm}$

3.10.2 Specimen Creation

To create a silicone rubber mould for dog-bone tensile testing samples, first some injection moulded polystyrene samples were obtained. These formed the plug for the silicone mould. RTV134 silicone rubber was used, as with the compact tension moulds described above, and was cast over the polystyrene ‘master’ in a shallow, flat-bottomed glass dish.

Once the mould had been created and sprayed with a PTFE mould-release, resin was cast to create testable samples. Once the resin had been mixed and degassed according to the method described above, it was poured into a preheated mould. The moulds were then placed back into the oven for the cure cycle. After the cure cycle the specimens were removed from the mould, and any defects eliminated with light polishing.

3.11 Composites Manufacture

3.11.1 Manufacture of Self-sensing Plies

Composite laminates were manufactured to test the heating of the composites systems which will be used to actuate the self-healing resin. These laminates are constructed with layers of prepreg and interleaves of insulating material which have electrical contact pads on them which make an electrical connection to the fibres in order to sense the changing resistance in the panel. The manufacture of these interleaves is one of the main aims of this work, refer to aim 2 and objective 3 from Section 1.2 on page 16.

Self-sensing plies were required to connect the sensing software, which was in this case TA instruments control hardware and associated software on a computer. The self-sensing plies were used to create an electrical contact with groups of fibres running through the composite in the required direction. As such it was a requirement of these plies that they must be compatible with the matrix, but also to be as flexible and lightweight as possible so as not to impact on the structural and mechanical properties of the original composite. In theory a non-flexible circuit board could be laminated into the structure to provide this functionality but would destroy the concept of the composite itself being self-sensing as a large portion of the properties would be that of the circuit board. It was also important to keep the resistance of the tracks as low as possible, as the sensing would be impaired if the resistance of

the fibres was small compare to that of the tracks. This would be due to their being a higher voltage drop over the higher resistance portion of the conduction path, the tracks, and there would be a less detectable difference in a changing resistance of the low-voltage drop region. It is also important when the same tracks are used to heat the appropriate section of composite, as there would be a higher resistive heating effect at the areas of higher resistance. This would mean that during a healing cycle the tracks would heat up more than the carbon fibres, wasting energy, failing to heal the damage, and potentially damaging or burning other areas of the composite. Various manufacturing techniques were trialed to attempt to create the lightest and cheapest interleave with the best electrical properties with which to sense the damage and then to apply a larger current for a resistive-heated healing event.

Photo-sensitive Film The traditional method for creating Printed Circuit Boards (PCBs) is to use photolithography on a copper-coated substrate. This is done by using a printed acetate mask over a photoresistive copper film in a high-intensity UV lightbox. However, as mentioned previously, this normal type of substrate would not be appropriate as a light, flexible system is required.

It was difficult to obtain pre-sensitised flexible circuit-boards so initially a photosensitive coating was applied to copper-coated polyimide film (R-flex 1000 from Rogers Corp.) in the form of a spray which was done manually. Kontakt-chemie Positiv 20+ Photo Resist Spray as used to provide a positive photo-resist coating. The mask was printed on LaserStar film from Mega Electronics using a laser printer. Using this method it was hard to achieve consistent results, as a perfectly consistent spray-coating which did not over-develop some areas of the film was almost impossible to achieve.

As an alternative to the spray-coating of positive resist, a dry film was ordered which could be laminated to the copper substrate to create much more consistent circuits. A negative dry-film photoresist was used from Mega Electronics who also supplied a

matching developer solution. The photoresist was laminated to the copper-coated substrate in the autoclave at 40 °C and 620 kPa for 1 hour.

For either method, the light-sensitive copper must be exposed to UV and developed before chemical etching which is described below. Once cut to size, the mask was placed over the photoresist and developed in a lightbox for 20 seconds for the dry film, or 2 minutes for the spray coating. The mask was removed, and the exposed film was placed in a developer solution to remove the light-activated portion of the coating. After developing, the film was washed repeatedly with water and then air dried.

Inkjet Masking As an alternative method for the photo-sensitive film which is quite expensive, and requires several processing stages before the etching can begin, the mask was printed directly onto copper-coated poly-imide film using standard inkjet printing to protect the tracks from the etchant. Printing was done on an unmodified Epson Stylus Office Bx630Fw printer and a range of different printing options were assessed to try to achieve the best mask possible. The properties thought to have the greatest effect on the quality, homogeneity and consistency of the print on copper were:

- Colour of the pattern
- Colour Precision
- Print Quality
- Resolution
- Media

These properties were investigated and results will be presented later. Copper-coated film was cut to the required dimensions and loaded into the printer using the paper tray. After printing, the effects of some ‘post-processing’ were investigated.

It was noted that the ink solvent remained conspicuously on the surface of the copper and appeared to be still in a liquid phase. Some time after printing the ink began to pool, recede, or separate, assumed to be associated with the equilibrium contact angle of the individual inks with respect to the unusual substrate. It was suggested that a faster drying of the ink solvent may be achieved to mitigate the effects of the ink movement by placing the printed copper straight into a pre-heated oven. This however could lead to other negative effects, most notably to oxidize the copper surface, so time and temperature of this process was critical and therefore investigated.

Chemical Etching Both of these methods were used to create a mask to use in the chemical etchant bath. Once the mask had been applied using any of the methods above, the film was placed in a heated wet chemical etchant bath, a Mega Electronics PA310, containing an iron chloride solution and was agitated by the machine with bubbling air. This step removes unprotected copper from the substrate to leave the desired track arrangement. Etching usually last approximately 7-30 minutes depending on the strength and age of the etching solution, but was checked periodically and stopped when the etchant had removed the required copper. As the etchant was extremely corrosive, thick gloves were worn when removing the film from the bath, which was then repeatedly washed with excessive cold water to remove any etching chemicals or residue.

Direct Silver Inkjet Printing The final approach which was used was direct silver deposition onto a polyimide film using an inkjet printer and silver ink. This method was the highest technology and despite the high capital investment in a high-precision printer, from an industrial perspective, the ease, consistency and speed of manufacture and reduced per-unit costs make this an attractive option. A Kapton 100HPP-ST polyimide film was obtained from DuPont which has good thermal, mechanical and chemical stability with respect to the composite systems

which were employed. Printing was done on a Microfab printer using parameters selected to create the best droplet size and printing consistency.

3.12 Composite Specimen Preparation

For the manufacture of the panels for the self-heating demonstration, a procedure was used which would be as similar as possible to that used in current industrial environments. Two size panels were made measuring 200 mm x 200 mm and 100 mm x 100 mm.

Prepreg material was used for these test panels, and Cycom 977-2 was used from Cytec Industries Inc. The overall concept of the self-sensing can be seen in schematic form in Figure 29.

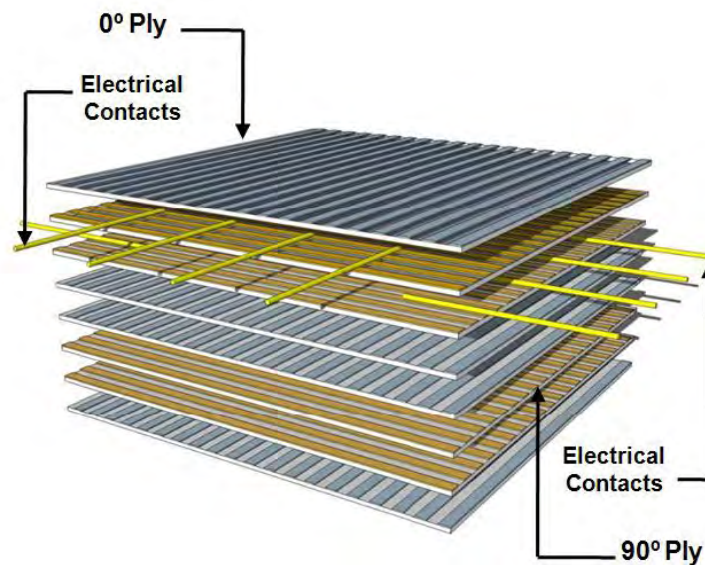


Figure 29: Schematic representation of the composite self-sensing system. Electrical contact was made with flexible circuit boards.

A standard bagging arrangement was used as recommended by the manufacturer as shown in Figure 30. Consumables were obtained from Cytec Industries Inc including Stretch-Vac™ 3000 nylon bag, with AB100 non-woven polyester breather and A5000 FEP release film, no peel ply was used. Standard sealant tapes and vacuum fittings

were used.

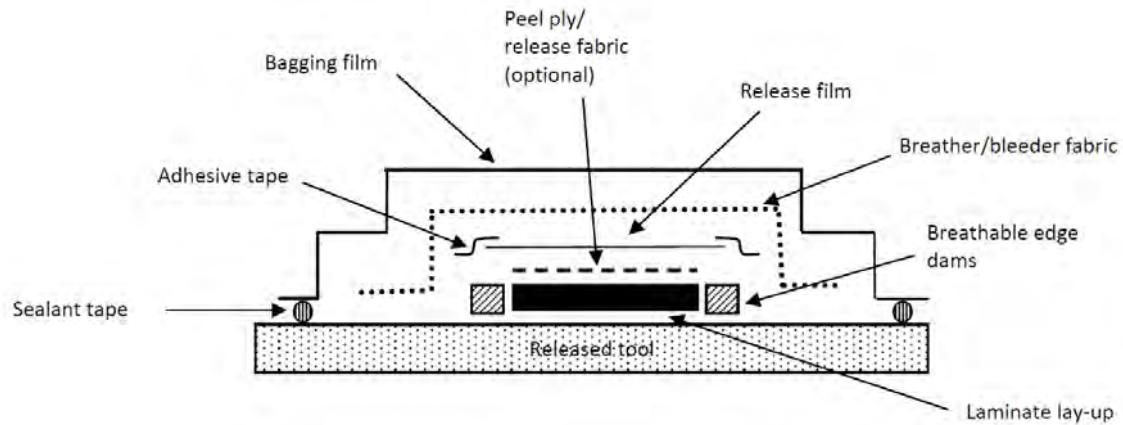


Figure 30: Composite manufacture bagging arrangement recommended by Cytec

Cure cycle for Cytec 977-2 was a ramp to 90 °C at 2 °C per minute, dwell for an hour and then a ramp to 177 °C for 3 hours. Final 200 mm x 200 mm square cured panel can be seen in Figure 31 which has two directions of self-sensing channels for damage triangulation. The 100 mm x 100 mm panels had a single direction (0°) for ease of manufacture and testing to prove the concepts for manufacturing.

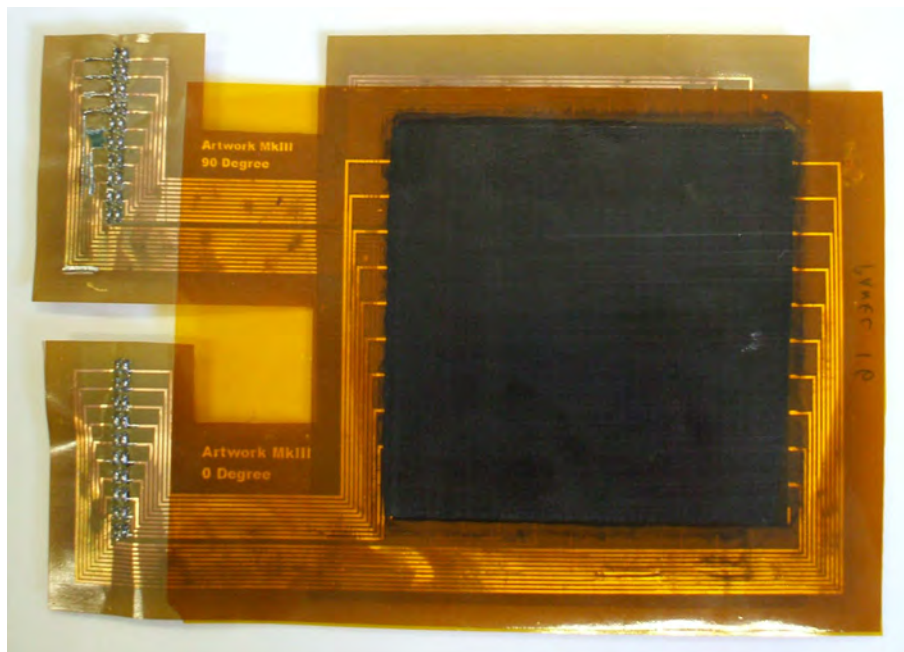


Figure 31: 200 mm x 200 mm carbon fibre panel with self-sensing polyimide circuit board inserts. Two connectors on left are for 0° and 90° directions.

4 Characterisation of Resin System

4.1 Introduction

This chapter provides an initial investigation of mechanical and physical properties of the resin system which has been developed for self-healing composite systems. This addresses Aim 1 by implementing Objective 1 from Section 1.2 on page 16. Modifications to the resin system will be examined in the following chapter. Previous tests included mechanical tests and comparisons of healability, which need to be presented alongside new results to aid the development of a new system. The results will be presented and discussed with a view to developing targets for the improved system.

The resin system which had been developed for the solid-state self-healing has been characterised using a variety of investigation methods. Mechanical testing was undertaken in order to assess the effects of the healing agent on the neat resin, and rheological profiles of the resin were measured to get baseline data for the development of improved resin systems in the later stages of the project.

4.2 Developmental Research

The diffusional solid state healing system is based upon the idea of thermal diffusion of a healing agent dissolved into a compatible matrix resin. The healing agent is a long linear polymer, a homologue of the host resin, which creates high levels of entanglement and inter-diffusion with the network and will reptate through the network and across cracks after damage, causing crack closure and a recovery of mechanical strength. Research had already been undertaken for a ‘proof of concept’ for this technology which has been demonstrated using uniaxial compression testing and charpy impact testing [96].

These tests were carried out on the system to show that the resin is able to recover

some mechanical properties after energy is introduced into the system to allow the molecules to move. However these are not tests which provide complete mechanical information about the performance of the resin, nor of the ability to heal itself. Therefore more complete data is presented alongside, with compact tension tests and rheology on the uncured resin and a rheological profile of the cure.

4.2.1 Uniaxial Compression Testing

Uniaxial compression testing was performed on the samples during the original research. The test specimen is compressed along its major axis at constant speed until the specimen fractures or until the load or the decrease in length reaches a predetermined value. The load sustained by the specimen is measured during this procedure. Output from the procedure can be seen in Figure 32, which shows the compressive stress/strain curves for the self-healing resin formulated with a variety of concentrations of healing agent. The measured results across the 5 repeats are summarised in Table 3, which shows the values for yield strength and strain for the different formulations. The yield stress and strain were defined as the maximum point on the stress-strain curve.

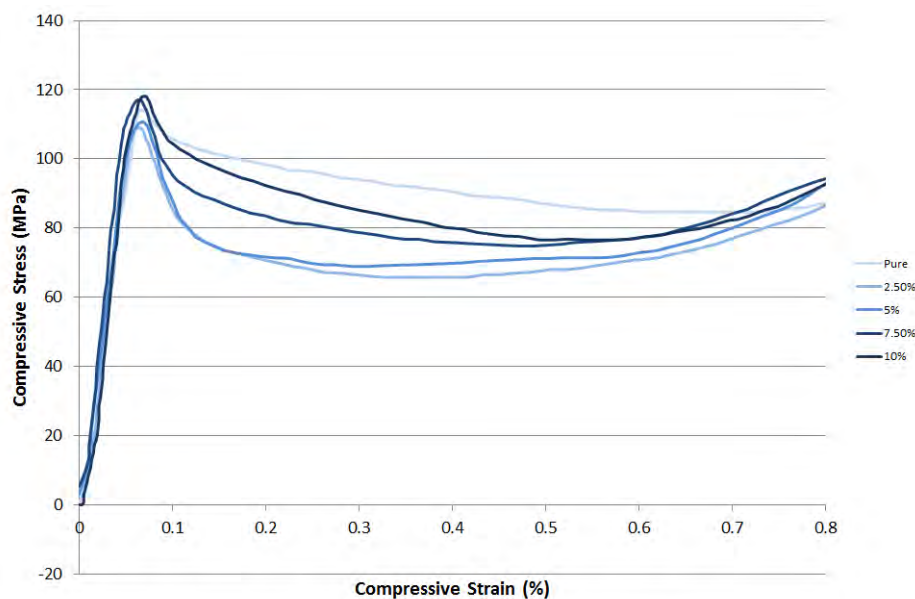


Figure 32: Stress/Strain curves of resin in uniaxial compression test.

Concentration (wt%)	Yield Strength (MPa)		Yield Strain (%)	
0	110.74	± 2.95	6.50	± 0.72
2.5	111.92	± 1.19	7.38	± 0.18
5	112.06	± 0.94	7.55	± 0.33
7.5	118.84	± 3.37	7.56	± 0.27
10	119.39	± 3.12	7.60	± 0.26
12.5	116.39	± 0.78	7.56	± 0.12
15	111.51	± 1.54	7.61	± 0.16

Table 3: Yield strength and strain from uniaxial compression testing of base resin with varying concentrations of healing agent.

Figure 33 shows the yield strength of the samples with regard to concentration of the healing agent. Figure 34 shows the results of the yield strain in the same fashion. Note that both Y axes have been expanded to emphasise the results for the purposes of comparison and clarity, and do not include the origin.

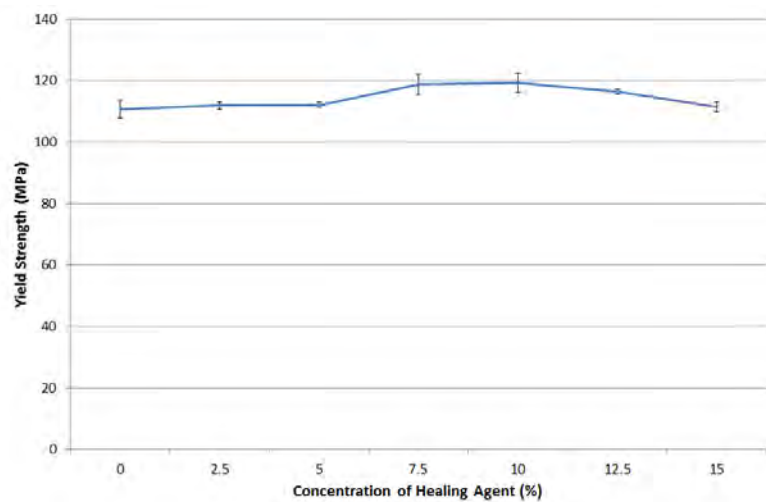


Figure 33: Yield Strength of base resin with varying concentration of healing agent from uniaxial compression testing.

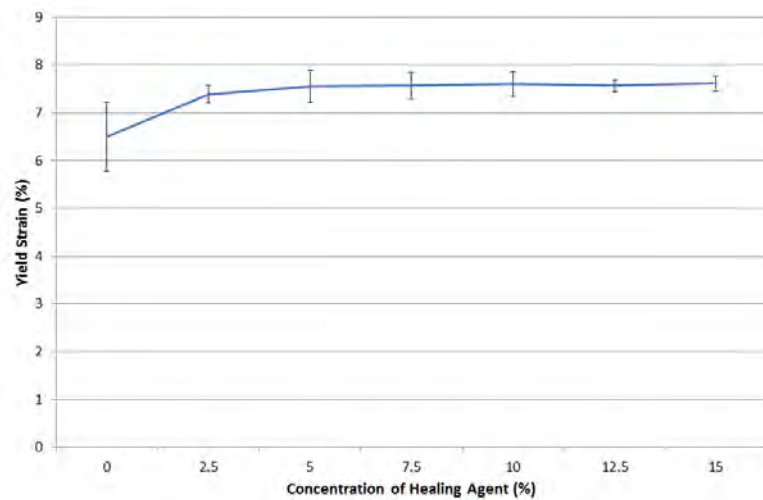


Figure 34: Yield Strain of base resin with varying concentration of healing agent from uniaxial compression testing.

4.2.2 Tensile Testing

Tensile testing had also been completed as part of the development work on this self-healing technology and this is an important aspect of the mechanical assessment of this technology. A complete picture of the performance of these resins is a requirement to be fully aware of the impact on every property of including new diluents.

Healing agent concentration (wt %)	Tensile strength (MPa)	Failure strain (%)	Young's modulus (GPa)
0	76.09 ±7.01	2.87 ±0.67	3.52 ±0.30
2.5	76.54 ±6.55	2.75 ±0.52	3.40 ±0.32
5	76.40 ±7.80	2.79 ±0.55	3.41 ±0.18
7.5	79.85 ±3.30	3.89 ±0.67	3.30 ±0.15
10	79.98 ±4.67	3.71 ±0.83	3.32 ±0.12
12.5	79.96 ±2.52	3.40 ±0.77	3.32 ±0.05
15	78.32 ±1.60	3.50 ±0.42	3.27 ±0.27

Table 4: Tensile testing results for modified 828 resin with ultimate tensile stress failure strain and modulus.

4.3 Compact Tension Self-Healing

Compact tension specimens have been used to further quantify the healing performance of the resins from the previous system. Compact tension testing is a much more repeatable method for testing a real material property, namely the critical stress intensity factor. There are issues associated with the use of compact tension testing, particularly with the setup which was used and these will be discussed in a later chapter.

Figure 35 shows the critical stress intensity factors for several concentrations of healing agent and the recovery of mechanical performance over each healing cycle. The healing cycle was done at 140°C for 6 hours. Each test was repeated with a minimum of 5 samples as per the standard specification.

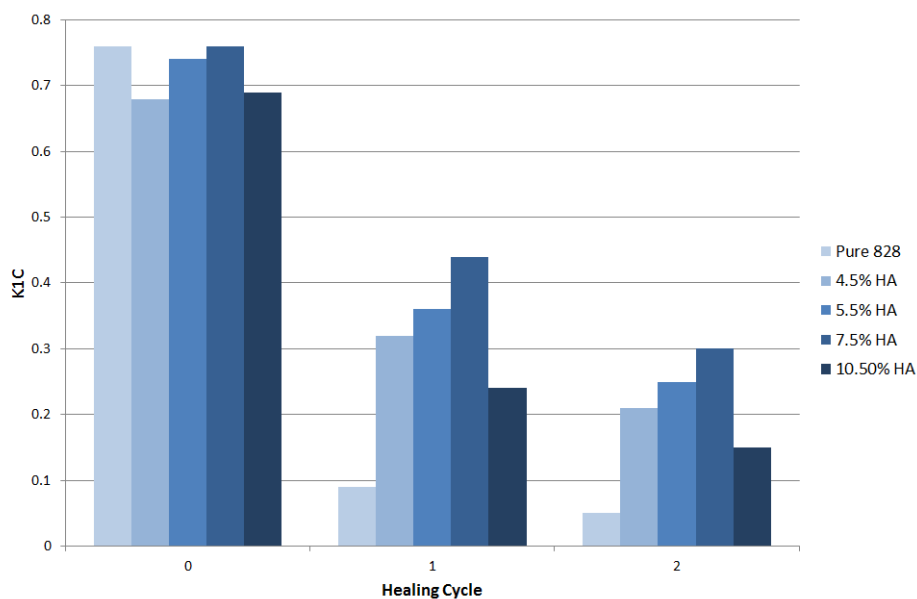


Figure 35: Recovery of K_{IC} for varying concentration of healing agent.

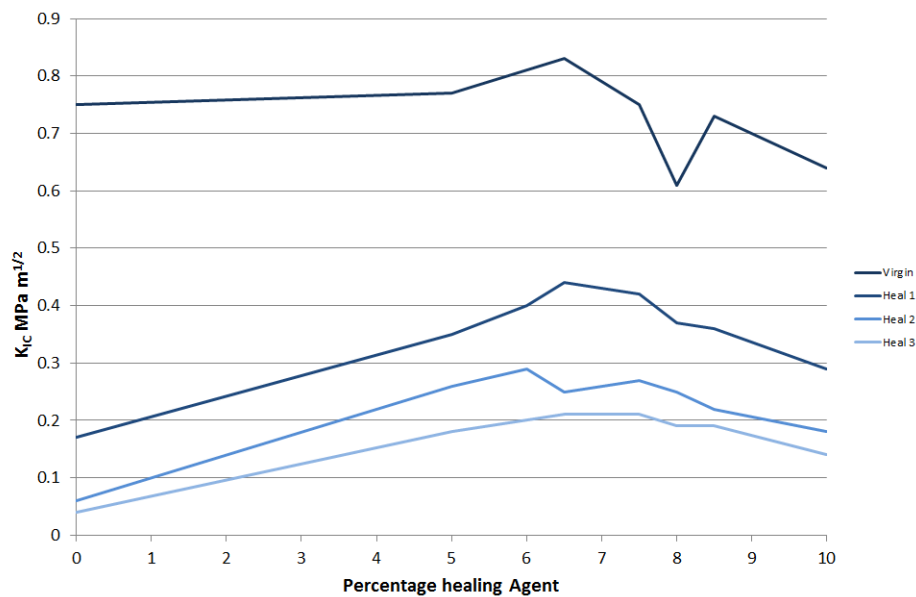


Figure 36: Recovery of K_{IC} across 3 healing cycles, with very concentration of healing agent.

4.4 Rheology of System

Although it had been noted that the handling of this resin was a problem especially at high healing-agent loadings [133] this effect has not previously been characterised. The results from rheometric analysis are shown in Figure 37. Rheometric analysis was used for the first time during this project and considerable information was drawn from the technique. All results in this chapter refer to the self-healing resin system developed in previous work[95, 96].

Viscosity was measured for base resin with different concentrations of healing agent dissolved in. This was done in flow mode as described in the Experimental section. Results are shown in Figures 37 and 38. Figure 38 shows a log plot of the same results at the higher temperature band where it becomes difficult to differentiate the individual formulations. Viscosity was measured on several runs and the results deemed most representative were chosen, as an averaging technique would not have achieved a smooth curve. Repeatability for the tests was good, and the equipment became unable to read the absolute viscosity of the solution at around the same

temperature during each run. Flow mode is traditionally ramped up in temperature, but a temperature ramp in both directions was completed, as the very high viscosity of the modified resin system at low temperatures prevented the rheometer from turning the plates to start the experiments. Therefore more data was collected on a decreasing temperature experiment. Cooling was done at a low value of $2^{\circ}\text{C}/\text{min}$ to allow for thermal equilibration and thermal lag within the system. By comparing the ramp up and ramp down experiments it was determined that thermal lag was negligible due to the responsive peltier plate heating element and the extremely small working volume ($\sim 1\text{ cm}^3$).

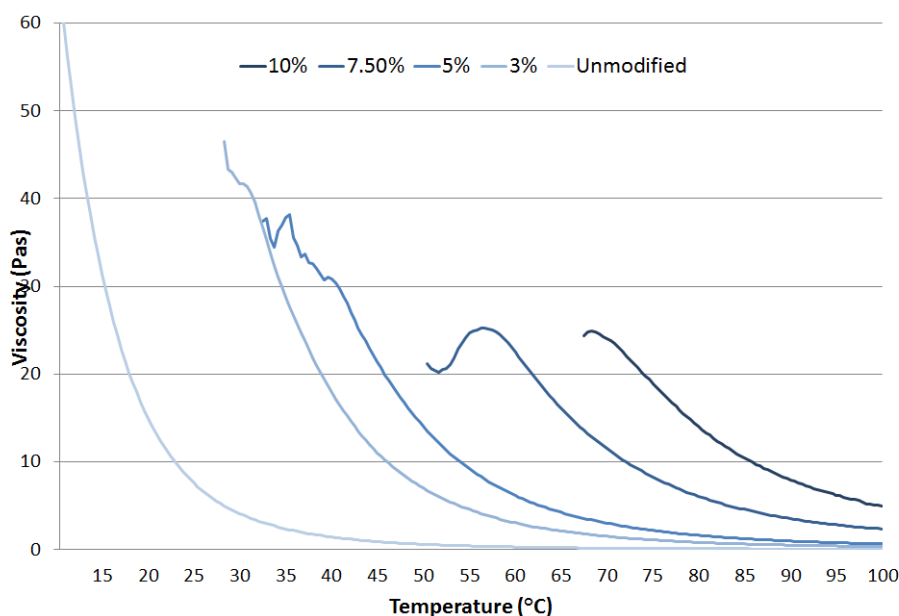


Figure 37: Temperature dependence of viscosity of resin with varying concentration of healing agent (0 wt%, 3 wt%, 5 wt%, 7.5 wt% and 10 wt%).

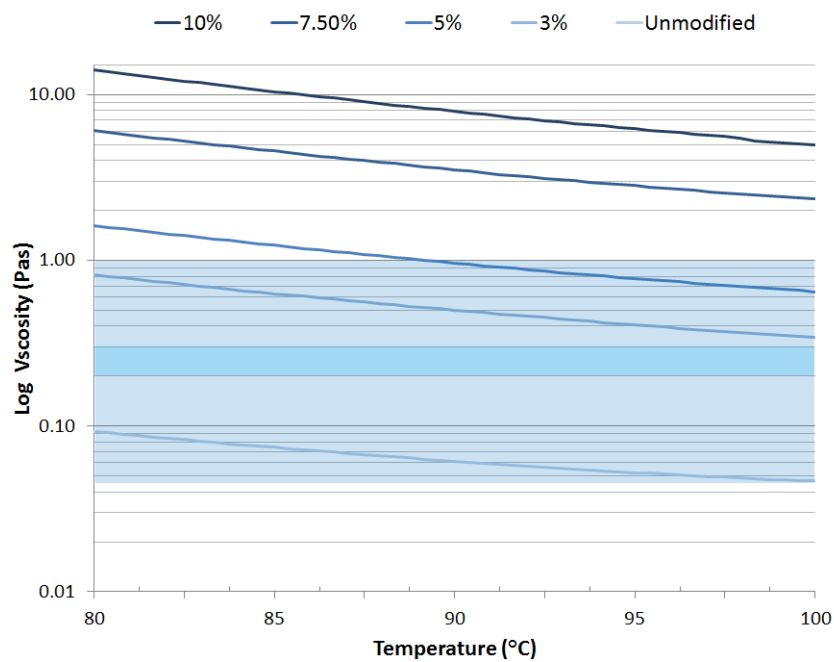


Figure 38: Log plot of viscosity vs temperature detail. Shaded area represents viscosity usable (light) and ideal (dark) for use in resin transfer moulding.

It can be seen from the Figures that the self-healing resins had too high a viscosity at room temperature to be measured in the flow mode experiments conducted. This was primarily due to the fact that the materials behaviour was dominated by the elastic properties once the temperature was so low. It can be assumed that the material is almost unworkable at these temperatures and hence the need for viscosity reduction. As a useful comparison, water is 0.001 Pa.s and maple syrup is around 0.5 Pa.s at room temperature. Even at 85 degrees the viscosity of the 10% resin is 10 Pa.s which is the approximate viscosity of butter. Figure 39 shows the normal force recorded by the rheometer during the viscosity measurements of the resin formulations shown above. This was the force perpendicular to the rotating plane of the plate geometry, away from the heating plate.

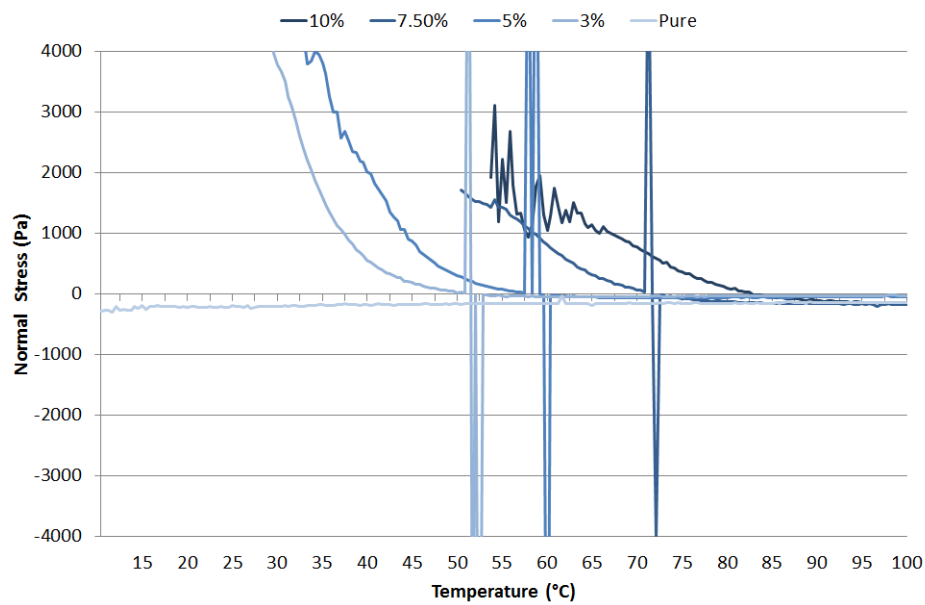


Figure 39: Normal stress recorded during the flow mode viscosity testing shown in Figure 37.

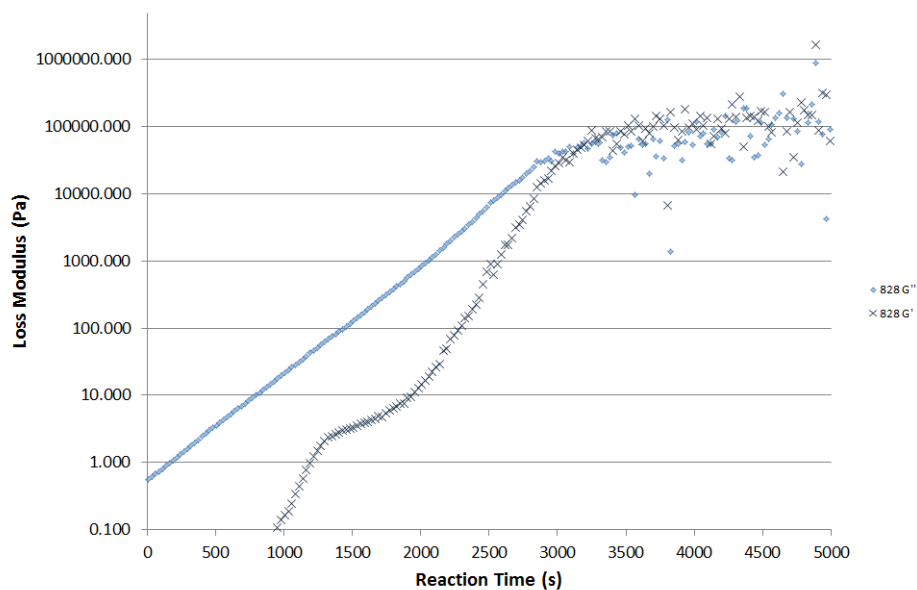


Figure 40: Loss and Storage moduli of the isothermal curing reaction at 90°C of the pure 828 resin with no modifying healing agent. The crossing point of the loss and storage moduli represents the gel point of the reaction.

Figure 40 shows the isothermal curing reaction of the pure 828 resin which is monitored by a reciprocating parallel plate geometry, or ‘oscillation mode’ rheometer. There are several definitions of the gel point of a reaction, which is when the

monomers have reacted to the extent that there is an effectively infinite polymer network, but one is that it is the crossing point of the loss and storage modulus of the reaction mixture. This also coincides with the point where the reactants stop displaying viscous flow, which appears on the plot as increasing noise as the reaction proceeds, as the molecules become less able to move past each other and lose energy. Another common definition of the gel point is when the material begins to display elastic properties. In theory the overall complex viscosity of the mixture approaches infinity at this point which of course causes different equipment and experiments to show a different absolute values for the gel point. The elastic behaviour begins to dominate the bulk properties as the reaction mixture is still deformable, but begins to show its viscoelastic hysteresis associated with the cured polymer network rather than a purely viscous one displayed by the monomers. This is not to say that the monomers have fully reacted, only a proportion of the reactive species need to have joined to form a network and much work has been devoted to creating models which can predict the extent of reaction using physical properties. The proportion of monomers reacted into the network depends on the functionality of the monomers, the degree of conversion reached by the reaction and the ratio of the reactive sites/groups of the two monomers.

4.5 Discussion

Epon 828, a bisphenol A epoxy resin has been modified with a healing agent of bisphenol A co-epichlorohydrin with a molecular weight of 44000 from Aldrich chemicals. The resin was modified with a range of concentrations and tested using a variety of methods to assess the mechanical properties. Chemical and other physical properties of the resin, and the effects of the addition of healing agent, have been investigated in other studies which may be found in the references. Compact tension testing has been the main tool of healability assessment due to the repeatability of this test, and also its measurement of a fundamental materials property, critical

stress intensity factor, which is a direct indicator of the ability of a material to resist fracture. Tensile and compression tests were also performed to determine whether there was a detriment to any other mechanical properties on the addition of the healing agent modification.

It can be seen from the compression tests that an increase in healing agent concentration was accompanied by a corresponding increase of compressive yield strength and strain. This is to be somewhat expected with the introduction of varying chain lengths into a normally heavily cross-linked resin system.

According to Chen and Schweizer [135, 136] there are 5 strain amplitude regimes: Linear stress growth, anelastic regime where stress increases more slowly, a local stress maximum or ‘peak yield’ followed by a period of dropping stress known as ‘strain softening’, a plastic flow regime of a near constant plateau, and finally, at high enough deformation, either a total failure or a period of increasing stress due to chain deformation known as ‘strain hardening’. Each of these domains can be seen in Figure 32, particularly of note is the increasing peak yield, and increasing strain softening, with increasing concentration of healing agent.

The strain softening seen in the system was significantly increased with the addition of healing agent, which can be attributed to the uncrosslinked healing agent allowing for a slightly more viscous type plastic deformation, allowing chains to move against each other with less energy than would be required to break covalent bonds in the structure. This, accompanied with the lower modulus of the higher healing agent concentrations shows that the healing agent acts as a plasticiser as the majority of inclusions would [137], lowering stiffness but increasing failure strain.

The tensile tests shown in Table 4 also support these findings. In general they show the same trends as the compressive testing as would be expected from an isotropic non-reinforced polymer matrix. The table also shows the decreasing Young’s modulus with increasing healing agent as calculated from the results.

Rheology was performed on these resins, for the first time, to complete the analysis.

This quantitatively demonstrated the viscosity of the resin, and how it changes with inclusions, with changing temperature, and during the cure cycle. It was found qualitatively in previous experiments that the room temperature viscosity of the self-healing resins was far too high to handle, even for procedures which can normally deal with high viscosity resins such as wet layup. Unfortunately it was found that the rheometer was unable to measure an absolute value for any of the modified resins below 30 °C.

It is likely that if spherical domains of the healing agent are formed that these would be deformed under shear loads and show elastic behaviour similar to a thermoplastic material. This behaviour could account for the observed maxima in viscosity in Figure 37. This is supported by the normal force measurements in Figure 39, whose data curves first begin to deviate from their expected values as temperature decreases and then begin to fluctuate dramatically as the data becomes unusable. This condition is not observed in the data plotted for the pure 828 resin which shows a standard and more expected linear temperature relationship associated with the polymers coefficient of thermal expansion. These data also serve to support a phase separation theory.

However this somewhat misrepresents the viscosity of the final curing mixture, which would be used in the final manufacturing procedure, as the curing agent had not been added. This was to avoid curing the epoxy resin during the testing which would have jammed the rheometer. The curing agents, including the NMA which was used during these curing studies, are generally the lower viscosity component of the two (resin and hardener). In this case the reaction was also accelerated with catalyst BDMA which has extremely low viscosity, but the inclusion of which would have been in such small quantities as to hardly affect the viscosity of the final mixture. It was thought that the extremely high molecular weight linear healing agent, which could be thought to be a thermoplastic polymeric material, at higher concentrations has such high intermolecular interaction with the lower weight, shorter chains of

the host epoxy resin that the macroscopic properties of the uncured resin became similar to that of a thermoplastic.

4.6 Conclusion

The resin system which had been developed has been assessed in further detail. Once the technology had been shown to be effective, it was most important to assess the mechanical performance to improve healability and to measure the rheological properties to form a baseline for improving the processability of further formulations. The increased viscosity which is associated with higher healing agent concentration can be seen to make handling of the self-healing resins at room temperature almost impossible above 15%. Viscosity would need to be reduced significantly to fall within the range suitable for industrial resin transfer moulding. It was decided that an investigation into 3 different methods for reducing the viscosity should be undertaken: the use of a lower molecular weight healing agent to try to mitigate the impact on the viscosity of the higher concentrations of healing agent needed for optimal curing, the use of further resin modification with the use of a reactive diluent, and the use of a bisphenol F type resin to modify the base resin viscosity.

5 Development of Resin System

5.1 Introduction

Having characterised the resin system from previous studies with a particular emphasis on the handling properties the next stage was to characterise the effects of various developments of the formulation. This section addresses Aim 1 by completing Objective 2 from Section 1.2 on page 16.

5.2 Characterisation of Systems

For each route of development the viscosity was assessed using flow-mode rheometric analysis as well as an assessment of the effect on the healing performance by comparison of the maximum load to failure and by fracture toughness assessment which was undertaken for the original system (see Chapter 4). It is important that the healability of the cured system is not impacted too heavily as it removes the advantages such a system provides. On the other hand it would be too ambitious to expect that any developments are likely to achieve improved mechanical properties, healing properties, easier handling and reduced costs.

5.2.1 Concentration Effects

It has been shown that viscosity increases dramatically with increasing concentration of the healing agent. This was an expected result although it has not previously been quantified. The first stage of resin development was to ascertain to what extent the healing agent was responsible for the difficult handling of the resin, and whether an acceptable level of healing may be achieved at a lower concentration of healing agent. Results obtained for the viscosity of the system and how this changes with increasing concentration of healing agent are shown in Figure 41. For the recovery associated with this concentration effect see Figure 35 on page 71.

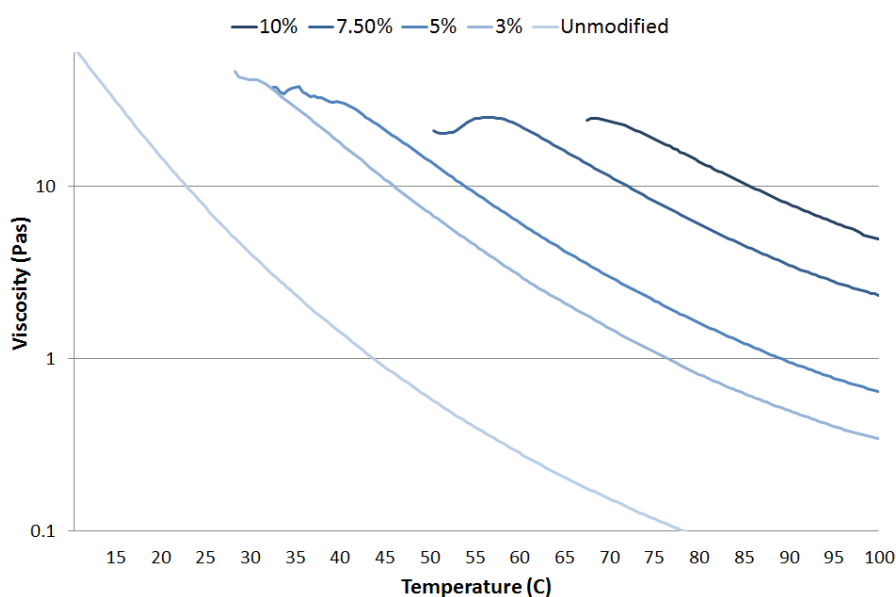


Figure 41: Log complex viscosity of epoxy resin modified with increasing concentration of healing agent. Healing agent Mw: approx. 44,000 g/mol

5.2.2 Molecular Weight Variance

Molecular weight is a very influential characteristic of the healing agent which has a strong influence on viscosity. The chain length is directly proportional to the amount of chain entanglements and hydrogen bonding between neighbouring molecules. This in turn is responsible for the sharp increase in viscosity, requiring much more energy to be available in order to get the chains mobile at room temperature. Because of this strong influence, it was decided that an investigation of the direct mathematical relationship of viscosity and molecular weight. To quantify this relationship, two other healing agents were sourced which were chemically similar but with a different length. These were dissolved into the base resin in the same way as the previous resin and the results tested using the rheometry method described.

The resins were all poly-diglycidyl ethers of bisphenol A, with the original healing agent weighing 44000 g/mol, and two new ones with molecular weights of 6100 g/mol and 4000 g/mol respectively. The weights were obtained from manufacturers technical data sheets. As the objective was to lower the overall viscosity of the resin it was decided that only lower weights would be used.

Rheological data is shown below in Figure 42 showing the unmodified epoxy resin compared to resins which had 7.5% concentration by weight of the 3 test healing agents.

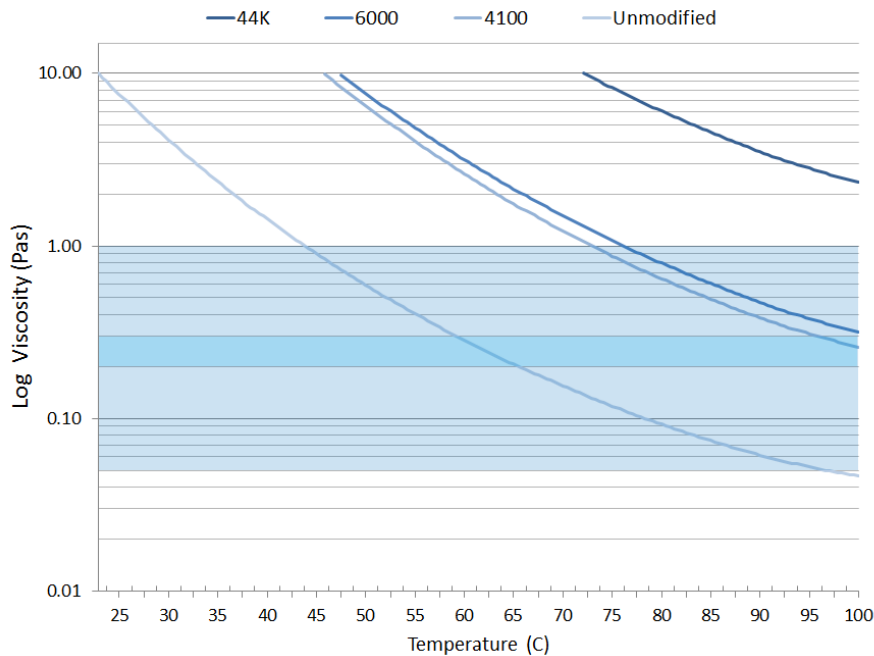


Figure 42: Viscosity of epoxy resin modified with 7.5 wt% of healing agents with different molecular weights as a function of temperature. Also shown is viscosity of the control resin, unmodified Epon 828. Shaded areas represent the usable (light) and ideal (dark) viscosity ranges for resin transfer moulding.

Compact tension testing was also conducted to compare the relative healability of these three systems. Critical stress intensity factors can be seen in Figure 43, comparing the recovery after 1 and 2 healing cycles with the virgin properties. The recovery of all 3 modified resins was extremely encouraging. The lower molecular weight healing agents appear to have provided approximately equal recovery performance to the previous versions of the resin, which was formulated with the heaviest healing agent, 44000 g/mol shown as the darkest colour bars in Figure 43. Recovery of all 3 modified resins are approximately equal, at around 60%. The lightest healing agent (4000 g/mol) shows recovery of 55%, the middle healing agent (6100 g/mol) shows a percentage recovery of 52% and the heaviest (44000 g/mol) shows a recovery of 58%. It should be noted that there is a reasonably well recognised

difficulty in obtaining accurate and consistent fracture toughness values for these types of brittle specimens and therefore these recoveries should be understood to be guideline quantities. This will be discussed further in the discussion section.

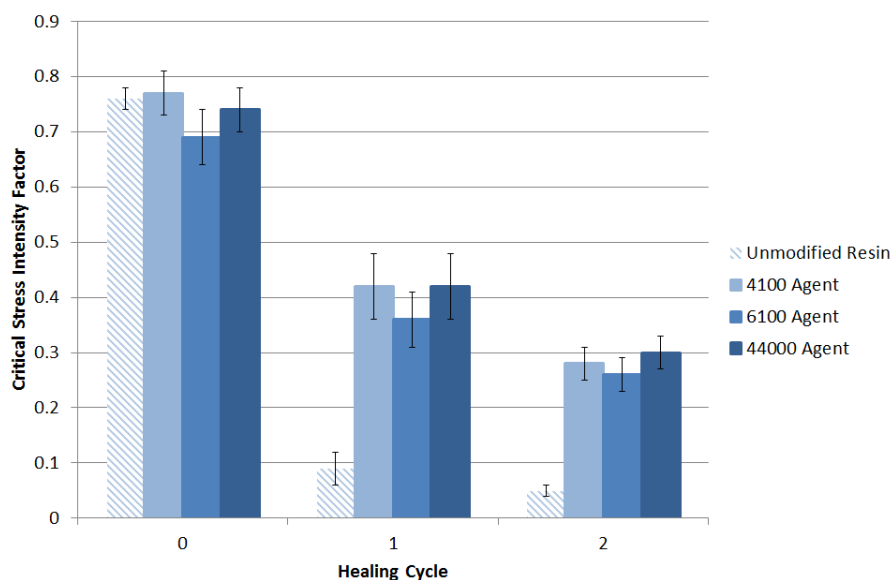


Figure 43: Recovery of fracture toughness with 7.5% of healing agents with a range of different molecular weights. Healing cycle ‘0’ refers to virgin properties. The ‘Unmodified Resin’ is the control with no healing agent.

5.2.3 Reactive Diluents

Diluents are a common form of modification for industrial resin blends. Diluents are generally a much lower molecular weight species which serves to promote molecular mobility in the liquid phase, and these are often solvents which are lost during cure. As the resin was to be modified for use in industrial manufacturing processes such as resin transfer moulding which uses closed moulds due to the pressure, a solvent would not be suitable as this would be trapped inside the matrix during cure and cause voids and would severely impair mechanical performance. Reactive diluents, on the other hand, can provide this same function for the uncured resin, but should react into the matrix during cure providing additional support. In many cases these actually serve to improve the mechanical properties of the cured system as they allow the resin cure to go further to completion as they enable the molecules to stay

mobile for longer into the reaction, and provide further reaction sites for trapped molecules in the gel. A candidate reactive diluent was selected from the literature for beneficial influence on the epoxy-acid anhydride cure system. This was propylene carbonate. This diluent was selected as it is very safe to handle, has extremely low viscosity, according to the manufacturer's data sheets, and has low volatility. Diluents are also not expensive components which would be very favourable from an industrial perspective as it would lower the overall cost of the blended system and therefore the application of this technology.

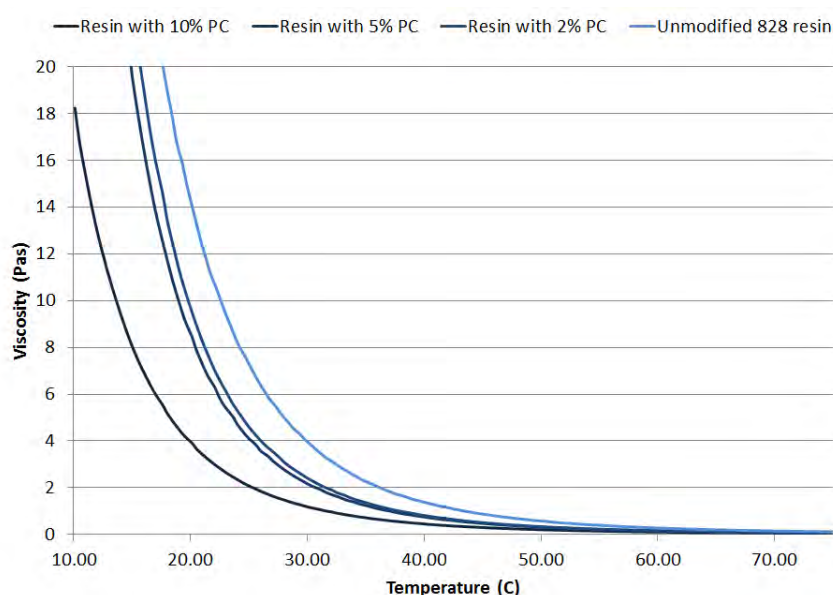


Figure 44: Change in viscosity with temperature of unmodified 828 resin, with increasing concentrations of propylene carbonate (PC) diluent

Figure 44 shows the change in viscosity of the base bisphenol-A resin across a range of useable temperatures with increasing concentration of diluent propylene carbonate. A noticeable reduction in viscosity is achieved uniformly across the range of temperatures tested.

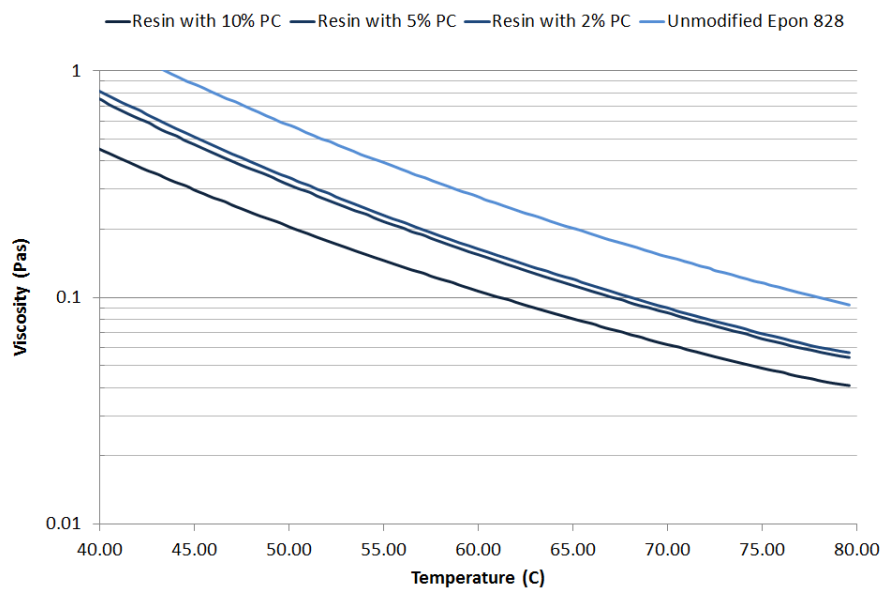


Figure 45: Log viscosity of resin without healing agent, modified by propylene carbonate

Figure 45 shows the viscosity on a log scale. This highlights the uniformity of the reduction in viscosity across the temperature range. A reduction in viscosity approximately equal to a 15 degree increase in temperature can be seen with a concentration of 10% propylene carbonate.

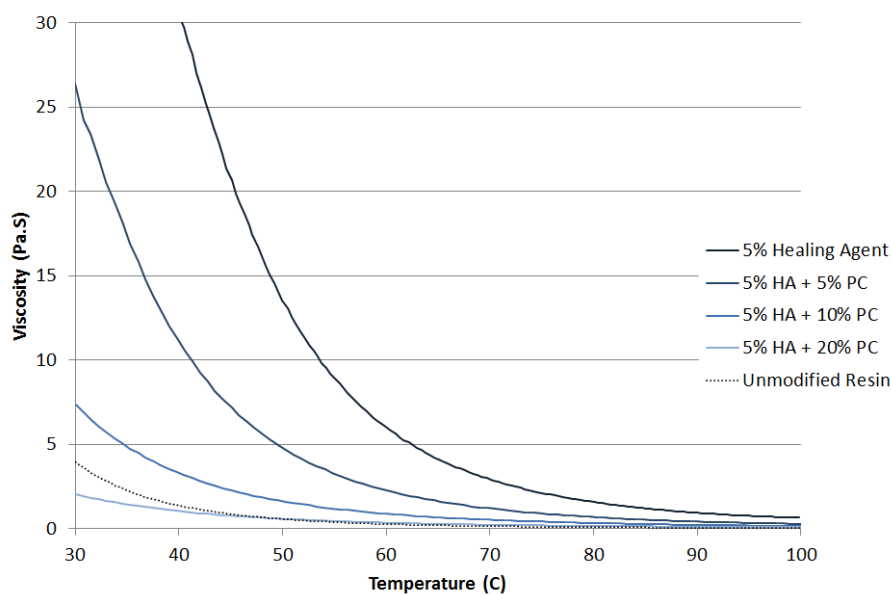


Figure 46: Change in viscosity of modified self-healing resin, with 5% healing agent and a range of concentrations of propylene carbonate (PC). Also shown is unmodified control.

It was decided that further testing would highlight the effect of the diluent when combined with the healing agent at a recovery level of concentration. Figures 46 and 47 show this data. The increase in viscosity caused by the healing agent is far in excess of the effect which the diluent imparts to the blend. To bring the viscosity down to a level of 1 Pa.s, which would be approximately required to utilise the resin for most manufacturing procedures the content of the diluent must reach a very large percentage (20%) in order to offset a small loading of the healing agent (5%). It can also be noticed that an increase of temperature does not provide the same reduction in viscosity after heavy modification. This can be seen in a small reduction in gradient of the curves for each of the samples in Figure 47.

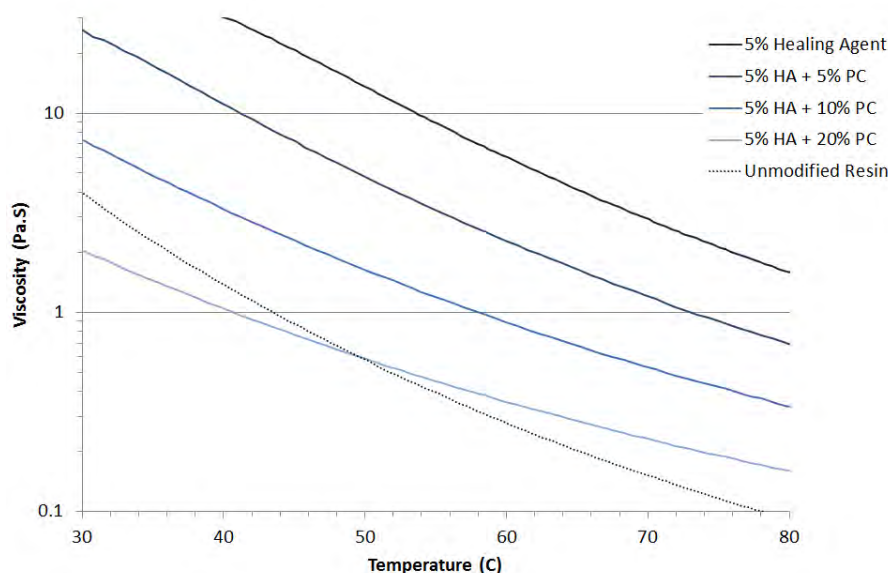


Figure 47: Log viscosity of self-healing resin modified with propylene carbonate (PC).

Compact tension testing was also done to compare the effect on the fracture toughness and its healability. These results are shown in Figure 48. The standard formulation of the self-healing resin which can be seen as the light blue bar shows by far the largest recovery in fracture toughness compared to the other resins. The resins which have been further modified with the diluent can be seen to have recovery as low as that of the control, shown as the shaded bar. Recovery of the standard

healing resin was approximately 60%, while the resins with diluent recovered only approximately 30% or less of the fracture toughness of their virgin specimens during the first healing cycle. The second fracture and healing event shows the same trend. Recovery of mechanical performance was similar to that of the control samples.

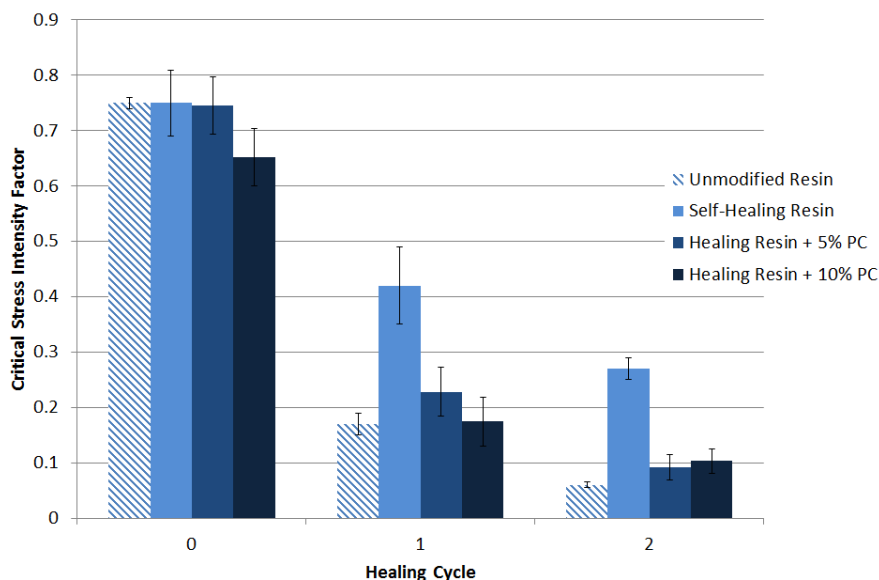


Figure 48: Recovery of fracture toughness of resin modified by healing agent and propylene carbonate (PC) diluent. ‘Unmodified’ resin contains no healing agent or diluent and represents the control

5.2.4 Bisphenol-F Blend

The inclusion of Bisphenol-F type resins was also suggested and was investigated. Bisphenol-F resins, as discussed in the experimental section, are generally lower viscosity at room temperature and give excellent mechanical and chemical performance after cure. They are often blended with bisphenol-A resins by resin manufacturers for these reasons. However there does tend to be a cost penalty for these resins which will be discussed. A standard bisphenol-F resin which was used is Araldite PY 306 from Huntsman Advanced Materials. As they have the same reactive chemical groups there is no change to the cure procedure other than to take the epoxy equivalents of the bis-f (159-170) resin into account.

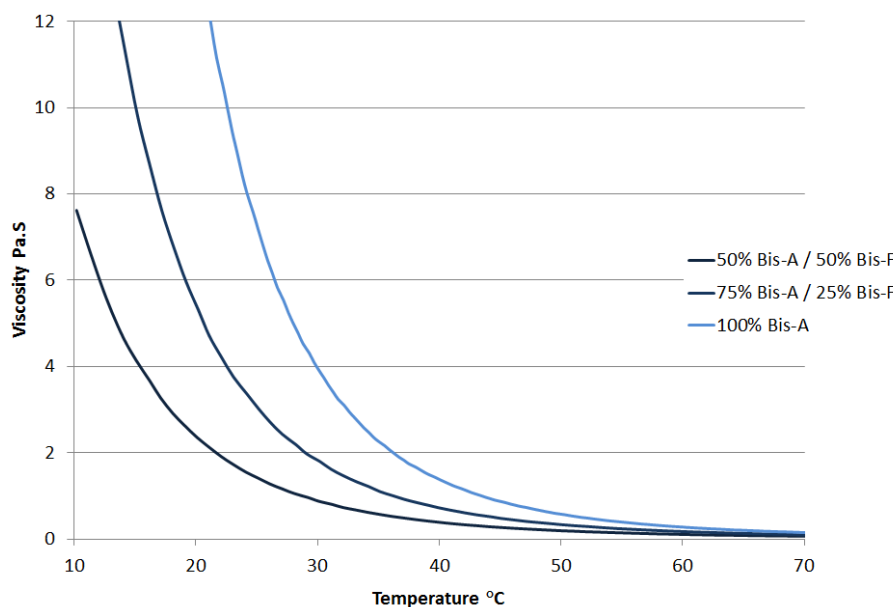


Figure 49: Change in viscosity with changing concentration of Bisphenol F resin (PY306).

5.3 Discussion

The solid state self healing method which has been described in chapter 4 has been further developed. The original formulation developed by previous studies involved the modification of a standard acid-anhydride-cured bisphenol-A epoxy resin with a long linear bisphenol-A thermoplastic material which could provide mechanical recovery after fracture. This has been found to provide reasonable healing with high temperature, but manufacture and handling of the resins were a significant problem. The extent of this problem was assessed in the previous chapter and targets for the modification were set.

The resin was modified by several methods which had been proposed from various sources. Methods of assessing the recovery and mechanical performance of the resin were compact tension and tensile testing procedures. Initial trials focused on the quantification of the viscosity problem which had been noted. Figure 41 on page 81 shows the viscosity of the blends with different concentrations of healing agent, from the previous chapter. This was discussed in more detail in Section 4.5 on page 76 but may be summarised by saying that too high a temperature is required for processing

of self-healing resins with a concentration of healing agent high enough to impart a useful degree of healing.

The viscosity of the blend with 7.5 wt% addition of healing agents of different molecular weights are shown in Figure 42 on page 82. The drop in viscosity with a lower molecular weight variant of the same healing agent is expected as there is less hydrogen bonding between the chains of the polymer network. There are also likely to be fewer chain entanglements. This leads to lower energy being required to move the chains through the structure, lowering viscosity. It also may be thought that chains which are more free to move through the monomers will create less 'friction' in the liquid which is measurable as viscosity. The 6100 g/mol healing agent and the 4000 g/mol healing agent both reduced the viscosity of the blend significantly even at the same level of loading. Figure 43 on page 83 shows the fracture toughness recovery for such blends and it appears that these lower molecular weights impart equally good healing to the resin within experimental error. It may be said that the lower molecular weight species have an effectively lower activation energy for their movement and therefore their healing actuation. As these samples were healed using the same healing cycle time and temperature conditions it may therefore be that the lower molecular weight species had effectively more energy with which to move. Therefore, although they might recover strength more quickly under the same conditions, it may be that the longer healing agent has the ability to recover more strength with its additional bonding but would require longer time to reptate and equilibrate in the structure. It is the opinion of the author that there will be a compromise in molecular weight of the healing agent. Not simply a balance of healing time to strength recovered, but that there will be an optimum length of healing agent molecule where the strength of the statistically probable quantity of chain entanglements exceeds the strength of the covalent bonds which bridge a crack. In this case, additional length of a healing species providing greater entanglement leads to no more healing capability, and will only serve to slow the healing process

by an effective increase in the activation energy for the healing process.

The heaviest molecular weight healing agent blend did not enter the useful viscosity range for RTM even at temperatures up to 100°C which was the upper thermal limit of the test. As the lowest working cure temperature of the 828 resin cured with NMA was 90°C it would be extremely unlikely that any process could use handling temperatures this high. Figure 40 on page 75 from the previous chapter shows that the gel time for this formulation at 90°C is around 50 mins. For safety reasons it is also unlikely that high temperatures would be used. The lower molecular weight variants, however, fall within the usable region at approximately 70°C. This is of course with no curing agent, and therefore the viscosity of the overall resin to be infused will be significantly lower. This work might serve as a useful starting point for a more detailed and focused investigation into the rheology of infusion resins which could include a complete test matrix of resins and components before mixing, and of isothermal cure by oscillation mode cure monitoring.

Figure 44 on page 84 shows the effect of the diluent on the viscosity of the unmodified resin. As expected the diluent decreased the viscosity, with a 10% loading by weight equating to a reduction in viscosity similar to an increase of approximately 15°C. This was an important find as it is the primary function of the diluent. It was further investigated how this was influenced by the addition of the healing agent to create a self-healing resin. Figures 46 on page 85 and 47 on page 86 show the combined effects of the diluent and the healing agent. The viscosity increase of the healing agent was largely offset by this use of an extremely low viscosity diluent. 20% diluent reduced the viscosity of the self-healing resin to less than that of the unmodified resin below 50°C. It would have been expected that 20% diluent would, however, have severely impacted the mechanical performance of the resin to the extent that it could not be used for any high performance application.

The compact tension testing of these samples, however, showed a much less beneficial effect. Figure 48 on page 87 shows the recovery of fracture toughness of the

diluent-modified resins. The self-healing effect has been almost completely removed. Samples with diluent recover approximately the same percentage of toughness as the control sample. The healing efficiencies of the new resins were 26.7% for the 10% diluent and 29.7% for the 5% diluent compared to 57% for the standard formulation of the self-healing resin, and 23% for the control resin without any healing agent. These findings make it clear that this diluent at least cannot be used for this purpose as it almost completely inhibits the healing function of the healing agent. There are several possibilities for the method of this action. It is possible that these small molecules consume required free space between molecules in the polymer network. It has been suggested in other work that the method of reptation of the healing agent requires a certain amount of free space to occur [133]. Without being able to reptate through the structure the healing agent cannot move across the crack interface and therefore cannot lead to any recovery in strength. Alternatively, it may be that the diluent simply does not react into the matrix. The acid anhydride curing reaction, which is detailed in the experimental section, does imply that further crosslinks of different chemistries would not be able to bond directly into the structure, which is almost a self-assembling alternating reaction of epoxy and anhydride monomers caused by a cycling polar attraction. If the diluent fails to react into the matrix then the mechanical properties would be damaged so severely that the healing agent would have little effect. This effect could be demonstrated with a simple tensile test to ascertain the ultimate tensile stress and Young's modulus. It would be immediately apparent if the diluent was contributing to or had improved the mechanical performance. Once this had been proven it would be of scientific interest why this diluent had removed the recovery of the self-healing resin.

The final assessment was of the use of a bisphenol F resin in place of the standard bisphenol A. The rheometry of the blends can be seen in Figure 49 on page 88. The reduction in viscosity of the bisphenol F resin blend was much more apparent than was expected. An inclusion of 50% bis-F resin reduced the viscosity by a factor of

10 compared with the pure bis-A. A pure Bis-F resin was not able to be tested as it was in powder form. It was expected that, since it would not affect the chemistry of the curing reaction, the self-healing technology would work equally effectively with a bis-F resin. However these resins are much more expensive and this would have to be taken into account when designing a component or manufacturing process to determine the level of bis-F required to optimise costs. Further testing could be done on a purely bis-F formulation of the resin with an assessment of the full mechanical properties as a follow-on project.

5.3.1 Compact Tension Testing Fracture

Compact Tension testing has been used a considerable amount in this study and in previous proof-of-concept studies which laid the foundations for this technology. The fracture toughness of a material is one of the most important fundamental properties of a material which does not change through size or geometry and is one of the most influential factors taken into account by engineers in the field when selecting materials for a particular application.

While fracture toughness assessment may be a sound approach, there are dangers in assuming that the results provide a complete assessment of the material being tested and, more importantly perhaps, of the technology being developed.

It is easy to apply methods which have been laid out in standards without understanding the limitations of those methods. In order to clarify where the problems may lie, a brief history of the development of fracture mechanics is presented which is important to our understanding of whence the equations have been derived.

As the understanding of the fracture of materials has increased, in the theoretical fields at least, and the solutions to load calculations become more complicated, understanding by the technical and research members who carry out the materials may have, if not fallen, then at least become more abstract. The fundamental understanding of relationships between material properties can be clouded by polynomial

equations which have been calculated to ‘best-fit’ a scatter of values.

5.3.2 Irwin and the development of Standards

Once Irwin had completed his seminal work[144] and it had been recognised how important the theory of fracture mechanics was, development started on Standards which could be used to quantify fracture toughness for all materials to allow for better design and material selection in the future. The test procedure for the measurement of fracture toughness was standardized by the American Society for Testing and Materials (ASTM) which, among other standards institutes, lays down guidelines to create repeatable testing and consistent methods to be used across many research institutions. While it is true that the appeal of the K concept for fracture toughness is in its universal applicability, there are a few requirements of the test procedure in order to ensure a plane-strain condition at the fracture tip for the resulting value to be a measure of fracture toughness.

1. All characteristic specimen dimensions must exceed 25 times the expected plastic zone size at the crack tip.
2. For plane strain conditions at the crack tip the specimen thickness must exceed at least the plastic zone size.

It is not easy for many experimenters to calculate or verify if their tests meet these requirements so there is a heavy reliance on the standards to produce methods which achieve consistent results.

5.3.3 Difficulties in implementation of Standard Testing

One of the issues with the use of standards is that often it is not taken into account what errors in the measurement of samples equates to in the subsequent calculation of fracture toughness.

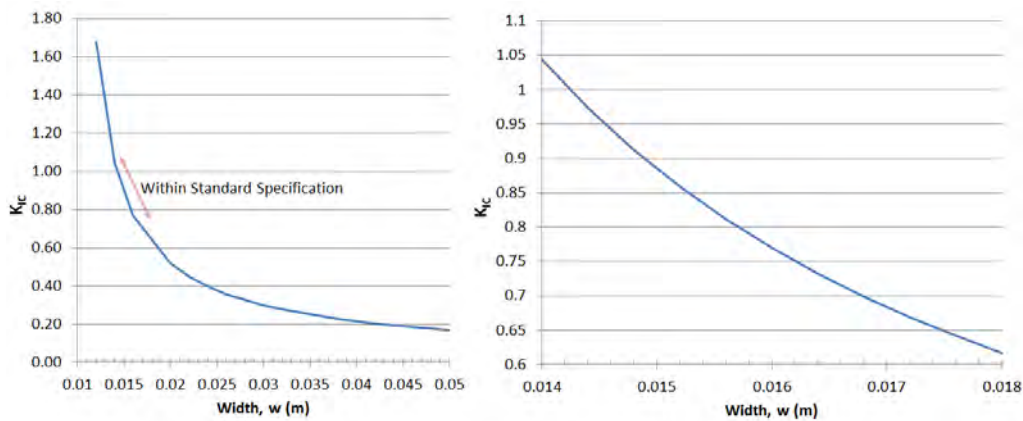


Figure 50: The effect on calculated K_{IC} of measuring the width of the specimen

Figure 50 shows the effect of the measurement of the width of the specimens on the calculated K_{IC} , and Figure 51 shows the direct effect of initial crack length measurement. Inset in both figures is detail showing the area which is permissible within the limits of the specification for the set load and crack length/width conditions.

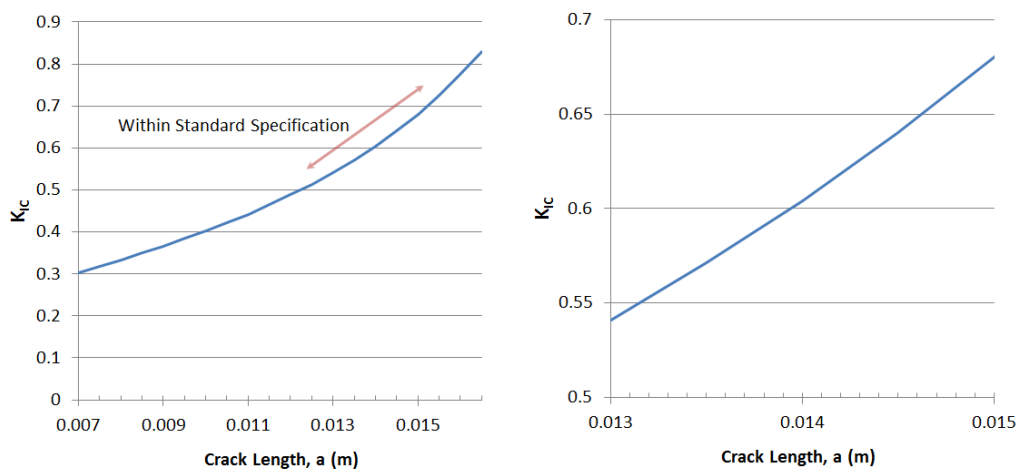


Figure 51: The effect on calculated K_{IC} of measuring the initial crack length

Further to this, Figure 52 shows a comparison of the polynomial calculations for geometry calibration factor for the two main competing standards. While these are extremely close in the narrow margin of the standard limits, there still exists a great effect on the final calculated fracture toughness for both calibration factors.

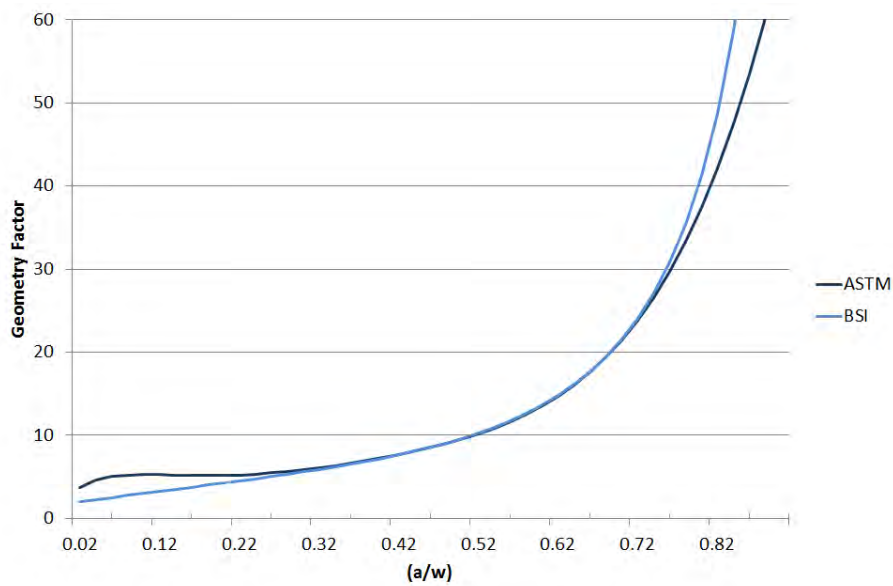


Figure 52: Comparison of ASTM and BSI polynomials for calculating the geometry factor from the initial crack length (a) and specimen width (w)

It can be shown that a measurement accuracy of $\pm 0.5\text{mm}$ of the initial crack length and width in a measurement of fracture toughness of $1\text{MPa}\cdot\text{m}^{\frac{1}{2}}$ with an error of $\pm 0.11\text{MPa}\cdot\text{m}^{\frac{1}{2}}$, represents an 11% error. This can be calculated using the following example measurements and equations from the ISO Standard shown in the Experimental section:

$$a = 0.012 \text{ m} \pm 0.0005 \text{ m}$$

$$w = 0.024 \text{ m} \pm 0.0005 \text{ m}$$

$$h = 0.012 \text{ m}$$

$$F = 200 \text{ N}$$

Lower Limit

$$f\left(\frac{0.0115}{0.0245}\right) = 8.81$$

$$8.81 \times \frac{200}{0.012 \times \sqrt{0.0245}} = 0.94 \text{MPa.m}^{\frac{1}{2}}$$

Upper Limit

$$f\left(\frac{0.0125}{0.0235}\right) = 10.70$$

$$10.7 \times \frac{200}{0.012 \times \sqrt{0.0235}} = 1.16 \text{MPa.m}^{\frac{1}{2}}$$

$$\therefore K_{IC} = 1.05 \pm 0.11 \text{MPa.m}^{\frac{1}{2}}$$

So large a margin of error can be found even with no range of measured values from repeat experiments. This means that such error is likely to be introduced in any measurement of fracture toughness by this method, even before repeat experiments are carried out, as per the standard. There are several factors that aggravate this situation. A process in which an individual researcher is responsible for every stage (as is inherent in PhD activity in the drive to gain experience at every level) admits the possibility that measurements confirming expectations might be favoured, albeit subconsciously. However, it is very often not noted down as a source of error, indeed is frequently not even perceived as such. So although used samples are compulsorily retained there is little or no recourse to re-measurement or independent verification. In other fields, notably medicine, measurements are purposely performed ‘blind’ in order to preclude this danger of expectation fulfillment. Another factor is the very nature of the property to be measured, a crack being intrinsically irregular and open to variations of measurement, albeit very small. In addition the inability

of the researcher to position the measuring instrument accurately and consistently conflicts with the equipment's precision of $\pm 0.01\text{mm}$ making it difficult to achieve measurements of incompletely fractured samples to the standard requirement of $\pm 0.02\text{mm}$. Yet without the specimen being split in two, which would preclude healing, a more precise measurement by microscope is not available. Thus small inaccuracies of measurement, when entered into a standard polynomial equation, can be magnified into seemingly significant results because the error margin cannot be quantified or verified. It is also very important to note that these errors are not systematic. It could be argued that a systematic error might be ignored as all the results would be skewed evenly and without bias by the type of test, so other tests done to the same standard would be similarly influenced. This is not the case with the errors described above.

5.3.4 Standard assessment of self-healing materials

The overriding source of difficulty for the presentation of data from self-healing composites is the materials testing standards which are detailed by British Standards Institute (BSI), the International Organization for Standardization (ISO) and the American Society for Testing and Materials (ASTM), which are not equipped to test materials designed to recover properties.

The main difficulty is that existing standards have largely been devised to test specimens to destruction, in order to create load/displacement data for the sample of material. For example, short-beam shear testing may be used on composite samples to determine the inter-laminar shear strength. However, in order for the test to complete under the terms of the ISO Standard, the laminate must separate, thereby destroying the geometry of the sample, and with it any hope of healing using chemical means, which is the only actuation method used in most intrinsic self-healing technologies. Hence non-standard methods have more commonly been employed in the field in order to evaluate the beneficial effects of the technology more

accurately. These novel methods range from ‘Mode-I’ 4-point bend testing [70, 73], ‘notched’ compact tension, ‘geometry-modified’ single edge notched bending [147], tapered double cantilever beam [148] and visual methods [149, 150, 95]. However, the industrial requirement for standards is so that materials may be directly compared in all aspects and an appropriate selection made. While it would be difficult for the Standards bodies to institute, or even make available, standards which would create comparable data for drastically contrasting technologies, it may be in the interest of the industry to create a new set of testing protocols.

The principle for the creation of the compact tension standard for metallic materials is that a fatigue crack is introduced in the sample at the notched, or chevron, edge. The sample is cycled below the plastic limit (less than 60% of the K_{Ic}) until a crack begins to grow and an extremely sharp crack tip is created. However for polymer samples other problems arise. It is often not possible to initiate a fatigue crack in very brittle samples, and largely they do not exhibit work-hardening effects which are the methods by which an embrittlement of material at the crack initiation site creates a brittle failure.

The two main standards for testing fracture toughness (ISO 13586:2000 and ASTM D5045-99) specify the procedure for single-edge notched bending (SENB) and also for compact tension testing (CT). Both of these procedures insufficiently define how to initiate an adequately sharp crack in a brittle thermoset polymer specimen. Details of crack preparation are often missing from published literature on these testing methods. One paper suggests that a typical procedure would be to cool a razor blade in liquid nitrogen before tapping it on the specimen, but points out that the crack sharpness is dependent on the blade temperature which will vary, and also that the crack needs to be demonstrated to be reproducibly sharp. It is mentioned in both standards, and the preceding discussion, that a sufficiently sharp crack is a prerequisite for toughness measurement.

The three stages of crack creation in a compact tension specimen are shown in

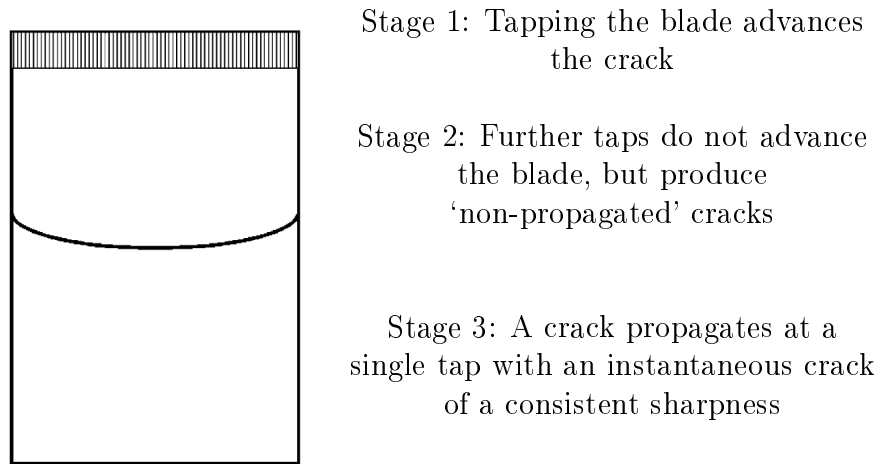


Figure 53: The three stages of crack propagation by razor tapping from [147]

Figure 53. The first stage the blade sinks into the sample a short way with each tap. At the second stage further taps do not appear to produce deeper penetration of the blade. At a certain time, quantity of taps or force later a stage 3 crack will propagate uncontrolled through the sample instantaneously with a tap. This uncontrolled crack would occasionally completely break the sample in half which would have to be disposed of. Often, and due to limited experience in gaining this delicate technique, it is believed that the tapping was stopped earlier so as not to risk destruction of the sample. This would add random errors in the collection of reliable fracture toughness data. This perhaps excessive reverence of samples was due to the large time and expense of creating them to begin with. There is intrinsic difficulty in casting the specimens as air bubbles can be introduced either in pouring the degassed mixture into the moulds, or as gasses evolved during the cure. These small bubbles are often not easily noticed at the time of creating the samples, but can cause significant problems with testing and mostly must be removed from testing. As the thermosets are extremely brittle, it was often the case that one or two were

cracked or lost during the machining process, which itself took a large amount of time and added expense. Furthermore, some of the samples while testing developed a crack which was not perpendicular to the testing direction and consequently was not arrested by the hole. This meant that the sample could not be healed and therefore was discarded. For these reasons, several times during the project, groups of samples would be created and, after several months, too few samples yielded valid test data to complete the minimum 5 specimens required by the specification and the entire process would need to be restarted. This not only cost a large amount of money, but caused time to be spent investigating avenues which the tests would show, much later, were non-starters. To circumvent this problem in future I would suggest either the number of specimens is increased 10-fold, which may be infeasible due to cost, or an alternative testing method should be sought. It has been suggested in the literature that an improved method of testing for fracture toughness is the modified single-edge notched beam method detailed in [147]. This method has the benefits of a well-defined crack preparation procedure, as well as a simple sample geometry which does not necessitate the use of a machine shop, which would enable many more samples to be created in less time and at less cost, vastly improving the quantity of results and the efficiency of obtaining them.

5.4 Conclusion

Several further developments to the formulation of new self-healing resins have been proposed, with their rheology and healing behaviour characterised. The use of an optimum healing concentration has previously yielded an improvement in healing efficiency and this can now be contrasted with its processing difficulties. Reductions in viscosity have been achieved by the use of lower molecular weight healing agents, inclusion of a reactive diluent and by the use of a lower viscosity host resin. The healability has not been improved, but several methods have shown that a reduction of viscosity and therefore an improvement in processability may be achieved without

necessarily a reduction in healability.

Rheology was used for the first time in the assessment of these resins and was very successful in producing a large amount of useful data which will serve as a starting point and reference for new students taking on more research in this area.

It has been shown that the determined fracture toughness of a test specimen is in a significant way affected by the measurement of, or rather the inability to measure, the initial crack length. Problems with inconsistent data are compounded by the difficulty in obtaining a consistent crack in specimens. Compact tension testing was assessed and several shortcomings highlighted particularly in the context of this type of study with limited staff, resources and time. Specimens took too long to manufacture, were too expensive and were inconsistent. An improved methodology is required, and a suggestion is made of the modified SENB test.

It is also discussed that standards need to be created to facilitate the measuring and comparison of self-healing thermosetting polymers, and that standards bodies or institutions would be instrumental in creating precise methodology which would remove several potential sources of error which at the moment may be clouding the veracity of the results. These new testing procedures could help bring the self-healing field sharply into focus.

6 Manufacture of Sensing Panel

6.1 Introduction

This chapter addresses Aim 2 by the completion of Objective 3 from Section 1.2 on page 16. The manufacture of the electronic connections to the carbon fibres is one of the difficulties for implementing a self-sensing system based on this design. Experimental details for this work is shown in Section 3.11.1 on page 61.

To activate the self-healing resin it must be heated to above the healing temperature which provides the healing agent molecules with enough energy to reptate through the interpenetrating network. The design of the sense-and-heal which is under investigation provides this heat targeted to the damage site so as not to compromise the wider integrity of the structure during an in-situ heal. The targeting may be achieved in a similar manner to how the damage is located, by resistive heating of the area by passing a high current down the carbon fibre channels where the damage was detected. In this way the heating is only applied to the area which has been damaged by an impact event and not to the whole panel. Resistive heating is an effective method to provide energy to the damage site as the carbon fibres themselves carry the thermal energy, and they have very high thermal and electrical conduction. Breaks and gaps between the fibres, such as are expected to occur at the the damage site provide areas of higher resistance and therefore increased localised heating.

6.2 Self-Sensing Plies

The manufacturing route of the self-sensing plies was one of the most important factors in terms of the quality of copper which was available on the flexible circuit boards. High quality tracks will lead to fewer faults in the circuits and lower resistance of the copper tracks. A low track resistance means that a greater voltage drop is available down the carbon fibres which allows for a greater resolution of sensing

damage. Furthermore, a lower resistance of track can allow a higher power to be applied for the actuation of the healing event.

Several manufacturing routes were tested as explained in the experimental section 3.11.1 on page 61. These included:

- Photo-sensitive Film
- Inkjet Masking
- Direct silver printing

The results from the manufacturing processes were assessed. The photosensitive film was the original method used for the manufacture and its use is detailed in Section 3.11.1 on page 61. However the quality of tracks have been slightly variable, therefore two alternative manufacturing routes have been conceived with which to compare the original results.

6.2.1 Inkjet Masking

The inkjet masking removed four stages of manufacture before the etching could take place. These stages were the adhesion of the dry photosensitive film to the copper substrate, the printing of a acetate UV-light mask, using the light box, and finally developing the mask before etching can take place.

The inkjet mask circumvents these steps by providing a mask directly onto the copper which the chemical etchant cannot remove. This had the potential to save more of the copper, as well as time and cost with expensive chemicals for etching and developing, and also to improve the consistency of the resultant tracks.

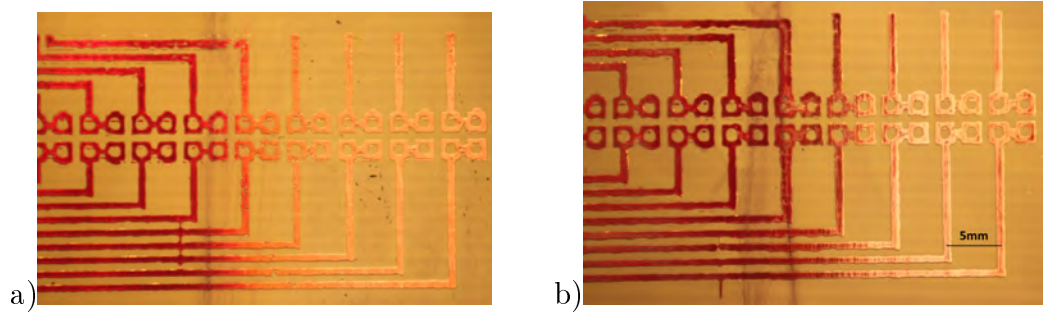


Figure 54: Images of Inkjet mask printed with various colours, with a 20 minute oven air dry post-print cycle. Right hand side of each image shows the mask partially removed with acetone. a) standard quality. b) photo quality

Figure 54 shows the images of the masks after etching, with their masks partially removed with acetone. The quality of the tracks looks good. Details of the tracks can be seen in Figure 55. Several printing options were investigated to determine the optimum parameters of the inkjet printing method. Print Quality determines the resolution of the print. It was thought that this would have an effect on the accuracy of the tracks. The two options for this parameter were ‘standard’ and ‘photo’.

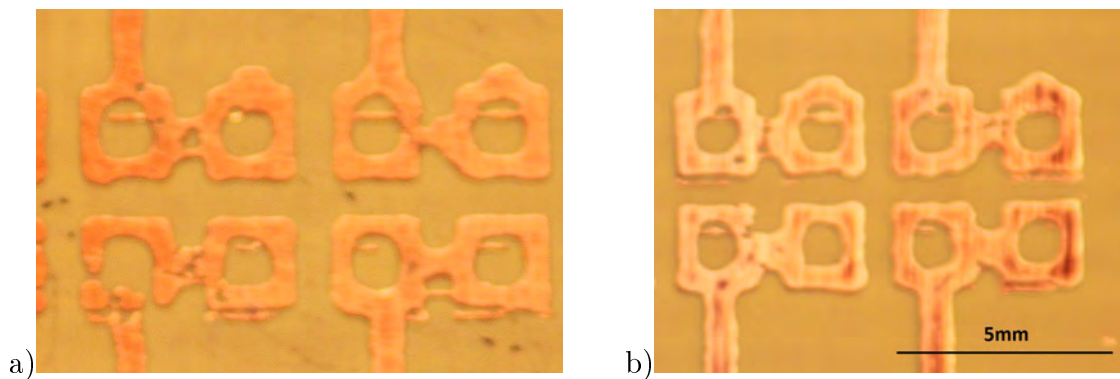


Figure 55: Detail of track quality: a) standard quality, and b) photo quality

There was no visible of electronic differences between flexible circuit boards made with either a standard or photo quality mask. This can be seen in Figure 55. The surface of the copper led to the ink pooling within a few seconds of it being removed from the printer. The wetting of the surface was noticeably poor compared to paper or acetate. This made the resolution of the printing irrelevant as a mask printed

with a slightly finer detail of pixels would pool together equally quickly. The masks which were printed with different colours, however, showed much more contrasting results. Detail of these tracks can be seen in Figure 56.

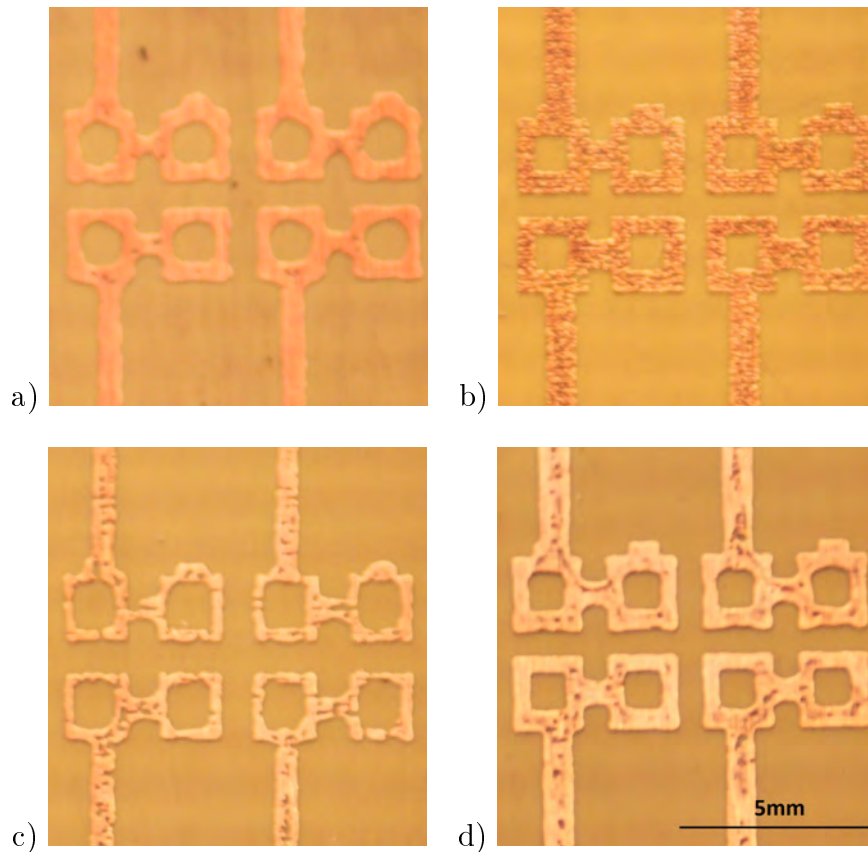


Figure 56: Track quality comparison of flexible circuit boards created by using a mask printed with the 4 colours of the inkjet printer head: a) cyan, b) magenta, c) yellow, and d) black.

Tracks on circuit boards made with inkjet masks of different colours provided results with much more variability. Figure 56 shows the results of masks of the 4 colours on the print-head; cyan, magenta, yellow and black. These are the most common colours for printing (CMYK). It is apparent that the inks have different wetting properties and create a contact angle with the substrate related to the surface energy of the ink. The cyan ink (Figure 56a) gave the most consistent track quality. Although the magenta ink showed the most accurate geometry of tracks, the copper had a stippled surface which gave a lower conductivity and occasional tracks breaks which can be very detrimental to the self-sensing ability of the panels created. Yel-

low ink does not seem to provide as much resistance to the etchant chemicals as can be seen in Figure 56c. Black ink appeared to provide tracks with a balance of accuracy and consistency of tracks.

In order to improve the wettability of the surface of the copper an attempt was made to change the surface chemistry. This was achieved with a pre-treatment of 15 minutes in an air convection oven at 90°C to slightly oxidise the surface. Resultant tracks can be seen in Figure 57.

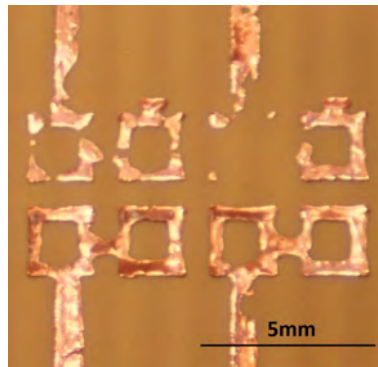


Figure 57: Mask created with a copper pre-treatment of 15 minutes in an air convection oven at 90°C.

The oxidation of the surface did appear to improve the quality of the printed mask, however the oxidised surface of the copper took twice as long to etch, and the mask did not provide enough protection to the copper underneath to prevent the removal of copper from the tracks, seen in Figure 57. Therefore this method was abandoned. A final approach was to combine the parameters to provide an optimum mask using the current inks and printer.

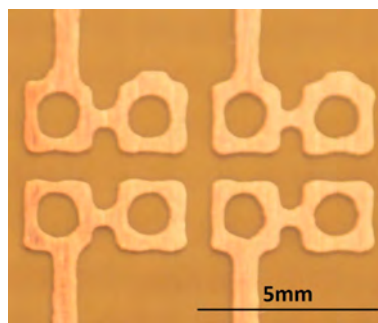


Figure 58: Final print mask quality.

Figure 58 shows the combination of beneficial parameters selected: Colour R0 B180 G0, Photo Print Quality, 20 minute air dry. These parameters provided the best quality and consistency of tracks.

6.2.2 Direct Silver Printing

An alternative manufacturing route was the direct printing of silver onto the Kapton film using a specialist printer. The first attempt of this trial can be seen in Figure 59. This method was by far the quickest and simplest in terms of the repeat manufacturing times, saving an enormous amount of time for the manufacture of the self-sensing panels. It was also much easier than the dry film method for changing the design of the artwork for each panel without having to replace a light mask. As no chemical developing or etchants were needed it also saved costs of these consumables, as well as removing hazardous materials and waste from the labs. Although the overall quality of the tracks can be seen to be high in Figure 59, there were some problems with the technique.

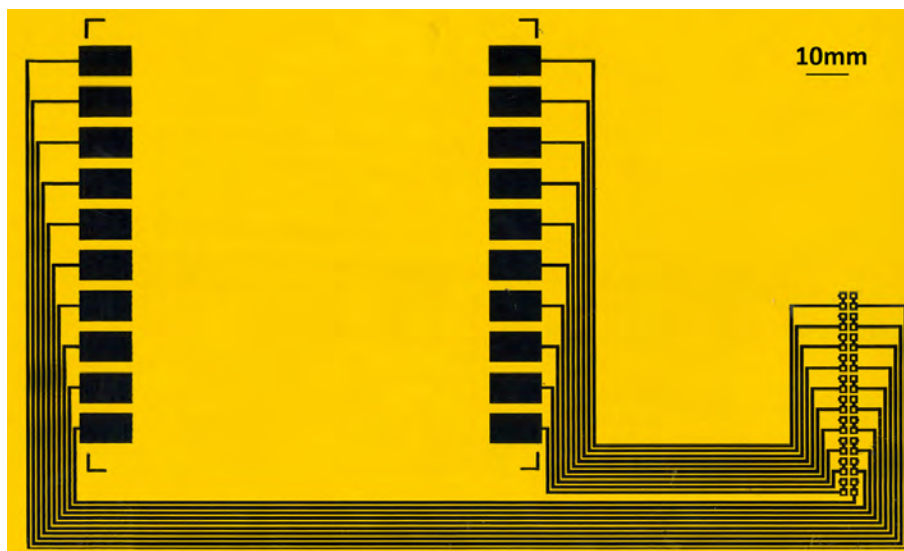


Figure 59: Artwork produced with direct silver printing.

Figure 60 shows selected details from the direct silver printing artwork shown in Figure 59. Figure 60a shows that a tiny fibre which had become attracted to the

electrostatic kapton film had electrically broken the silver track during the printing. This was a significant problem with the silver printing as it was very difficult to prevent such particles from becoming attracted to the film during preparation in the lab. Further tests were conducted with an additional step of washing the film surface with acetone prior to printing but similar effects were seen. Particles of extremely small dimensions would still cause significant problems to the consistency of the tracks produced.

Figure 60b shows that line spacing while printing tracks perpendicular to the moving direction of the print head had issues. It was thought to be associated with small amounts of movement of the film during the printing process which caused misalignment of the printing lines on a very small geometric scale. An increase of line-printing density partially ameliorated the problem. An alternative method to remove this problem was to program the printer to move in a vector mode, always printing parallel to the track direction, rather than standard raster mode as most printers. While this would have been possible with the equipment which was being used, time and cost limitations put this type of work outside the scope of the current project.

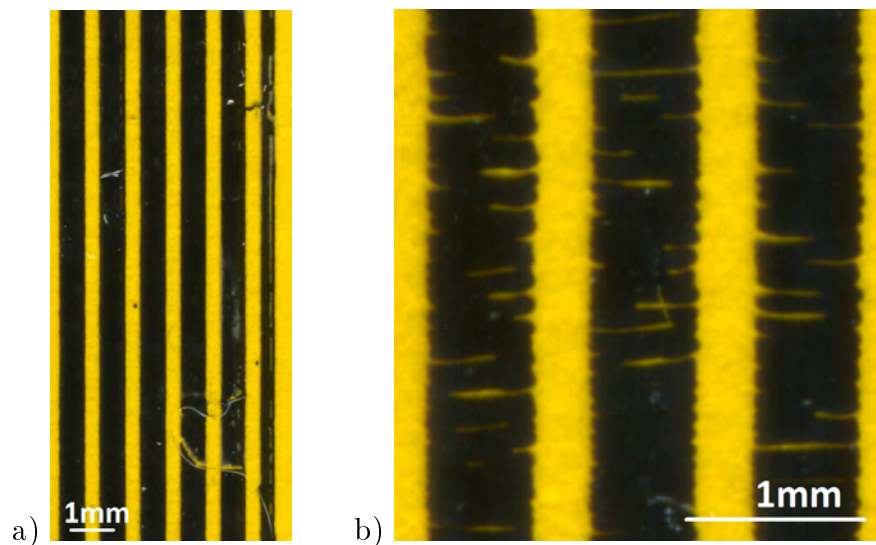


Figure 60: Silver printed artwork detail. a) Inclusion causing track damage. b) Line spacing causing track break.

6.3 Small Panel Resistive Heating

To test the heating actuation of the self-healing resin system it was necessary to produce some small-scale panels. These panels were manufactured from prepreg material and laid-up as described in the experimental section. It was decided that the dry-film track etching method was the most consistent and suitable for the best contacts and panel performance.

6.3.1 Thermography

To assess the ability of the panels to provide heating to a damage-affected zone, 4 panels were manufactured and then impacted. Heating was achieved by connecting the panel to a current-regulated supply system, so that the current and voltage could be balanced to achieve the target heating power. Two power levels were selected to try and detect the temperature rise down the channel. Two watts and six watts were used and the temperature was equilibrated for 3 minutes. Thermal imaging was done using an Electrophysics PV320 infra-red camera connected to a PC via USB with Velocity 2.1 software to perform the data capture and analysis. Panels which had been impact damaged were used to see whether the damage area was targeted by the heating. Results can be seen in Figures 61-64 from panels with a range of different contact widths. The main points to notice in these figures is the point of impact in the centre of the image, the contact area connecting the electrical sensing circuitry to the carbon fibres which is at the top centre and bottom centre of the images and the ‘channel’ area of heating between the 2 contact areas.

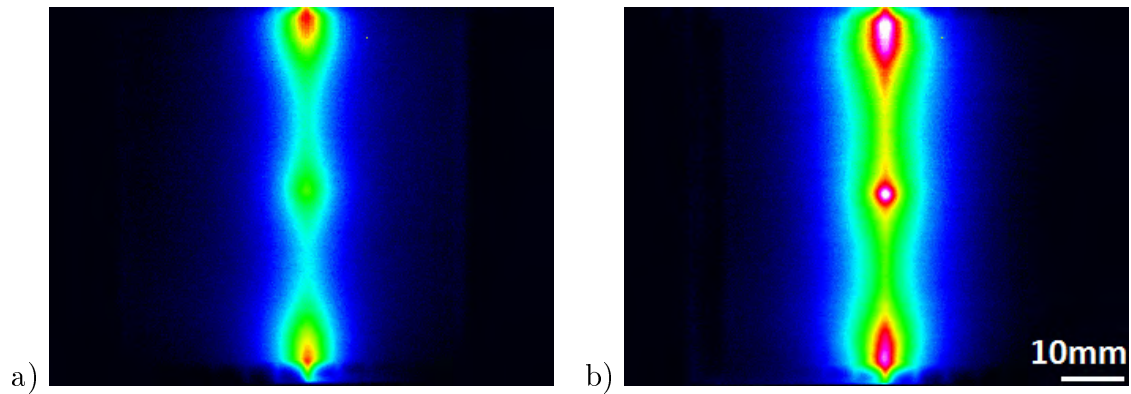


Figure 61: Infra-red thermography of a panel with **1.25mm** contact widths targeting damage using 2W of heating power: a) Front face, and b) Back face

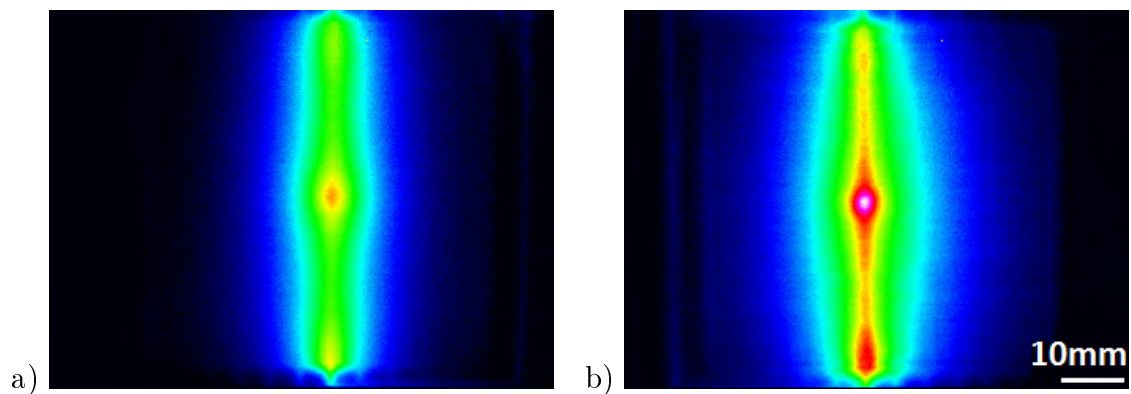


Figure 62: Infra-red thermography of a panel with **2.5mm** contact widths targeting damage using 2W of heating power: a) Front face, and b) Back face

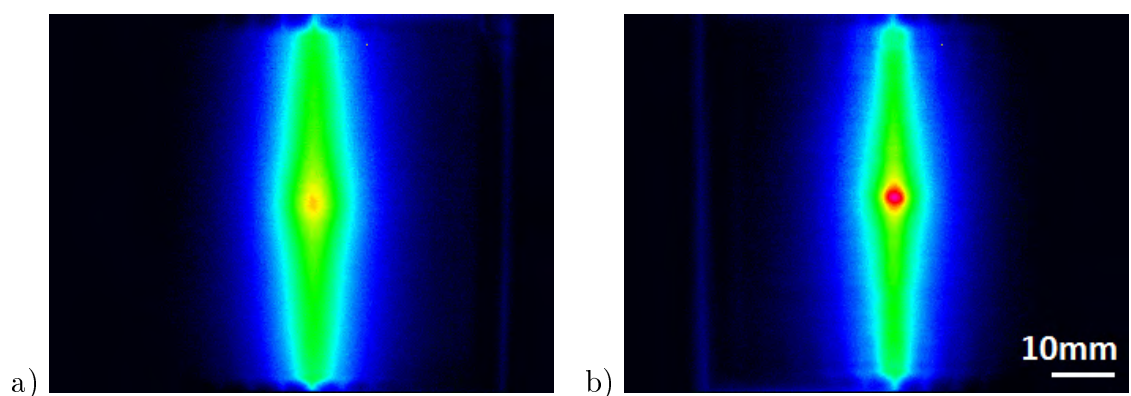


Figure 63: Infra-red thermography of a panel with **5mm** contact widths targeting damage using 2W of heating power: a) Front face, and b) Back face

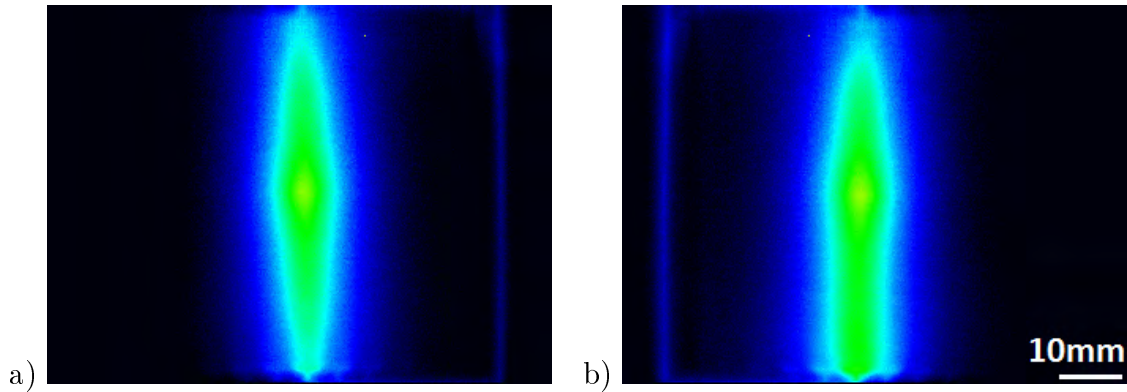


Figure 64: Infra-red thermography of a panel with **7mm** contact widths targeting damage using 2W of heating power: a) Front face, and b) Back face

Figure 61 shows a panel with the thinnest contact widths in contact with the carbon fibres of the prepreg. It can be clearly seen that even without calculations or interpretation of the data that there is significant heating of the contact zone at the edges of the panel. Moreover, heating of the contact zone is even higher than at the damage site. The extent of this increase in temperature will be investigated in further detail later. For contact widths of 2.5mm shown in Figure 62 this effect is significantly diminished. Here the temperature is seen to rise only to around that which is shown at the damage site. This correlation is further demonstrated with the other increasing contact widths, with 5mm showing an even more targeted effect. However it may also be noticed that the copper track which goes around the edge of the panel begins to heat up increasingly with increasing track width. This can be seen as the blue line at the edges of the figures, increasing in intensity to a maximum in Figure 64. This is due to the increasing relative track resistance to that of the target channel. As the contact width increases, so too does the number of carbon fibres which are connected across the panel width. As the current has many more pathways this has an effect similar to connecting many small resistors in parallel. The resistance of the channel drops, meaning a higher current is drawn for the same voltage. At a lower voltage, a higher percentage of the voltage drop is across the circuit board, rather than the panel. This in turn means that the resistance of the

copper tracks on the circuit board, which has not changed, is proportionally larger and therefore dissipates that higher proportion of the energy being used to heat the panel.

While this in itself is not considered a failing, it does put more electrical load on the connections, wiring, power supply and tracks of the flexible circuit board, and is also considered to be a waste of energy.

It is possible to plot the pixel intensity as a graph in order to show the relative intensity of the heating for 2 watts and 6 watts as shown in Figure 65.

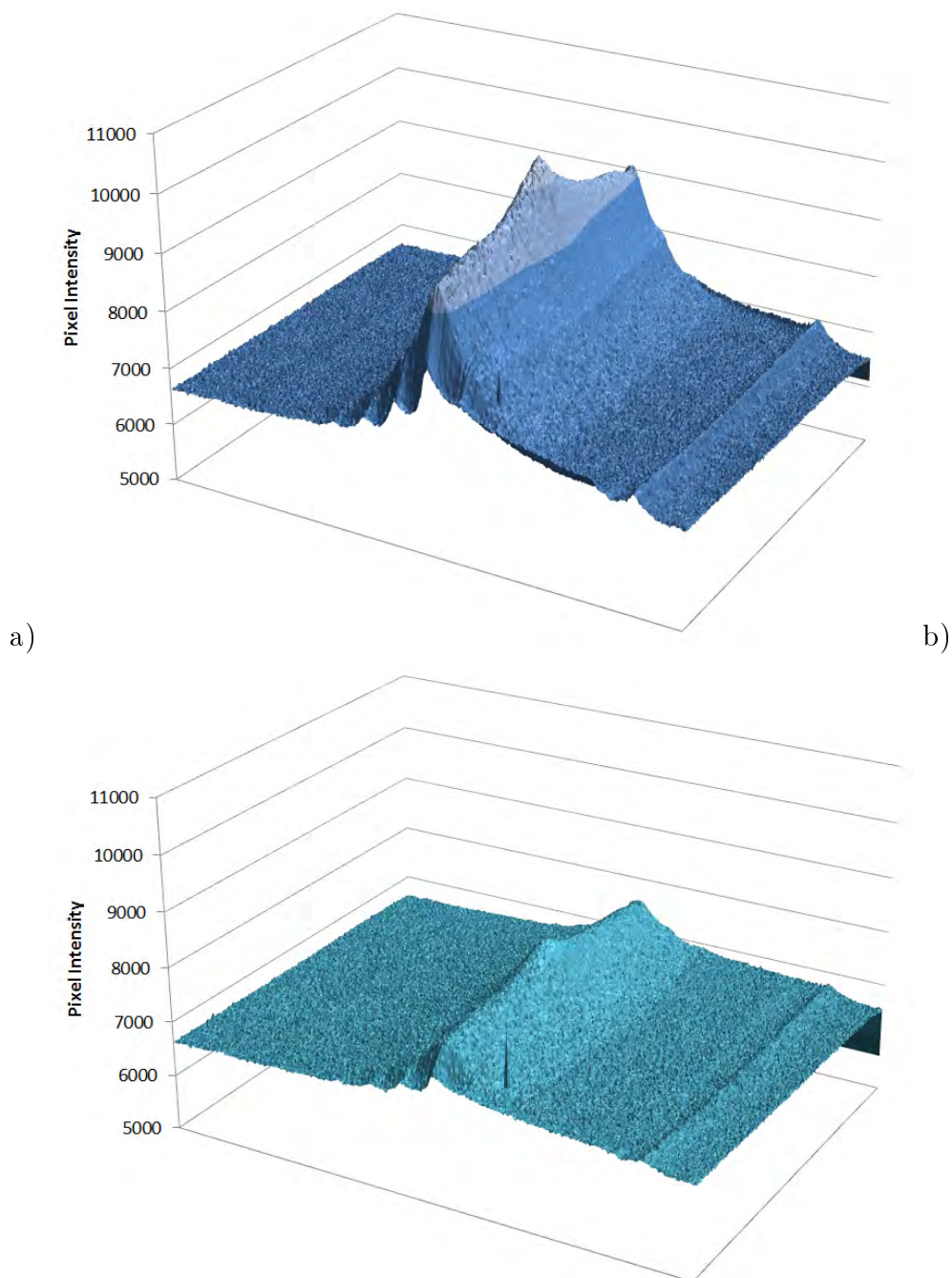


Figure 65: 3-dimensional graphical representation of temperature increase across the panel area during single-channel heating of a damaged specimen (damage can be seen as a temperature spike in the centre). Both tests were done on a panel with 5mm contact widths like those in Figure 63. a) 6W of heating power, and b) 2W of heating power.

When equating the intensity of a pixel to an exact temperature a formula was used to calibrate the results. For each of the tests conducted, thermocouple readings were

taken at the contact point and the area of highest damage. This was to calibrate against the infrared camera data which is less reliable with absolute quantities. This data is shown in Table 5 on page 116. To reduce the pixel intensities a simple linear first order equation was used as there were two known points measured with surface thermocouples which could be used for the calibration. It had been noted during the experiments that the infra-red camera sensor readings had a tendency to ‘creep’, meaning an object being viewed under isothermal conditions would gradually read a higher and higher temperature in the IR camera software. This was thought to be due to the internal electronics warming up. It was recommended to turn on the camera for at least 30 minutes before use to allow the internal ambient temperature compensation system to equilibrate, however this seemed to ameliorate rather than eliminate the issue.

Two basic parameters were calculated for the conversion as it was assumed that there would be no exponential element to the correlation between intensity and temperature. While this assumption may not be true, only two absolute temperature readings were taken and therefore were available for calculation. The high temperature conductivity of the carbon fibres meant that a fairly low spatial resolution of thermocouple readings would have been possible and, had a large number of thermocouples been used, this would have led to an extremely short time frame for reading each value. While this may be argued to have improved the accuracy of the absolute temperature graphs, errors would likely have been exacerbated by an excess of data obscuring the overall picture of the results.

Therefore this conversion is only meant as a guide to interpretation of the data. The thermocouple temperature readings were being measured over a larger area and therefore would not have registered the high temperature spots which can be seen on the thermographic images. The highest measured temperatures were correlated to the highest readings on the thermographic images, therefore this is going to yield an extremely conservative estimate of the power efficiency of the system when

comparing the input power and the temperatures achieved. This was also done over a short time, as a longer time to ‘equilibrate’ the panel temperature would lead to the whole panel heating up and removing any distinction in the heating. It is recommended to bear this in mind while viewing the calculated temperature graphs. The general formula used for the calibration was gradient/intercept form of the general linear equation:

$$y = ax + b \quad (13)$$

Where:

$$a = \frac{y_2 - y_1}{x_2 - x_1} \quad (14)$$

$$b = \frac{x_2y_1 - x_1y_2}{x_2 - x_1} \quad (15)$$

This equation may be used to for a calibration for each of the sets of data shown in Table 5.

Table 5: Absolute thermocouple temperature readings of the contact and damage area after heating for 3 minutes.

	Power	Face	Current	Voltage	Max. Damage Temp. ($^{\circ}\text{C}$)	Max. Contact Temp. ($^{\circ}\text{C}$)
1.25mm	6W	Front	1.006A	5.96V	48.6	54
	6W	Back	1.006A	5.96V	61.1	69
	2W	Front	0.577A	3.48V	33.2	36.1
	2W	Back	0.577A	3.48V	36.3	38.1
2.5mm	6W	Front	1.323A	4.54V	59.3	43.1
	6W	Back	1.323A	4.54V	57.6	44.6
	2W	Front	0.757A	2.64V	35.5	31.9
	2W	Back	0.757A	2.64V	43	36
5mm	6W	Front	1.532A	3.92V	48.5	35
	6W	Back	1.532A	3.92V	48.8	34.2
	2W	Front	0.882A	2.27V	35.3	29
	2W	Back	0.882A	2.27V	37.6	28.2
7.5mm	6W	Front	1.782A	3.337V	58.3	40.8
	6W	Back	1.782A	3.337V	52.3	35.6
	2W	Front	1.011A	1.99V	34.9	29.7
	2W	Back	1.011A	1.99V	35.3	29.2

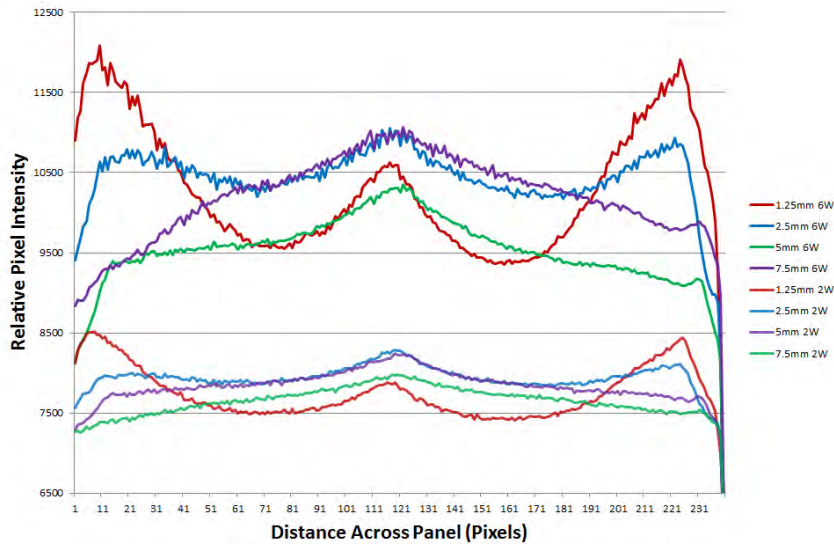


Figure 66: Intensity of the infra-red camera pixels down the centre of the heated channel. Comparison of contact widths (colour) and heating power (upper and lower traces).

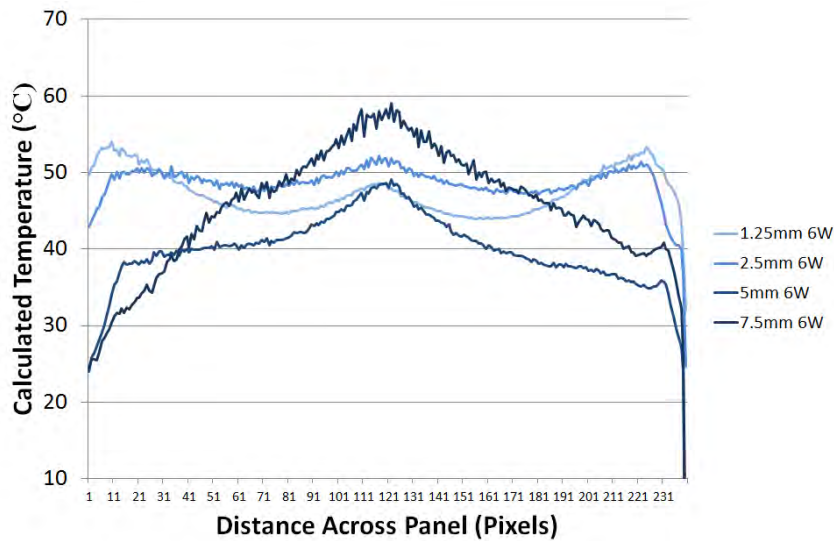


Figure 67: Temperature-calibrated profile through the cross-section of the panel with the damage in the centre.

Figure 66 shows the raw pixel intensity data of the channels with both 2 W and 6 W data. The different colours represent the different contact widths on the panel. Figure 67 shows the temperature-corrected data using the absolute values measured by thermocouple. It can be seen that the increase of temperature at the contact interface decreases rapidly with the wider contact panels. The 7.5 mm contact panel looks well targeted, with the edges of the panel moving barely above ambient temperature under a heating of 2 watts. However, it is not easy to identify the best targeting or efficiency with this qualitative information. To analyse these effects further some 2-dimensional processing can be done.

To demonstrate the targeting effect of the different track widths some statistical analysis was performed on the raw sensor data from the IR camera. The panel data was split into individual areas which were averaged to provide a single reading. The panel was split up into the areas shown in Figure 68:

- A ‘cold’ area at the edge of the panel to provide an ambient temperature for the panel (25 x 4 pixels). Denoted by the area outlined in purple.
- A ‘hotspot’, in the centre of the damage, which was the highest measured pixel

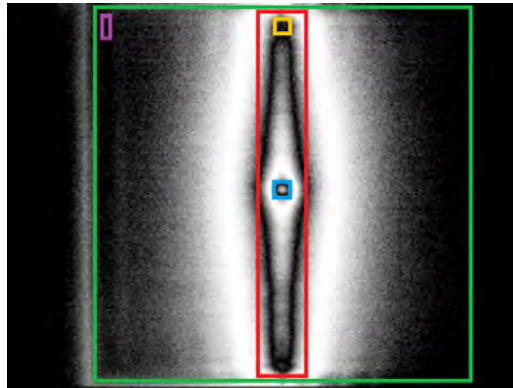


Figure 68: Calculation areas for the targeting characteristics of the resistive heating. Green: Panel area. Purple: Ambient panel temperature. Red: Channel area. Blue: Damage zone, the ‘Hotspot’ is in the centre of this zone. Orange: Contact area.

intensity. Central pixel of the area outlined in blue.

- A ‘hot zone’ which was the area around the hotspot (± 5 pixels). Area outlined in blue.
- A ‘contact area’, an area around the hottest pixel within 20 pixels of the panel edge (± 5 pixels). Area outlined in yellow.
- A ‘channel area’, the area surrounding the carbon fibres which are providing the heating. This area was the full length of the panel with edges ± 10 pixels from the edge of the ‘hot zone’. Area outlined in red.

Each of these areas were averaged for each panel and the results compared against each other (Figure 69).

As can be seen in Figure 69, the average temperature rise of the whole panel remains fairly constant with the changing contact widths. This is to be expected as the total amount of power is constant (2W) for each test and the average temperature rise should be equal to the power being dissipated. It would be ideal therefore if the gradient of this line were 0. The slightly anomalous values shown may be attributable to a different ambient temperature of the room when testing different panels, or an internal heat-compensation problem with the camera as discussed previously.

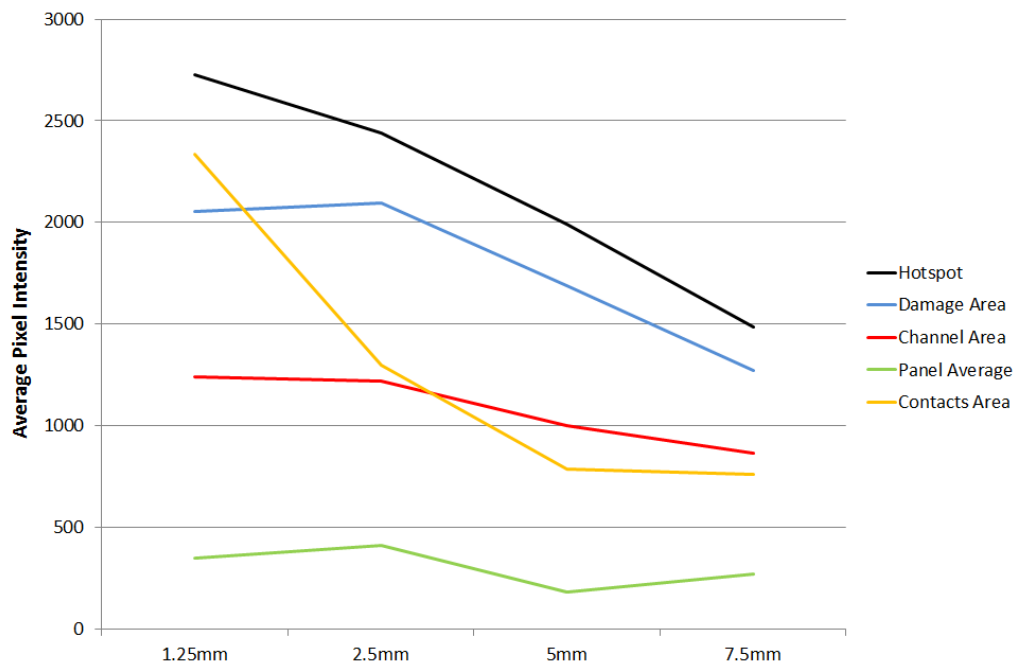


Figure 69: Damage-targeting ability of self-heating panels with changing contact width. Calculation zones can be seen in Figure 68.

The increase in temperature in the channel area, equally, might be expected to be approximately equal to the power input. However, the selected channel area boundaries did not change for different panels as it was difficult to decide upon fair constraints for the affected area. It was decided that a consistent area (consisting of the full length of the panel ± 10 pixels either side of the hottest pixel) would be fairest. The wider contacts made a wider electrical path through the composite, and therefore spread the heating effect more across the panel. This may account for the decreased channel area heating with increasing contact width. Alternatively, the decreased heating effect may be due to the energy lost in resistive heating of the copper tracks on the flexible circuit board as explained earlier.

The most significant effects, however, can be seen in the temperatures of the damage and the contacts. The ideal self-heating system would be most targeted to the damage (i.e. high hotspot and damage heating) and would have extremely low contact heating (to prevent damage and wasted energy). At a contact width of only 1.25mm, the limited number of carbon fibres with good electrical contact with the

copper of the flexible circuit board meant that contact resistance is very high. This high resistance leads to a greater voltage drop at this area, and a greater heating effect. This can be seen clearly in Figure 69 and the corresponding thermographic image in Figure 61a. The temperature at the contacts exceeds the damage area on average which is not ideal. Wider contact widths decrease the temperature increase at the contacts rapidly, and at 5mm can be seen to be lower than the average channel area temperature.

6.4 Large Panel Targeted Heating

A larger panel was created 200mm x 200mm to assess the ability of the self-sensing system to detect damage over a longer range, and equally if the heating system could be demonstrated with longer fibres. There were also both X and Y sensing plies to demonstrate detection in two planes, and again to target heating even more to the damage zone.

6.4.1 Thermography

Images taken with the infra-red camera in the method described in Section 6.3.1. The flexible circuit board for these panels was made using the ink printed mask method described in Section 6.2, not the photoresistive film method which was used to create the panels in the previous section. These images also show an undamaged panel and therefore the track resistance is far lower. It can be demonstrated that the heating effects can be targeted to any section of the panel by applying the heating current (6W in Figure 70) to the desired channels in the X and Y directions. Steerable heating was achieved for the first time with this method.

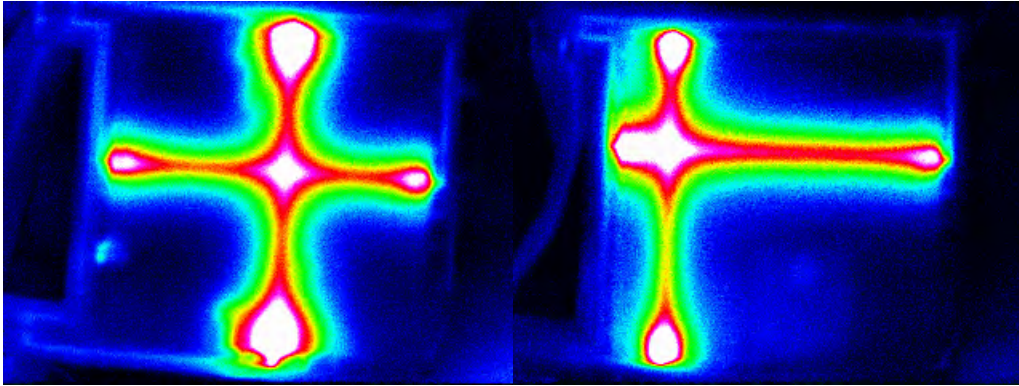


Figure 70: Thermography of 200 mm x 200 mm self-heating panel targeting 2 arbitrary sites on an undamaged panel to demonstrate steerable heating effects. 6W of power applied. Large contact heating noticeable.

While Figure 70 shows the ability of the system to target heating to any area of the panel it also highlights the high contact area heating. This is due to an imperfect contact being made between the copper contacts on the flexible printed circuit board interleave and the carbon fibres in the prepreg. Although every care was taken to clean the contact area it is possible that the copper oxidised slightly during the curing process. As these flexible printed circuit boards were made using the ink mask method which was removed with acetone, it is possible that some of the ink remained and provided a dielectric layer on the surface of the contact area. A final problem is that excess resin from the prepreg will be drawn out the sides of the panel during cure by the pressure of the autoclave. As the circuit board is nonporous this may create a resin-rich interlayer which separates the copper contacts from direct connection with the carbon fibres.

This high contact area heating effect can be visualised better as a 3-dimensional plot, shown in Figure 71.

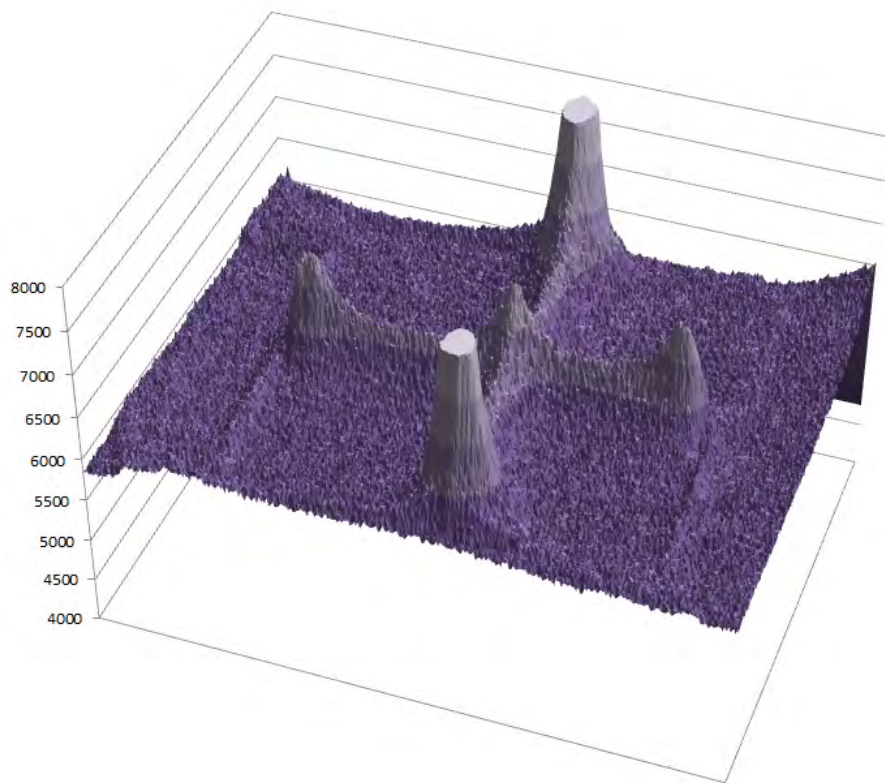


Figure 71: A 3-dimensional plot showing the pixel intensity of the infrared camera viewing an undamaged large carbon-fibre panel which is being resistively heated down an arbitrary X and Y channel.

The contact heating shown in Figure 71 is of a higher intensity than that of the smaller panel. However to a certain extent this effect was expected as this test was conducted on an undamaged panel. The damage in the previous panels causes broken fibres which breaks the electrical pathway between the connections. This causes a higher resistance at the damage site and consequently a lower percentage resistance at the contacts. Conversely it can be shown that the extremely low resistance from the carbon fibres across the panel will accentuate even a moderate contact resistance.

6.5 Discussion

Resistive heating via the carbon fibres to deliver heating for initiating healing has been assessed. Several new manufacturing routes have been developed to provide

the best quality of tracks for this technology in the future.

Inkjet mask printing was trialed as a new manufacturing method for the embedded circuitry to deliver current the fibres. Although this had the potential to save several steps in the procedure as well as cost and time, this method provided the lowest consistency and therefore could not be used further in the project. It is shown in Figure 55 that the track quality in general was very high, but even occasional track breaks where ink had run would ruin a panel. Although all relevant parameters for printing were investigated, including some heat treatment after printing, the inks failed to wet the surface of the copper. This was thought to be due to the surface of the copper which the inkjet inks were not designed for. However, it would be possible to improve this technology for future flexible circuit-board manufacture with an appropriate specialised ink.

It is thought that direct silver printing will provide faster, cheaper and more automated production of flexible circuit-boards in the future. It has been shown that this process gives additional manufacturing flexibility, as different artwork may be created easily, different materials can be printed with different thicknesses and solvents, and many different substrates may be used to provide the best mechanical and electrical properties of the final panel. However, within the limits of the current work, several difficulties prevented consistency of the final tracks produced. Quantity of inks which were available, time on the equipment and inefficient raster-type printing all contributed. Therefore, dry film etching was chosen as it provided the best consistency of tracks within the time frame of the current project.

The resistance of the fibres is extremely low. The design of the self-sensing system must be constructed to lessen the effect of the connections to the fibre ends. With larger panels, which will almost certainly be the case in a real-world application, this problem will be a little easier to solve as the resistance of longer fibres across a larger panel will be much higher, giving a lower percentage resistance to the connections. It would be a useful piece of further work to develop a new connection method for

the contact area to improve the current transfer between the tracks and the carbon fibre, lessening the resistance of the area. This would improve the efficiency of the system, and very likely the accuracy of the self-sensing of damage.

The resistance in the carbon fibres increases dramatically during damage. This is of course the basis of the sensing technique which has been developed in other studies, but it also carries large benefits for the self-heating system which has been demonstrated. The efficiency is improved as a higher percentage of the power is dissipated on the carbon fibres rather than losses in the system carrying the power to the panel. It also promotes targeting of the healing directly to the damage site as the area with the highest resistance will be directly around the broken fibres and fracture of the composite as this is where electrical pathways are limited and therefore more ohmic heating is caused.

The size of the connections are extremely important and will be related to the size of the final panel on which the technology will be used. As can be seen from Figure 69, the area of the panel surface surrounding the copper contacts is heated due to the higher resistance of the limited carbon fibres which have made a good electrical connection with the copper. Figure 69 shows the for the thinner contact widths (1.25mm and 2.5mm) the heating is much great, but then falls significantly for the larger contact widths. For the larger contact widths, more carbon fibres are connected and therefore a lower resistance is created but at the cost of accuracy in targeting the damage, and also resulting in an increase of power overall to heat the area, as a larger area is to be heated. This in turn puts a much higher electrical load on the power equipment and copper tracks which will create more losses resulting in inefficiency. Therefore a compromise must be reached in the size of the contact area related to the panel dimensions. To create a general rule, it is hypothesised that the ideal contact width is when the contact area temperature falls below that of the average track temperature, seen in Figure 69. This would make the ideal track width between 2.5mm and 5mm.

Although the resistance of the carbon fibres is low it is possible to provide resistive heating as long as the resistance of the copper tracks and of the contact between the flexible circuit board and the carbon fibres was sufficiently low. The overall efficiency of the heating effect may be characterised by the ratio of the total resistance to that of the carbon fibres, thus determining the losses in the non-heated part of the system. This type of self-heating system could be used with many of the healing systems being developed. The targeting system shows how the same electronics may be used for both a sensing and an actuation of healing by heat. This system could be used in service parts for aerospace or energy structures which may be difficult to remove from service, or in space applications where parts may be inaccessible.

6.6 Conclusion

To summarise the results shown it can be said that several new manufacturing methods have been developed and discussed. Different methods of manufacturing the tracks have been explored and discussed. Several of these have been trialled for the first time, including thermography of the self-heating system. Steering of the heat for the self-healing system has been demonstrated, and an assessment of the targeting ability of the system has been made. It would be possible to expand this work to model a thermoelectric mathematical view of the system which could form better sensing and targeted heating with increased accuracy.

Larger panels of up to 200 mm square have been demonstrated using this technique. The results also point to improvements in system design for even larger scales of manufacture in industry, thus scaling of this self-heating technology is not thought to be an issue for industrial manufacture. Sensing must also be improved in parallel with this development, and has been covered by other unpublished research, but has been out of scope for the current work. The most appropriate size for the contacts for the panel have been discussed, and a proposal for determining the optimum size made.

7 Concluding Summary

This work has detailed the investigation into the manufacturing and technological development of a solid state self healing polymeric system for use in composites for aerospace applications. The basic operation of this system is based on the use of a soluble linear polymer integrated into a standard epoxy resin system. The healing agent used for this system has been a bisphenol-a type linear polymer without epoxy end groups to prevent covalent reaction into the network. These molecules reversibly bond with the crosslinked network by hydrogen bonds and chain entanglements. The healing agent can be given enough energy when heated to move or reptate through the structure and across crack faces, which are still in contact, and bridge them to regain mechanical strength.

It has been shown that the mechanical properties of the modified resin are not intrinsically negatively affected by this technology. The modified resins have been shown to exhibit improved tensile and compressive strength and strain, as well as similar (or marginally improved) fracture toughness and fracture energy. These gains however could be argued to be offset by a decreased tensile modulus. These trends continued up to the highest concentrations of healing agent tested ($\sim 10\%$).

The fracture toughness recovery during cure was shown to be most effective at a concentration of 6-7 wt% of the resin where approximately 60% of the fracture toughness was recovered.

Rheometry has been used for the first time in this work for the study of solid state self healing resins. A large amount of information about the rheological properties and on the cure cycle of the resins has been documented. Rheometry is an extremely useful tool for characterisation and developmental formulation of new resins especially when considering manufacturing routes with requirements of very specific viscosities. It was shown the the initial viscosity of the modified resin was extremely high. At the optimum concentration for fracture toughness recovery as determined

by the compact tension measurements, the initial viscosity of the modified resin was almost 100 times that of the unmodified resin. Reductions in viscosity have been achieved by the use of lower molecular weight healing agents, inclusion of a reactive diluent and by the use of a lower viscosity host resin. The healability has not been improved, but several methods have shown that a reduction of viscosity and therefore an improvement in processability may be achieved without necessarily a reduction in healability.

Compact tension testing has been examined thoroughly and several issues with it discussed. It has been shown that the determined fracture toughness of a test specimen is in a significant way affected by the measurement of, or rather the inability to measure, the initial crack length. Problems with inconsistent data are compounded by the difficulty in obtaining a consistent crack in specimens. Compact tension testing was assessed and several shortcomings highlighted particularly in the context of this type of study with limited staff, resources and time. Specimens took too long to manufacture, were too expensive and were inconsistent. New standards will be required to adequately represent and compare different healing resins. Improvements to the efficiency of this type of work have been proposed, including refinements to the testing and manufacturing procedures which may yield more data in future studies. Sources of error in both the methodology and study design have been examined and highlighted for future reference.

Different methods of manufacturing the flexible circuit boards for self-sensing and self-heating have been explored and their effectiveness discussed. Several of these methods have been trialled for the first time, including thermography of the self-heating system. Steering of the heat for the self-healing system has been demonstrated, and an assessment of the targeting ability of the system has been made. It would be possible to expand this work to model a thermoelectric mathematical view of the system which could form better sensing and targeted heating with increased accuracy.

Larger panels of up to 200 mm square have been demonstrated using this technique. The results also point to improvements in system design for even larger scales of manufacture in industry, thus scaling of this self-heating technology is not thought to be an issue for industrial manufacture. Sensing must also be improved in parallel with this development, and has been covered by other unpublished research, but has been out of scope for the current work. The most appropriate size for the contacts for the panel have been discussed, and a proposal for determining the optimum size made.

Overall it can be said that the manufacturing of the complete sense and heal system based on the solid state method has encountered many difficulties, some of which have been overcome in this research. There is a significant way to go to bring the manufacturing readiness up to the required level for industrial implementation, but a tackling of these issues head on has brought some of the problems and potential avenues for improvement into the fore.

8 Future Work

Sensing and healing is an important next step for the materials of the future, especially in fibre composites, in fields such as aerospace. While it has been demonstrated that a self-healing concept in the solid state is possible, there are many areas which would require serious attention if this is to become an industrial reality.

The high viscosity of this system is still a problem for industrial manufacturing procedures to produce panels with a self-healing resin. The methods used to solve this problem have done so largely at the expense of healability and therefore are not suitable. There are many other methods which may be tested to overcome this problem. Reduced viscosity host resins would enable the final mixture to be easier to handle. Alternative reactive diluents may be trialled. This area is expansive and has the potential to yield the biggest gains. The diluent tested was not a favourable one and in fact the chemistry, on reflection, did not suit this self-healing resin chemistry. It is possible that by testing more diluents a further improved healing resin may be developed. A lower molecular weight healing agent has been shown to provide equally good healing at a lower viscosity than the original self-healing formulation. Further development of this resin is likely to lead to significant gains. It is thought that a bisphenol-f self-healing resin may be possible which would have a reduced viscosity and would provide high healing. A bisphenol-f based healing agent which has a lower viscosity may also prove to be a valuable healing agent even within bisphenol-a systems as these are extremely compatible and might prove to reptate through the structure more easily, providing greater healing at lower activation energy.

Oscillation mode rheometry may be used to study viscosity of components individually, and blended, and during curing which would serve as an extremely useful reference work for further development.

In addition to the development of the resins, a full sensing system must also be

developed. It has been shown that the sensing system described may also be used to provide resistive heating targetted to damage located within a laminate, and this system must be extended to use larger panels in a resin-infusion experiment in order to demonstrate the technology to consumers for it to reach the next level of production-readiness. Using thermography it would be possible to expand this work to model the thermoelectronics mathematically, which could form better sensing and targeted heating with increased accuracy.

References

- [1] Gunston, B. (ed.), *"The Chronicle of Aviation"*, Chronicle Communications Ltd., London, p. 39, (1992)
- [2] Donald, D. (ed), *"The Encyclopedia of World Aircraft"*, Blitz Editions, Enderby, p. 585, (1997)
- [3] Fulghum, D., *"Away Game."*, Aviation Week & Space Technology, 8 January 2007
- [4] Whittle F., *"Improvements related to liquid-fueled burners and vaporisers"*, UK Patent Number (577,972), May 1946
- [5] Mitchell R., *"Construction of wings for aircraft"*, Supermarine Aviation Works (Vickers) Ltd., UK Patent Number (472,839), Oct. 1937
- [6] Chaplin, H., *"Improvements in or relating to Means for carrying Bomb and like-loads on Aircraft"*, Fairey Aviation Company Ltd., UK Patent Number (600,576), Apr. 1948
- [7] *NACA Report, "Sixth Annual Report of the National Advisory Committee for Aeronautics"*, Washinton D.C, Report Number: NACA-AR-6, Nov. 1920
- [8] Kelly, A., *"Very stiff fibres woven into engineering's future: a long-term perspective"*, Journal of Materials Science 43(1) pp. 6578-6585 (2008)
- [9] *"Red Ink at Rolls-Royce"* Time Magazine, Monday, Nov. 23, 1970
- [10] Russell, J., *"Composites affordability initiative: Successes, failures - Where do we go from here?"*, SAMPE Journal 43(2) pp. 26-36 (2007)
- [11] Tajima, N., Sakurai, T., *"Overview of the Japanese Smart Materials Demonstrator Program and Structures System Project"*, Advanced Composite Materials, 13(1) pp. 3-15 (2004)

- [12] Uglea, C. V., Negulescu I. A., "*Synthesis and Characterization of Oligomers*", CRC Press Inc., p. 103 (1991)
- [13] Gardziella A., Pilato L., Knop A., "*Phenolic Resins: chemistry, applications, standardization, safety and ecology*", Springer (1999)
- [14] Pontén, A., Zimerson, E., Sörensen, Ö., Bruze, M., "*Chemical analysis of monomers in epoxy resins based on bisphenols F and A*", Contact Dermatitis, 50(5), pp. 289 - 297 (2004)
- [15] Crosby, P., "*In-situ Cure Monitoring of Epoxy Resin Systems*," PhD Thesis (1996)
- [16] May, C. A., "*Introduction to Epoxy Resins. Epoxy Resins Chemistry and Technology*", Marcel Dekka Inc., New York (1988)
- [17] Shechter, L., Wynstra, J., "*Glycidyl ether reactions with amines.*", Industrial and Engineering Chemistry, 48(1) pp. 94-97 (1956)
- [18] Rozenburg, B. A., "*Kinetics, thermodynamics and mechanism of reactions of epoxy oligomers with amines.*", Advances in Polymer Science, 75(2) pp. 113-165 (1985)
- [19] Shechter, L., Wynstra, J., Kurkijy R.P., "*Glycidyl Ether Reactions with Amines*", Industrial and Chemical Engineering, 48(1) p. 95 (1956)
- [20] Zhang, Y. X., Vyazovkin, S, "*Effect of substituents in aromatic amines on the activation energy of epoxy-amine reaction*", Journal of Physical Chemistry B, 111(25) pp. 7098-7104 (2007)
- [21] Fisch, W., Hofmann, W., "*Chemischer aufbau von gehärteten epoxyharze. III. Mitteilung über chemie der epoxyharze*", Die Makromolekulare Chemie, 44(1) pp. 8 - 23 (1961)

- [22] May, C. A., (ed.), *“Epoxy resins: chemistry and technology”*, Marcel Dekka Inc., New York, p. 62 (1988)
- [23] Dearborn, E. C., Fuoss, R. M., MacKenzie, A. K., Shepard, R. G., *“Epoxy Resins from Bis-, Tris-, and Tetrakis-Glycidyl Ethers”*, Industrial and Engineering Chemistry 45(12) p. 2716 (1953)
- [24] Hogg, P. J., *“Composites in Armor”*, Science 1100, p. 314 (2006)
- [25] Tomblin, J., Lacy, T., Smith, B., *“Review of Damage Tolerance for Composite Sandwich Airframe Structures”*, Office of Aviation Research, Washington D.C., FAA Report Number: DOT/FAA/AR-99/49
- [26] Hexcel Composites *“Pre-impregnated composite material for curing at specified curing temperature for making high performance composite parts, comprises reinforcing fibers, and matrix comprising thermoplastic particle component”*
Patent Number: US2011147670-A1; US8097333-B2
- [27] Mouritz, A. P., Chang, P., Isa, M. D. *“Z-Pin Composites: Aerospace Structural Design Considerations”* Journal of Aerospace Engineering 24(4) pp. 425-432 (2011)
- [28] Gyan, S., Ganguli, R., Naik, G.N. *“Damage-tolerant design optimization of laminated composite structures using dispersion of ply angles by genetic algorithm”* Journal of Reinforced Plastics and Composites 31(12) pp. 799-814 (2012)
- [29] Zhou, G., *“The use of experimentally-determined impact force as a damage measure in impact damage resistance and tolerance of composite structures”*, Composite Structures 42 (1998) pp. 375-382
- [30] Richardson, M. O. W., Wisheart, M. J., *“Review of low-velocity impact properties of composite materials”*, Composites Part A 27, pp. 1123-1131 (1996)

- [31] Sela, N., Ishaib, O., “*Interlaminar fracture toughness and toughening of laminated composite materials: a review*”, Composites 20(5) pp. 423-435 (1989)
- [32] White, S. R., Sottos, N. R., Geubelle, P. H., “*Autonomic healing of polymer composites*”, Nature 409(6822) pp. 794-797 (2001)
- [33] Davies, G.A.O., Olsson, R., “*Impact on composite structures*”, Aeronautical Journal, 108, pp. 541–563 (2004)
- [34] Cantwell, W.J., Morton, J., “*The impact resistance of composite materials – a review*”, Composites, 22 (5), pp. 347–362 (1991)
- [35] Hull, D., Shi, Y.B., “*Damage mechanism characterization in composite damage tolerance investigations*”, Composite Structures, 23, pp. 99–120 (1993)
- [36] Trask, R., Williams, H., Bond, I., “*Self-healing polymer composites: mimicking nature to enhance performance*”, Bioinspiration & Biomimetics 2(1) pp.1-9 (2007)
- [37] Dry, C., “*Passive tunable fibres and matrices.*”, International Journal of Modern Physics B (IJMPB) 6(15-16) pp. 2763-71 (1992)
- [38] Dry, C., McWillan, W., “*Three-part methylmethacrylate adhesive system as an internal delivery system for smart responsive concrete*”, Smart Materials Structures 5(3) pp. 297-300 (1996)
- [39] B.J. Blaiszik, S.L.B. Kramer, S.C. Olugebefola, J.S. Moore, N.R. Sottos, and S.R.White “*Self-Healing Polymers and Composites*” Annu. Rev. Mater. Res. 40:179–211 (2010)
- [40] Bergman SD, Wudl F. 2008. “*Mendable polymers.*” J. Mater. Chem. 18(1):41–62
- [41] Wool RP. 2008. “*Self-healing materials: a review.*” Soft Matter 4(3):400–18

- [42] Kessler MR. “*Self-healing: a new paradigm in materials design.*” Proc. Inst. Mech. Eng. G 221(4):479– 95 (2007)
- [43] Yuan YC, Yin T, Rong MZ, Zhang MQ. “*Self healing in polymers and polymer composites. Concepts, realization and outlook: a review*” Express Polymer Letters 2(4):238–50 (2008)
- [44] Youngblood JP, Sottos NR, Extrand C. “*Bioinspired materials for self-cleaning and self-healing*”. MRS Bulletin 33(8):732–41 (2008)
- [45] White SR, Caruso MM, Moore JS. “*Autonomic healing of polymers.*” MRS Bulletin 33(8):766–69 (2008)
- [46] Bond IP, Trask RS, Williams HR. “*Self-healing fiber-reinforced polymer composites.*” MRS Bulletin 33:770–74 (2008)
- [47] Williams, K., Dreyer, D., Bielawski, C., “*The Underlying Chemistry of Self-Healing Materials*”, MRS Bulletin 33(1) pp. 759-65 (2008)
- [48] Williams, G., Trask, R., Bond, I., “*A self-healing carbon fibre reinforced polymer for aerospace applications*”, Composites Part A: Applied Science and Manufacturing 38(6) pp.1525–1532 (2007)
- [49] Bleay, S., Loader, C., Hawyes, V., “*A smart repair system for polymer matrix composites*”, Composites Part A: Applied Science and Manufacturing 32 pp. 1767-76 (2001)
- [50] Motuku, M., Vaidya, U. K., Janowski, G. M., “*Parametric studies on self-repairing approaches for resin infused composites subjected to low velocity impact*”, Composite Structures 35(3) pp. 263-269 (1996)
- [51] Bleay, S. M., Loader, C. B., Hawyes, V. J., “*A smart repair system for polymer matrix composites*”, Composites Part A: Applied Science and Manufacturing 32(12) pp. 1767-1776 (2001)

- [52] Wu, D., Meure, S., Solomon, D., “*Self-healing polymeric materials: A review of recent developments*”, Progress in Polymer Science 33 pp.479-522 (2008)
- [53] Caruso, M., Blaiszik, B., White, S., “*Full recovery of fracture toughness using a nontoxic solvent-based self-healing system*”, Advanced Functional Materials 18(13) pp. 1898-1904 (2008)
- [54] Kessler, M.R., White, S.R., “*Cure kinetics of the ring-opening metathesis polymerization of dicyclopentadiene*”, Journal of Polymer Science Part A: 40 (14) pp. 2373–2383 (2002)
- [55] Kessler, M.R., Sottos, N.R., White, S.R., “*Self-healing structural composite materials*”,Composites Part A: Applied Science and Manufacturing 34 pp. 743–753 (2003)
- [56] Kessler, M.R., White S.R. “*Self-activated healing of delamination damage in woven composites*” Composites Part A: Applied Science and Manufacturing, 32 (5), pp. 683–699 (2001)
- [57] Brown, E. N., Sottos, N. R., White, S. R., “*Fracture testing of a self-healing polymer composite*”, Exp. Mech. 42, pp. 372–379 (2002)
- [58] Brown, E. N., Sottos, N. R., White, S. R., “*Microcapsule induced toughening in a self-healing polymer composite*”, Journal of Materials Science 39, pp. 1703–1710 (2004)
- [59] Brown, E. N., White, S. R., Sottos, N. R., “*Retardation and repair of fatigue cracks in a microcapsule toughened epoxy composite—part I: manual infiltration*”, Composites Science and Technology 65, pp. 2466–2473 (2005a)
- [60] Brown, E. N., White, S. R., Sottos, N. R., “*Retardation and repair of fatigue cracks in a microcapsule toughened epoxy composite—part II: in situ self-healing*”, Composites Science and Technology 65, pp. 2474–2480 (2005b)

- [61] Brown, E. N., Sottos, N. R., White, S. R., “*Fatigue crack propagation in microcapsule toughened epoxy*”, *Journal of Materials Science* 41, pp. 6266–6273 (2006)
- [62] Sanford, M. S., Henling, L. M., Grubbs, R. H., “*Synthesis and Reactivity of Neutral and Cationic Ruthenium(II) Tris(pyrazolyl)borate Alkylidenes*”, *Organometallics* 17 (24), pp 5384–5389 (1998)
- [63] Samojowicz, C., Bieniek, M., “*The doping effect of fluorinated aromatic hydrocarbon solvents on the performance of common olefin metathesis catalysts: application in the preparation of biologically active compounds*”, *Chemical Communications* 47(1) pp. 6282 - 6284 (2008)
- [64] Kessler, M. R., “*Self-healing: a new paradigm in materials design*”, *Proceedings of the Institution of Mechanical Engineers, Part G: Journal of Aerospace Engineering*, Vol. 221 (2007)
- [65] Hamilton AR, Sottos NR, White SR. “*Pressurised vascular systems for self-healing materials*”, *Journal of the Royal Society Interface*. 9 70 pp. 1020-1028 (2012)
- [66] H.R. Williams, R.S. Trask, I.P. Bond “*Self-healing sandwich panels: restoration of compressive strength after impact*” *Compos Sci Technol*, 68 (2008), pp. 3171–3177
- [67] Norris, C.J., Meadway, G.J., O’Sullivan, M.J., Bond, I.P., Trask, R.S. “*Trask Self-healing fibre reinforced composites via a bioinspired vasculature*” *Adv Funct Mater*, 21 pp. 3624–3633 (2011)
- [68] Norris, C.J., White, J.A.P., McCombe, G., Chatterjee, P., Bond, I.P., Trask R.S. “*Autonomous stimuli triggered self-healing in smart structural composites*” *Smart Mater Struct*, 21 p. 094027 (2012)

- [69] Norris, C. J., Bond, I. P., Trask, R. S. "Healing of low-velocity impact damage in vascularised composites" *Composites Part A: Applied Science and Manufacturing* 44 pp. 78-85 (2013)
- [70] Toohey, K. S., Sottos, N. R., Lewis, J. A., "*Self-healing materials with microvascular networks*", *Nature Materials* 6(8) pp. 581-585 (2007)
- [71] Toohey, K.S., N.R. Sottos, and S.R. White, "*Characterization of microvascular-based self-healing coatings*". *Experimental Mechanics*, 2009. 49(5): 707-717
- [72] Toohey, K.S., C.J. Hansen, J.A. Lewis, S.R. White, and N.R. Sottos, "*Delivery of two-part self-healing chemistry via microvascular networks.*" *Advanced Functional Materials* 19(9) pp. 1399-1405 (2009)
- [73] Hansen, C.J., W. Wu, K.S. Toohey, N.R. Sottos, S.R. White, and J.A. Lewis, "*Self-healing materials with interpenetrating microvascular networks.*" *Advanced Materials* 21(41) pp. 4143-4147 (2009)
- [74] Norris, C. J. , Bond, I. P. & Trask, R. S. "*Healing Of Low-Velocity Impact Damage In Vascularised Composites*" *Composites Part A: Applied Science and Manufacturing* 44(1) pp. 78-85. (2013)
- [75] Zako M., Takano, N., "*Intelligent Material Systems Using Epoxy Particles to Repair Microcracks and Delamination Damage in GFRP*", *Journal of Intelligent Material Systems and Structures* 10 pp. 836 (1999)
- [76] White, S., Caruso, M, Moore, J., "*Autonomic Healing of Polymers*", *MRS Bulletin* 33(1) pp. 766-769 (2008)
- [77] Soutis, C., Lee, J., "*Scaling effects in notched carbon fibre/epoxy composites loaded in compression*", *Journal of Materials Science* 43(10) pp. 6593 (2008)

- [78] Sage, I., Lloyd, P., Bourhill, G., “*Damaged composites come to light*”, *Material World* 8(3) pp. 23-24 (2000)
- [79] Pang, J., Bond, I., “*‘Bleeding composites’—damage detection and self-repair using a biomimetic approach*”, *Composites Part A: Applied Science and Manufacturing* 36(2) pp. 183–188 (2005)
- [80] Kessler, M.R., Sottos, S.R., “*Self-activated healing of delamination damage in woven composites*”, *Composites Part A: Applied Science and Manufacturing* 32(5) pp.683-99 (2001)
- [81] M. Zako, N. Takano, “*Intelligent materials systems using epoxy particles to repair microcracks and delamination damage in GFRP*” *J Int Mater Sys Struct* 10(10 p. 836-41 (1999)
- [82] Malkin, R. , Trask, R. S. & Bond, I. P. “*Control of unstable crack propagation through bio-inspired interface modification*” *Composites Part A: Applied Science and Manufacturing* 46, pp. 122-130 (2013)
- [83] van der Zwaag, S. (ed.) “*Self-healing Materials. An Alternative Approach to 20 Centuries of Materials Science*” Springer, p.45 (2007)
- [84] Diels, O., Alder, K. “*Synthesen in der hydroaromatischen Reihe*” *Justus Liebig’s Annalen der Chemie* 460: 98 (1928)
- [85] Chen X., Wudl F., Mal A., Shen H., Nutt S., “*New thermally remendable highly cross-linked polymeric materials.*” *Macromolecules* 36, p. 1802-1807 (2007)
- [86] S. Bergman, F. Wudl, “*Remendable Polymers*”, S. van der Zwaag (ed.) *Self-healing Materials*. Springer, p.53 (2007)
- [87] Chung C.M., Roh Y.S., Cho S.Y., Jim J.G “*Crack healing in polymeric materials via photochemical [2+2] cycloaddition*” *Chem Mater* 16 p. 3982-3984 (2004)

- [88] Scott, T., Schneider, A., Cook, W., Bowman, C.N., “*Photoinduced Plasticity in Cross-Linked Polymers*” *Science* 308(5728) p. 1615 - 1617 (2005)
- [89] Williams, K., Boydston, A., Bielawski, C. “*Towards electrically conductive, self-healing materials*” *J. R. Soc. Interface* 4, 359-362 (2007)
- [90] Meure, S., Wua, D. Y., Furman, S. “*Polyethylene-co-methacrylic acid healing agents for mendable epoxy resins*” *Acta Materialia* 57(14) p. 4312-4320 (2009)
- [91] Kim, Y.H. and R.P. Wool, “*A theory of healing at a polymer-polymer interface.*” *Macromolecules*, 1983. 16(7): 1115-1120.
- [92] de Gennes, P.G., “*Scaling Concepts in Polymer Physics*”. 1979, Ithaca, New York: Cornell Univ. Press.
- [93] Wool, R.P., “*Polymer entanglements*”. *Macromolecules*, 1993. 26: 1564-1569.
- [94] Wool, R.P., “*Relation for healing, fracture, self-diffusion and fatigue of random coil polymers.*” *American Chemical Society, Polymer Preprints*, 1982. 23: 62-63.
- [95] Hayes SA, Zhang W, Branthwaite M, Jones FR “*Self-healing of damage in fibre-reinforced polymer-matrix composites*” *Journal of the Royal Society Interface* 4(13) p. 381-387 (2007)
- [96] Jones, F., Zhang, W., Hayes, S. “*Thermally induced self-healing of thermosetting resins and matrices in smart composites*” *Self-healing materials. An alternative approach to 20 centuries.* 100, pp. 69-93 (2007)
- [97] Hayes, S.A., Jones, F.R., Marshiya, K., Zhang, W. “*A self-healing thermosetting composite material*” *Composites: Part A* 38 pp. 1116–1120 (2007)
- [98] Zhang, W. “*Self Healing Epoxy Resins and Composites*” PhD Thesis University of Sheffield (2008)

- [99] Kemp, M. “*Self-sensing Composites for Smart Damage Detection using Electrical Properties.*” 2nd European Conference on Smart Structures and Materials 2361(1) pp.136-139 (1994)
- [100] Han, C. “*Multiphase flow in polymer processing*”, Academic Press, New York (1981)
- [101] Paul, D., Newman, S. “*Polymer Blends*”, Academic Press, New York (1978)
- [102] Plochocki, A. P. “*Melt rheology of polymer blends the morphology feedback*” Polymer Engineering and Science 23(11) pp. 618 - 626 (1983)
- [103] Gan, W., Zhan, G., Wang, M. “*Rheological behaviour and structural transitions in a polyethersulfone-modified epoxy system during phase separation*” Colloid Polym Sci 285(2) pp.1727 (2007)
- [104] Kim, H., Char, K. “*Effect of Phase Separation on Rheological Properties during the Isothermal Curing of Epoxy Toughened with Thermoplastic Polymer*” Ind. Eng. Chem. Res 39(6) pp. 955-959 (2000)
- [105] Kim, B., Chiba T., Inoue, T. “*Phase Separation and apparent dissolution during cure process of thermoset/thermoplastic blend*” Polymer 36(1) pp. 67-71 (1995)
- [106] Barzegari, M., Yousefi, A. “*Rheology of co-continuous phase in physical thermoplastic elastomers*” Polymer International 53(10) pp. 1448-1455 (2004)
- [107] Yamanaka, K., Takagi, Y., Inoue, T. “*Reaction-induced phase separation in rubber-modified epoxy resins*” Polymer 30(10) pp. 1839-1844 (1989)
- [108] Ratna, D. “*Phase separation in liquid rubber modified epoxy mixture. Relationship between curing conditions, morphology and ultimate behavior*” Polymer 42(9) pp. 4209-4218 (2001)

- [109] Bucknall, C. , Partridge, I. “*Phase separation in epoxy resins containing polyethersulphone*” Polymer 24(5) pp. 639-644 (1983)
- [110] Todoroki, A., Tanaka, M., Shimamura, Y. “*Measurement of orthotropic electric conductance of CFRP laminates and analysis of the effect on delamination monitoring with an electric resistance change method.*” Composites Science and Technology, Vol. 62, pp. 619-628. (2002)
- [111] Abry J. C., Choia Y. K., Chateauminois, A., Dalloz, B., Giraud, G., Salvia., M. “*In-situ monitoring of damage in CFRP laminates by means of AC and DC measurements.*” Composites Science and Technology, Vol. 61, pp. 855-864. (2001)
- [112] Irving, P.E, Thiagarajan, C. “*Fatigue damage characterization in carbon fibre composite materials using an electrical potential technique.*” Smart Materials and Structures, Vol. 7, pp. 456-466. (1998)
- [113] Chung, D.D.L. “*Continuous carbon fiber polymer-matrix composites and their joints, studied by electrical measurements.*” Polymer Composites, Vol. 22, pp. 250-270. (2001)
- [114] Hou, L., Hayes, S.A. “*A resistance-based damage location sensor for carbon-fibre composites.*” Smart Materials and Structures, Vol. 11, pp. 966-969. (2002)
- [115] Todoroki, A., Samejima, Y., Hirano, Y., Matsuzaki, R. “*Piezoresistivity of uni-directional carbon/epoxy composites for multiaxial loading.*” Composites Science and Technology, Vol. 69, pp. 1841–1846. (2009)
- [116] Angelidis, N., Irving, P. E. “*Detection of impact damage in CFRP laminates by means of electrical potential techniques.*” Composites Science and Technology, Vol. 67, pp. 594-604. (2007)

- [117] Angelidis, N., Wei, C.Y. Irving, P.E., Discussion on paper '*The electrical resistance response of continuous carbon fibre composite laminates to mechanical strain*' Composites: Part A 35, 1135–1147 (2004).
- [118] Angelidis, N., Wei, C.Y. Irving, P.E., Response to discussion of paper: '*The electrical resistance response of continuous carbon fibre composite laminates to mechanical strain*' Composites Part A, Vol. 37, pp. 1495-1499. (2006)
- [119] Brydson, J. A. "*Flow Properties of Polymer Melts*" 2nd Edition. George Goodwin Ltd. Fleet St. London EC4P 4HL (1981)
- [120] Fox T. and Allen V. "*Dependence of the Zero Shear Melt Viscosity and the Related Friction Coefficient and Critical Chain Length on Measurable Characteristics of Chain Polymers*" Journal of Chemical Physics 41(2) p. 344 (1964)
- [121] Zhang, L., Dong, X., Zhang, H. "*Application research on self-healing technology with microcapsules for automobile brake pad*" Journal of Wuhan University of Technology - Materials Science Edition 24(1) (2009)
- [122] Barton, J.M., Hamerton, I., Howlin, B.J. "*Studies of cure schedule and final property relationships of a commercial epoxy resin using modified imidazole curing agents*" Polymer 39(10) pp. 1929-1937 (1998)
- [123] Chambon, F, Winter, HH "*Linear viscoelasticity at the gel point of a cross-linking PDMS with imbalanced stoichiometry*" Journal of Rheology 31(8) pp. 683-697 (1987)
- [124] Gillham, J.K., Benci, J.A., Noshay, A. "*Isothermal transitions of a thermosetting system*" Journal of Applied Polymer Science 18(4) pp. 951-961 (1974)
- [125] Laza, J.M., Julian, C.A., Larrauri, E., Rodriguez, M., Leon, L.M. "*Thermal scanning rheometer analysis of curing kinetic of an epoxy resin: 2. An amine as curing agent*" Polymer 40(1) pp. 35-45 (1999)

- [126] Ampudia, J., Larrauri, E., Gil, E.M., Rodriguez, M., Leon, L., “*Thermal scanning rheometric analysis of curing kinetic of an epoxy resin. I. An anhydride as curing agent*” *Journal of Applied Polymer Science* 71(8) pp. 1239-1245 (1999)
- [127] Tung, C.Y.M., Dynes, P.J. “*Relationship between viscoelastic properties and gelation in thermosetting systems*” *Journal of Applied Polymer Science* 27(2) pp. 569-574 (1982)
- [128] Scanlan, J.C., Winter, H.H., “*Composition dependence of the viscoelasticity of end-linked poly(dimethylsiloxane) at the gel point*” *Macromolecules* 24(1) pp. 47-54 (1991)
- [129] Raghavan S.R., Chen L.A., McDowell C., Khan S.A., Hwang R., White S. “*Rheological study of crosslinking and gelation in chlorobutyl elastomer systems*” *Polymer* 37(26) pp. 5869-5875 (1996)
- [130] Mijovic J., Kenny J.M., Nicolais L., “*Comparison of kinetic and rheological evaluation of gel time for an amine epoxy system*” *Polymer* 34(1) pp. 207-209 (1993)
- [131] <http://www.alchemie.com/wp-content/uploads/2011/06/PRELIMINARY-TDS-RTV-134.pdf>, Accessed on 20/04/2012
- [132] British Standards Institute, “*Plastics — Determination of tensile properties*” BS EN ISO 527-4:1997
- [133] M. S. B. M. Jamil PhD thesis, University of Sheffield, 2012
- [134] S. Oprea, S. Vlad, A. Stanciu, M. Macoveanu “*Epoxy urethane acrylate*” *European Polymer Journal* 36 p. 373 (2000)
- [135] Chen K., Schweizer K. S. “*Molecular Theory of Physical Aging in Polymer Glasses*” *Phys. Rev. Lett.* 98, p. 167802 (2007)

- [136] Chen K., Schweizer K. S. “Theory of aging, rejuvenation, and the nonequilibrium steady state in deformed polymer glasses” *Phys. Rev. E* 82, p. 041804 (2010)
- [137] Wypych, G. “*Handbook of Plasticizers*”, ChemTec Publishing 687 pages (2004)
- [138] H. Liebowitz “*Fracture : an advanced treatise*” . New York ; London : Academic Press, (1972)
- [139] C. E. Inglis, *Trans. Inst. Naval Architects*, 55, p. 219 (1913)
- [140] Griffith A. A., *Phil. Trans. Roy. Soc.*, 221(1) p. 163 (1920)
- [141] Griffith, A.A. “*The phenomena of rupture and flow in solids*” *Philosophical Transactions, Roy. Soc. London A221*, pp. 163-198 (1921)
- [142] Griffith, A.A. “*The theory of rupture*” In: *Proc. First Int. Congr. Appl. Mech.*, pp. 55-63 (1924)
- [143] Irwin, G.R. “*Fracture dynamics. In: Fracturing of Metals*” *Amer. Soc. For Metals*, pp. 147-166. (1954)
- [144] Irwin G, “*Analysis of stresses and strains near the end of a crack traversing a plate*”, *Journal of Applied Mechanics* 24, 361–364. (1957)
- [145] Irwin, G.R. and Wells, A.A. “*A continuum-mechanics view of crack propagation*” *Metallurgical Reviews* 10(38) p. 223 (1965)
- [146] Shank, M. E. “*A Critical Survey of Brittle Fracture in Carbon Plate Steel Structures Other Than Ships*” National Research Council. Institute of Technology (1953)
- [147] Jun Ma, Qing Qi, Jessica Bayley, Xu-Sheng Du, Mao-Song Mo, Li-Qun Zhang “*Test Method Development of SENB toughness measurement for thermoset resins*” *Polymer Testing* 26 pp. 445–450 (2007)

- [148] E N Brown, “*Use of the tapered double-cantilever beam geometry for fracture toughness measurements and its application to the quantification of self-healing*” *The Journal of Strain Analysis for Engineering Design* 46 p. 167 (2011)
- [149] Cordier P, Tournilhac F, Soulie-Ziakovic C, Leibler L., “*Self-healing and thermoreversible rubber from supramolecular assembly.*” *Nature* 451(7181) pp. 977–80 (2008)
- [150] Yamaguchi M, Ono S, Terano M. 2007. “*Self-repairing property of polymer network with dangling chains.*” *Mater. Lett.* 61(6) pp. 1396–99 (2007)

Appendix A

Epoxy-Amine Cure Chemistry

Generalised Reaction Route

It is generally accepted that there are two main reactions that occur during the curing of epoxy-amine based systems. Primary amines initially present in the reaction mixture react with the epoxide ring to produce secondary amine and hydroxyl groups. Further reaction of the secondary amine groups with the epoxide ring leads to the formation of tertiary amine groups. Addition reactions of epoxy to primary and secondary amine groups are catalysed by acids, phenols and alcohols. In the initial stages of the reaction the primary amines are in the majority and the reaction depicted in Figure 72 is dominant. This is a ring-opening reaction epoxy group by the primary amine to create a secondary amine species.

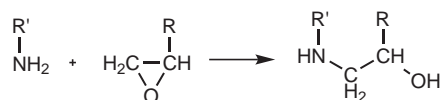


Figure 72: Primary amine-epoxy addition reaction.

This secondary amine can further react with another free epoxy to create a tertiary amine and a fully reacted species. The amine at the centre of this molecule is now unable to react any further which is why most curing agents have several of the same type of reactive group in order to provide as much cross-linking of polymers as possible (see Table 1).

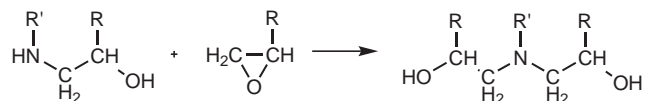


Figure 73: Secondary amine-epoxy addition reaction.

Further to these two common reactions are two others which will degrade the properties of the cured polymer. In Figure 74, the etherification reaction shown is rare

and has been proven to occur only under certain conditions, for example when the epoxy groups are in excess [17]. The ether links however are detrimental to the structure, as the bonds formed are less stable (thermodynamically favourable) yet consume epoxy groups. It has been established that the tertiary amines produced in the second reaction (Figure 73) catalyse the etherification reaction route [18], but only when the curing agent is an aliphatic amine. In the case of aromatic agents, steric accessibility prevents such reactions even at elevated temperatures.

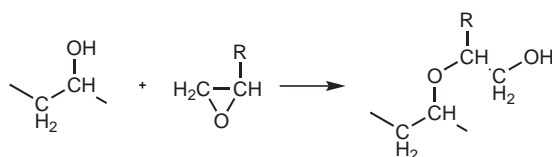


Figure 74: Hydroxyl-epoxy etherification reaction.

It is also possible, in an excess of epoxy groups, for the epoxy to polymerise with itself, a process known as homopolymerisation, shown in Figure 75. In the same way as the previous reaction, this homopolymerisation produces weakness in the structure due to the less stable ether links.

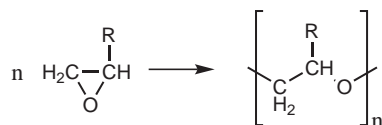


Figure 75: Epoxy-epoxy homopolymerisation reaction.

Reaction Mechanism

The reaction mechanism for the epoxy-amine reaction has been the subject of much research over the past 30 years. Mostly the mechanism has been documented using widely known and commercially available resins, such as phenyl glycidyl ether which is a reactively simple epoxy. As can be seen from Figure 76, the reaction is promoted by hydroxyl groups and is therefore self-catalysing. It was shown by Wynstra and Shechter [19] that some solvents catalysed the reaction, possibly due to the hydrogen

bonding properties. It is important that the epoxy oxygen is hydrogen bonded, making it more electronegative and therefore more susceptible to nucleophilic attack.

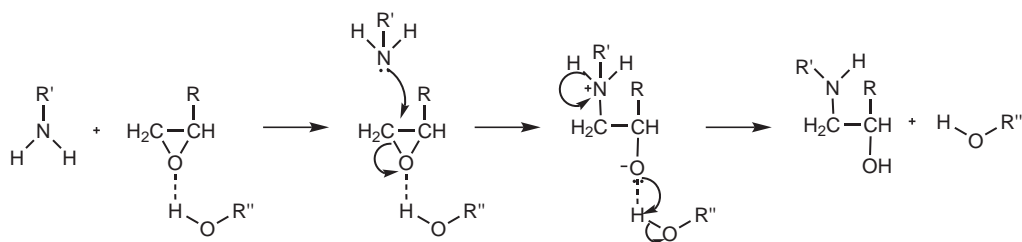


Figure 76: Mechanism of hydroxyl-catalysed epoxy-amine addition.

It has been shown by Zhang and Vyazovkin that large negative charges on any substituents of the amine curing agent cause an increase in activation energy for the epoxy reaction [20], which would mean that slower reaction times, and therefore higher processing temperatures are required for the cure.